Royal Netherlands
Meteorological Institute
Ministry of Infrastructure and the Environment

Cb-Tcu classification based on radar and satellite observations

J.P.J.M.M. de Valk and R.M. van Westrhenen

De Bilt, 2015 | KNMI Scientific Report; WR 2015-01

Cb-Tcu classification based on radar and satellite observations

Paul (J.P.J.M.M.) de Valk Rudolf (R.M.) van Westrhenen, 2015

Contents

Executive Summary

Cumulonimbus and towering cumulus clouds form a threat for save aviation conditions. Their detection in the vicinity of airports is an ICAO requirement. The detection is still predominantly done by human observers. At KNMI an automated Cb detection algorithm is developed based on radar and satellite observations. It became operational in 2011 at three airports in the Netherlands.

This report describes the derivation and performance of the Cb-classification software as used at the KNMI. It details the 2014 version of the software. The 2014 version substitutes the 2010 version, De Valk and van Westhrenen, 2010. This manual should be read in conjunction with the 2010 report and the operational manual, De Valk and van Westrhenen 2011.

The report and especially its appendices should enable the reader to develop an automatic Cb-classification from scratch based upon radar and satellite observations at any location within the viewing geometry of the SEVIRI instrument on board of METEOSAT. It requires the coverage of the area of interest by both radar and satellite observations and a supervised Cb classification over the same area. They serve as input for predictor and their coefficients determination which is based upon an algorithm that determines the predictor values over the areas of interest. The algorithm should produce contours, averages, minimum and maximum values of the observed values.

To derive the predictors and their coefficients an open source statistical software package “R” is used. The probabilistic equation based on the predictors and their coefficients enables a Cb classification. The choice by the developer of probability thresholds will determine the performance characteristics.

Improvements of the 2014 version in comparison to the De Valk and van Westhrenen, 2010 version are:

- extension of the number of Aerodromes to 26 for which a classification is produced

- slight modifications of the predictors and their coefficients in comparison to the 2010 version. Even though the modifications were slight the underlying research was thorough.

- clutter, i.e. false radar echos, impacted the results over sea in the summer. A rudimentary clutter removal has been applied to reduce the impact on the performance.

The results are summarised in the adjacent table on the next page. For the table an independent classification data set is used of a limited set of 8 stations for 2013. A colour coding has been applied to the table to enable a swift interpretation of the performance.

The table shows that overall the algorithm performance is good but that for the night especially in the winter the performance is poor.

2013	Sd **pod**	Sd far	Sn **pod**	Sn far	Wd **pod**	Wd far	Wn **pod**	Wn far
EHAM	**63**	23	**72**	32	**70**	45	**50**	50
EHBK	**65**	30	**60**	40	**70**	45	**40**	70
EHGG	**80**	25	**70**	40	**45**	60	**45**	55
EHRD	**70**	30	**60**	40	**60**	40	**45**	55
EHFZ	**55**	45	**60**	35	**60**	40	**60**	60
EHJR	**70**	30	**50**	55	**70**	40	**65**	60
EHMA	**70**	25	**70**	45	**45**	55	**45**	55
EHPG	**50**	40	**45**	55	**65**	40	**50**	55
Green	POD > 60 FAR <40							
light green	(POD > 55 FAR <45) or (POD>60 and POD-FAR >20)							
yellow	POD > 50 FAR <50							
orange	POD > 45 FAR < 55							
red	FAR >60 or POD < 40							

Table 1. Results of the updated 2014 version of the classification algorithm on the independent 2013 evaluation data set. Sd: Summer day, Sn : Summer night, Wd Winter day, Wn Winter night, POD: probability of detection in percent, FAR : false alarm ratio in percent. In chapter 4, Table 4.2 Table 4.3 and Table 4.4, page 62-63 these results are compared to previous versions of the classification algorithm. Please note that light green consists out of two groups.
POD and FAR are explained in chapter 2 page 4.

Acronyms

ARP: Aerodrome Reference Point

Cb: Cumulonimbus

FIR: Flight Information Region

NWP numerical weather prediction

Tcu Towering cumulus

1 Introduction

Convection in the atmosphere can cause turbulence which forms a hazard to aviation. Near to airports within the aerodrome undesired relative small vertical displacements of air-crafts induced by turbulence at take-off or landing may cause a disaster. Convective clouds can also produce lightning, can contain supercooled water and produce significant precipitating. Such phenomena can form a threat to save aviation. Therefore it is an ICAO requirement to report those convective clouds when they occur in the vicinity of an airport. In the world these reports are still predominantly man made.

Next to safety issues Cb occurrence has also economical implications. Due to flight safety rules Cb occurrence limits the flight capacity of the airport, and causes re-routing of air-planes, with increased fuel costs. In the convective clouds observations False Alarms should therefore be minimized and misses should preferably never occur.

In 2011 an operational algorithm was implemented at KNMI at three airports to produce an Automated Cb classification based on radar and satellite observations, De Valk and van Westrhenen, 2010. It replaced an automated algorithm operational since 2007 at two airports. The latter 2007 version used radar observations only. It's performance showed ample room for improvement.

In 2011 the request came to extend the implementation of this algorithm to all aerodromes represented by ARP (airport reference points) within the Dutch Flight Information Region (FIR). To enable this an evaluation data base of all the aerodromes within the FIR for a full year was required. The production of such a data base for the year 2010 for every 30 minute slot at every aerodrome was a huge effort. A rough 450000 evaluations were done.

The 2014 version of the detection algorithm described in this report is based on the 2010 data-base. The performance of the 2011 version evoked suggestions by the forecasters. Additional research was done to comply with the suggestions and to improve upon the 2011 performance in the 2014 version. Simultaneous with the research a limited evaluation was performed for a selection of 7 to 9 rainy days per month in 2013 and a limited number of stations, 8. This latter data set serves as an independent data set to evaluate the performance of both the operational and the 2014 version of the algorithm.

This report describes the process to create a classification algorithm based on radar and satellite observations in detail. It is aimed to be self explanatory.

Required input and conditions for a successful performing algorithm are:

-The region of interest is well covered by radar and satellite observations

-There is a data base of Cb occurrence which serves as the truth, preferable produced by forecasters.

-There is an algorithm available which can ingest radar and satellite observations, and produces information for a predefined collocation area like contours, minimum and maximum values of the observations. This information is required for the determination of predictors.

The report contains a theoretical part, with a description of convection, the description of the required classification in Meteorological Aerodrome Report, (METAR) and runway specific report or ACTUAL, methods to evaluate classifications and methods to produce a classification. A data part with a description of the data used, data issues and how to produce such data. The sections results, conclusions, and outlook finalise the report.

Appendices give the detailed information required to come to a classification algorithm.

2 Theory

Convection

A parcel of air with a certain temperature and moist content can be displaced in the atmosphere. Due to the displacement it can have a different buoyancy compared to the surrounding air caused by temperature differences. When the buoyancy is positive the air parcel will accelerate upwards. A number of physical processes occurring in the air parcel, expansion, condensation, latent heat release, may cause a further acceleration, and can result in strong updrafts. Entrainment of surrounding air will occur and the parcel will experience friction with the air, these processes will decrease the upward momentum. Condensation and glaciation are the sources of precipitation. The falling precipitation drags the air downward causing downdrafts. The updrafts and downdrafts will cause significant turbulence within and around the cloud.

The ice particles can split within the cloud. This is essential for the electric charging process. The charging may result in lightning, another threatening phenomena for aviation. There is an abundance of literature describing the processes of convection. For further reading we refer to S Petterssen (2008) or Mcintosh and Thom (1969).

These above mentioned phenomena are the physical principles of convective cloud formation. with the solar heating of the surface as an important energy source. There are two cloud types identiified as hazardous for aviation:

- the towering cumuli (Tcu) , which produces no precipitation yet, but has strong vertical motions,
- the cumulonimbus(Cb), which next to turbulence also produces precipitation.

The horizontal spatial scales of convection at mid latitudes in Europe ranges from 1 km (fair weather cumuli) till 300 km (09-06-2014, Pinkpop, Landgraaf, the Netherlands), see Figure 1. The temporal scale may range from 20 minutes till 6 hours.

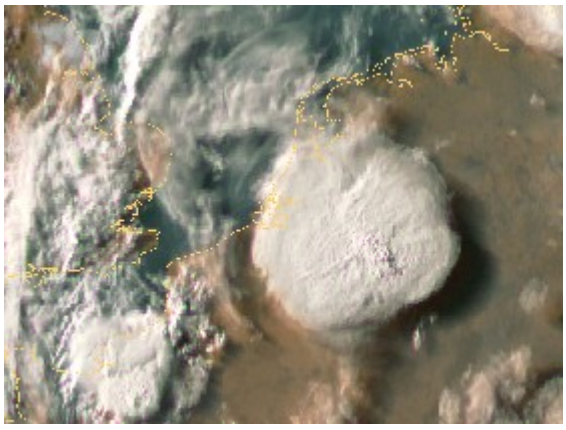

Figure 1: A mesoscale Cb over the Netherlands on June 9, 2014 at 18:00 UTC. The Cb caused casualties in Germany and severe damage. Notice the overshooting top south west of the centre of the CB.

The complexity and details of the process is hard to capture in numerical weather prediction (NWP) models. The 3 dimensional grid used for calculations in the NWP models to forecast the weather is still, in 2014, too coarse to capture and fully resolve all the associates scales contributing to convection. NWP may describe the vertical temperature and humidity profile adequate, and NWP could forecast favourable conditions for convection occurrence but it will predominantly miss the correct location and triggering moment, see for example Zbyněk Sokol and Petr Pešice, (2009).

Therefore the detection of Cb remains important, as there is no other source of information for their occurrence.

METAR and ACTUAL

METAR

The METAR (Meteorological Aerodrome Report) is produced every thirty minutes. It is issued at 25 and 55 minutes past the hour. The METAR reflects the weather conditions representative for the aerodorme of the airport ten minutes previous to the moment of reporting.

The AERODROME METEOROLOGICAL OBSERVATION AND FORECAST STUDY GROUP (AMOFSG)

February 2010 states that:" VCTS Thunderstorm in the vicinity are a "Primary requirement (thunderstorm)(ICAO Standard), but requires remote sensing to provide this in automated reports, requiring substantial work from many States to comply."

It is recognized by this group that it is a challenge to automate the detection of Cb/Tcu.

ICAO prescribes the format and the content of the METAR, see for details the appendix 2 of De Valk and Westhrenen, 2010.

The cloud part includes the vertical visibility, the coverage at several layers, when observable, and the cloud base height. Relevant and mandatory to report is the occurrence of Tcu or Cb. When a Tcu and a Cb occur at the same cloud level the observer is obliged to report only Cb. As the observer can only report a Cb when he or she can observe the top of the cloud, the coverage can never become "overcast".

The time required to develop from a Tcu to a Cb is relatively short in comparison to the total life cycle of a Cb. The observation frequency of Tcu is therefore considerably lower compared to the Cb occurrence frequency.

ACTUAL

Where METAR reports the conditions for the airport, the ACTUAL is a runway specific weather report. Its update frequency is depending on the used observation method, e.g. the automated wind observation has an observation frequency of 12 seconds and its ACTUAL update frequency is every 1 minute. The ACTUAL may change, reported in a SPECIAL when for example the runway is changed. For the Cb- algorithm the radar observation frequency determines the update frequency, which is a 5 minutes interval. This frequency may change in the future, when new radars are installed. The AUTO METAR report for Cb is determined for an aerodrome. This disables a differentiation per runway. The AUTO ACTUAL and AUTO METAR cb part will therefore have the same content but a different update frequency.

Verification

Cb/Tcu occurrence is a dichotomous phenomenon. The frequency of Cb/Tcu occurrence at mid latitudes is relatively low in comparison to the total number of METARs. The value of a forecast or classification can be assessed by comparison to an observation. Frequently used for assessment is the contingency table, table 2.1 (Wilks 1995). Here the occurrences of forecast/classification in comparison to observations are represented.

From the table a number of scores can be calculated. Given the large number of correct negatives for this specific Cb-Tcu classification this number is only incorporated in the *Hanssen and Kuipers discriminant* HKS and *Symmetric extremal dependence index* SEDI score, and neglected in the other scores, see below.

	observed yes	observed no
forecasted yes	hits	false alarms
forecasted no	misses	correct negatives

Table 2.1. Contingency table,(Wilks, 1995). Relationship between the number of observed and forecasted cases of a dichotomous phenomenon. The sample size is the sum of the hits, misses, false alarms and correct negatives.

Considered are next to SEDI and HKS, the Probability of Detection (POD), The False Alarm Ratio (FAR) the Critical success index (CSI) or threat score, and the BIAS.

POD = Hits/ (Hits + Misses)

FAR = False Alarms / (Hits + False Alarms)

It is relevant to note the difference between False Alarm Ratio and False Alarm Rate= False Alarms / (Correct Negatives + False Alarms). For both the abbreviation FAR appears in literature. When the number of Correct Negatives is high the False Alarm Rate can become a small number.

CSI = Hits/ (Hits + Misses + False Alarms)

BIAS= (Hits + False Alarms) / (Hits + Misses)

The BIAS is a ratio of the observed events and the classified events. The bias is not an accuracy measure. It states whether the event is classified more (bias >1) or less (bias < 1) than observed. Bias is 1 only states that Hits and Misses are in balance with Hits and False Alarms.

To evaluate the performance additional scores are considered. The *Hanssen and Kuipers discriminant (also named: true skill statistic, or Peirce's skill score)* HKS

HKS=Hits/ (Hits + Misses)-False Alarms / (Correct Negatives + False Alarms)

(also denoted TSS and PSS)

For rare events the HKS tends to the POD. A perfect score is 1.

http://www.cawcr.gov.au/projects/verification/

This score is included to serve as a reference for the *Symmetric extremal dependence index(SEDI)*

SEDI=[ln F - ln H - ln (1-F) + ln (1-H)]/ [ln F + ln H + ln (1-F) + ln (1-H)]

with H = POD and F = False Alarms / (Correct Negatives + False Alarms).

Note that the latter F, the False Alarm Rate, is different from the FAR, the False Alarm Ratio.

The SEDI perfect score is 1. The score can vary from -1 till 1. Zero indicates a poor performance. The SEDI score is introduced here as the occurrence of Cb is a relatively rare event and SEDI enables the evaluation of the performance of rare events detection or forecasting.

(http://empslocal.ex.ac.uk/people/staff/ferro/Publications/edi.pdf)

(http://www.wmo.int/pages/prog/arep/wwrp/new/documents/14_2_Nurmi_Extremes.pdf)

Brier Score

To assess the performance of probabilistic forecasts it is convenient to capture it in a scalar number Wilks, (1995). The most commonly used is the Brier score (*BS*). The score is the average of the squared differences between the forecast probability *c* and the dichotomous observable *o*.

$$BS = \frac{1}{n}\sum_{k=1}^{n}(c_k - o_k)^2$$

with *n* the sample size and *k* the index.

The Brier score is negatively oriented. The performance of an algorithm improves when the *BS* decreases.

From the Brier score a skill score *BSS* can be computed.

$$BSS = 1 - \frac{BS}{BS_{ref}}$$

with BS_{ref} the reference *BS*, usually the climatological occurrence frequency. When the *BSS* becomes negative the *BS* is worse than the climatological BS_{ref}. A *BSS* close to 1 indicates a very good performance. A *BSS* equal to 0 indicates that the BS and BS_{ref} have an equal score, so that the forecast does not contribute significantly relative to the climatological BS_{ref}.

Logistic regression

In De Valk and Westhrenen, 2010, some two hundred potential predictors are determined to classify the binary predictand: Cb/Tcu or non Cb/Tcu. For this 2014 study we could rely on the previous experience and limit the number of predictors to a mere hundred. A successful approach to come to binary results is the Logistic regression, Wilks (1995) and Carbajal-Henken et al (2009). Logistic regression models result to a classification or prediction of a binary predictand while the predictor variables can be of any type. A non-linear equation can fit the predictand *c* using a multiple number of predictors *x*.

$$P(c) = \frac{1}{1+\exp(-(b_0 + b_1 x_1 + b_2 x_2 + \ldots b_n x_n))}$$

With *P(c)* the probability that *c* occurs, b_i the regression parameters and x_i the predictor variables. The function is bounded between 0 and 1 due to its mathematical form allowing only for properly bounded probability estimates. The function drawn will always result in a S- shape curve. To come to a yes-no Cb classification a probability threshold or cut-off value is required.

Logistic regression is well known in social and medical sciences. In meteorological research it is commonly applied, e.g. for severe thunderstorm occurrence Schmeits et al (2008).

It is not possible a priori to indicate which predictors will lead to the best result in the desired classification. The dependencies and correlations between them are too complex.

The forward stepwise regression, Wilks (1995), enables the determination of those predictors which contribute significantly to the desired classification. In consecutive steps predictors are added to the equation and based on the statistical scores it is decided if the additional predictor contributes to the overall performance. It is up to the user to decide how many steps or predictors contribute significantly to the classification performance. Using all predictors may lead to an over-fit regression, Wilks (1995). In an over-fit regression too many predictors are used in the equation to describe the observations. The regression will fit to the used observations but the equation may fail to describe other observations not used for its determination.

To assess the performance of the algorithm and to optimize the choice of the predictor set the A*kaike information criterion, Wilks (1995)* AIC score is evaluated. AIC can be interpreted as a trade-off between the model complexity and the goodness of fitting the data. It is a relative score of quality of a statistical model and the lowest score usually indicates the best performance obtained by the best associated predictor set.

3 Data

Radar Data

In the Netherlands two Doppler radars, C-band, are operated for precipitation detection. The C-band radar emits and receives pulsed 6 Ghz radio waves with a wave length of circa 5 cm. The lowest inclination of a radar beam is 1 degree. Due to the inclination, the lower part of the atmosphere is not observed. This lower part increases with increasing distance to the radar due both to the curvature of the earth and the inclination. The atmospheric cone observed by the radars with a good signal to noise ratio has maximum radius of 320 km. The height from the lowest radar beam to the surface (at sea level) varies form 800 m near the radar site to 3 km, at the edge of the observation cone.

The reflection signal is proportional to the sixth power of hydrometeor diameter, when the particles are smaller than the wavelength, Holleman (2000). Due to the sixth power the variance of the reflectivity value is several orders of magnitude. A decibel or logarithmic scale is used to represent the signal. The radar reflections are projected on a grid with grid cells of 2.5 by 2.5 km. Since 2008 a radar software upgrade can also provide the reflections on a 1 by 1 km grid.

Z [dBZ]	7	15	23	31	39	47
R [mm/h]	0.1	0.3	1	3	10	30

Table 3.1 Relation between radar signal and rain rate.

In the table 3.1 examples of reflectivity *Z* values and corresponding precipitation rates *R* are given.

At KNMI the following equation relates reflections to approximate rain rate:

$$Z = 200 * R^{1.6}$$

with R in mm/hr.

The radar observes the atmosphere at various scanning angles, thus producing a 3D precipitation observation. The results of the 3 D scan are projected to a horizontal plane at a certain altitude in a pseudo-CAPPI, pseudo-Constant-Altitude Plan-Position Indicator, representation. http://www.knmi.nl/~beekhuis/rad_intro_nl.html#pCAPPI

It is relevant to note the next considerations about radar observations in relation to Cb/Tcu detection:

– The operational radars are sensitive to precipitation and not to cloud occurrence. Therefore developing convection without precipitation can not be observed by the radar. Hence radar observations can not detect Tcu which by definition is a non-precipitating cloud.

– Additionally the radar cannot distinguish between significant stratiform (non convective) precipitation or convective precipitation. This can cause false alarms when frontal precipitation occurs.

– The theoretical range of 320 km will not be reached in all atmospheric conditions. For example heavy rain will reduce the radar signal strength and therefore may mask any precipitation shielded by this heavy rain from the radar location.

satellite data

Meteorological satellites provide a near instantaneous view of the atmospheric state at observation time. The geostationary satellites are a valuable source of information for nowcasting. The latest generation of operational geostationary satellites provides an image every 15 minutes over Western Europe. They are operated by EUMETSAT. The Spinning Enhanced Visible and Infrared Imager (SEVIRI) on board the METEOSAT 8 and its follow-ons, 9, 10 and 11, are in operation since January 2004. SEVIRI as a passive instrument does not emit a signal, like the radar does. SEVIRI observes the solar radiation reflection by the earth in spectral bands from 0.5 μm to 3.9 μm and the emission of the earth in spectral bands ranging from 3.9 μm to 13.4μm. Next to the eleven spectral bands, there is a high resolution visible (HRV) channel, that has a spectral response function ranging from 0.4 μm to 1.1μm. The sampling grid distance in the nadir point of the satellite is 1 km for the HRV channel and 3 km for the other channels.

The observation cycle consists of a 12.5 minutes scan of the earth from south to north. Then the scan mirror returns to its starting position and calibration occurs in 2.5 minutes remaining from the 15 minutes cycle.

Further details on the satellite platform and the SEVIRI instrument can be found at www.eumetsat.int.

It is relevant to note the next points of satellite observations in relation to Cb/Tcu detection:

- Satellite view is obscured when higher cloud layers block the view to the lower atmosphere. Cirrus may hamper a correct interpretation of the occurring clouds within the satellite observation.
- During the night, there is no information in the HRV or other reflection channels. This affects the performance of the detection of clouds.
- The satellite observes predominantly the top layer of the cloud.
- The horizontal spatial resolution degrades when moving away from the nadir point. At the latitude of the Netherlands, the spatial resolution is approximately 3.5 km West East and 6 km North South, for the 11 channels and 1.2 by 2 km^2 for the HRV channel. Clouds smaller than the pixel size can not be classified correctly.
- One should correct for the slanted view of the satellite to collocate radar and satellite signals when both are used. A correction may require shifts up to several radar pixels, depending on the cloud top height. The slanted view correction is not applied in the present algorithm. This implies that the areal coverage of the satellite and the radar may differ slightly. When clouds occur the satellite covered area is located to the south of the radar covered area.

Timeliness of the observations

The time stamp assigned to the observation differs between radar and satellite observations. The time stamp of the radar indicates the end of the observation scan. The time stamp of the satellite indicates the start of the scan. A satellite scan has a recurrence frequency of 15 minutes. The radar observations have a recurrence frequency of 5 minutes.

The satellites observe the area of the Netherlands around 11 minutes after the start of an observation scan. Within less than a minute, the whole FIR is covered. The satellite data become available 1-2 minutes after the end of the scan. A processing step is required to extract the input data required by the classification algorithm.

The algorithm requires a limited processing time to come to a classification. For the development of the algorithm the processing time is irrelevant. A limited processing time is essential in an operational environment. In the operational mode a number of sequential data transfers and

process steps are required within a very short time window. Should one of these transfers be delayed the previous satellite image will be used. This previous image may have an observation time difference of more than 15 or even 30 minutes with the moment the required observations should be available.

To elucidate the timeliness issue:

For the METAR of 11.55, which should cover an observation period of 11:45 till 11:55 the radar image of 11.50 is optimum and the satellite image of 11.45. These cover the METAR time the best with an observation window for radar from 11:45 till 11:50 and a satellite observation window from ~11:50 till 11:52. In operational practice however the radar observation window of 11:40 till 11:45 is used. [Check], and the satellite of 11:15 observing the area around 11:25 till 11:27.

EUMETSAT also provides a rapid scan service with the hot standby spare satellite. The Rapid Scan Service provides every five minutes a satellite observation over the Netherlands. When the Rapid Scan Service imagery could be used this time difference could reduce to less than 10 minutes. For the 11:55 METAR example given above the satellite time stamp of 11:40 with an observation time window of 11:43 till 11:44 would be used.

Lightning detection data

The so called SAFIR network provides information about lightning. The lightning detection was shown to be a non significant contributor to Cb detection in the evaluation study done over 2005 on the operational algorithm-2007, The (2006). Lightning is unlikely to occur in the early stages of convection, therefore it can not contribute to early convection detection.

Nevertheless the lightning observations are used in the METAR producing TELNET software. The lightning information is merged into the METAR message at the end of the processing chain in the third party software installed on hardware at every METAR producing station. The occurrence of lightning within a circular area with a radius of 30 km overrules all other classification information and will report Cb in the METAR.

Unfortunately the SAFIR system also occasionally reports lightning erroneously. This can lead to Cb classification in a clear sky conditions. In such case the ACTUAL or METAR contains FEW015CB. This can cause confusion at the airport. At the moment of writing there is no solution to avoid such an error. For the major airports the forecaster may add “BECMG CAVOK” to the ACTUAL/METAR as mitigation.

In 2015 the lightning detection system will be replaced. There are differences in performance, The new system appears to have a better performance in cloud to ground lightning detection. It is unknown what the cloud to cloud lightning performance will be. The latter is still relevant for aviation.

Verification data

Forecasters have created an evaluated Cb classification data set. It is an expert classification of Cb within the aerodrome, a circle with a radius of 15 km around an ARP. Within their classification various information sources are used: Analyses of the weather maps, NWP profiles, METAR, lightning information, radiosondes, radar observations and satellite observations.

Various forecasters produced Cb classifications for 2010, for 26 aerodromes and for 2013 for 8 aerodromes. The robustness of the method was tested by a comparing the results from two forecasters for the whole month of August 2007, for 4 airports, a rough 6000 evaluations. There was 95 percent correlation on the Cb classifications, indicating that the method is robust.

For the 2013 evaluation a limited number of days is considered. Of each month the 7-10 days with the highest precipitation rate, judged from radar observations were evaluated by forecaster. The high number of precipitation free days and the limited resources available for evaluation were the motivations for this limitation.

The 2013 data set is used to assess and compare the performance of both the 2010 operational algorithm and the improved 2014 version.

In Appendix 2 a detailed method description is given of the evaluation and the method to convert the information in an accessible data format for automatic merging and processing.

In Figure 2 the stations for which a METAR is produced is shown. It includes the METAR code name per station. There are two METAR stations for which no automatic Cb classification will be generated. EHAK, because it is too remote from the radar sites, and EHFS, Vlissingen, as it is not an aerodrome. At the start of the expert classification it was not recognized that a METAR at EHFS is produced because it fills a gap in the FIR. Therefore it was neglected in the classification.

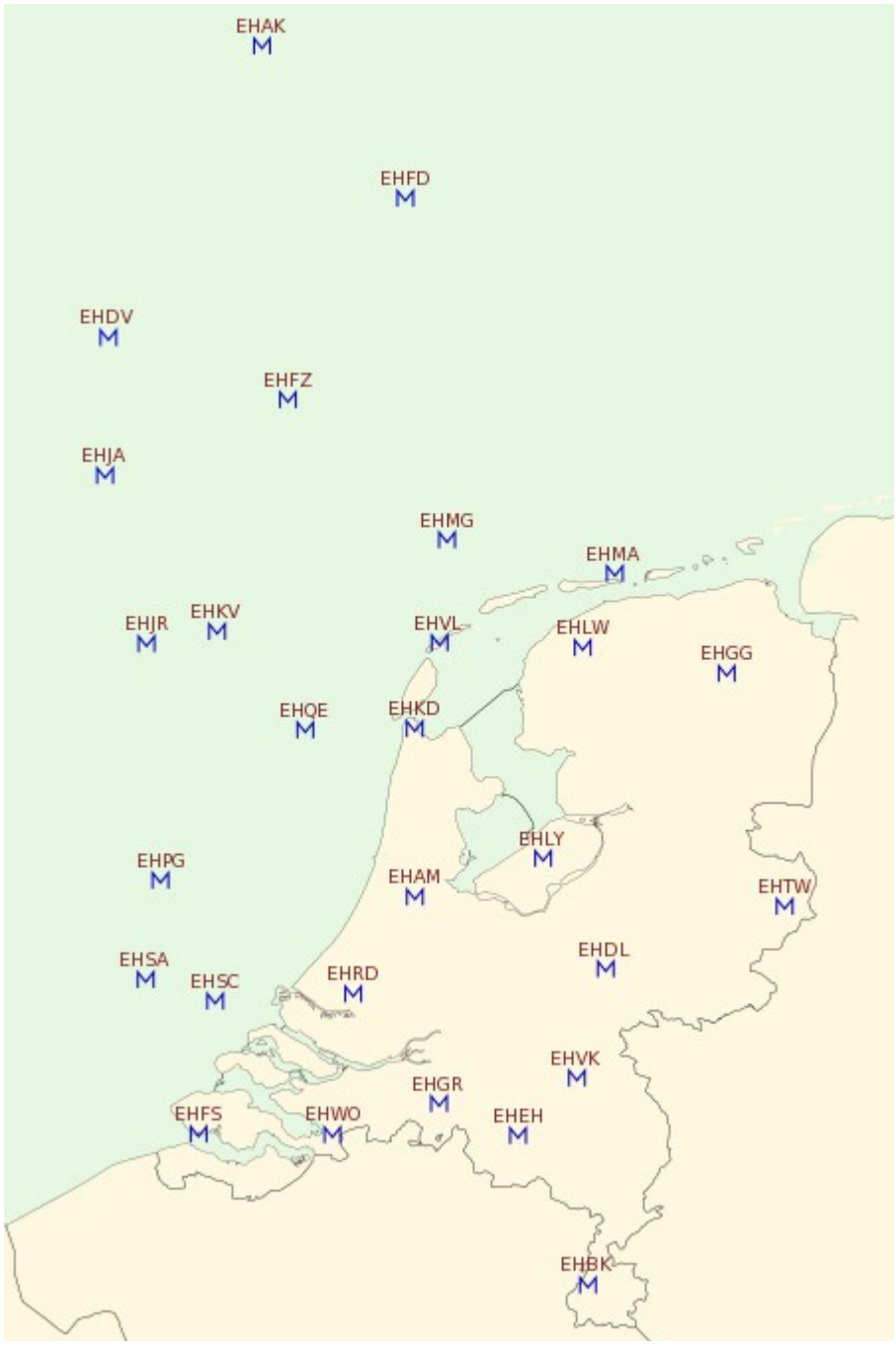

Figure 2. Areal distribution of ARP's with their respective METAR code. EHFS is not an ARP. A METAR is produced for this station as it fills a void in the Dutch FIR. EHFS is not included in this study. EHAK is not included as the station is too remote from the radar observation sites.

4 Results

Predictor derivation (related to section 3.2 of WR 2010-4)

The base of the algorithm is the determination of a set of predictors with a high explanatory correlation with the predictand. A large number of studies is focussed on the Cb occurrence and detection within satellite imagery, Mecikalski and Bedka (2006) , Mecikalski (2007), and Zinner(2008) and are described in De Valk and van Westrhenen, 2010.

The commonly applied methods use satellite observations as predictors. A number of the studies in the literature use the radar observations for evaluation purposes. In the method described here both radar and satellite observations are used simultaneously.

In De Valk and Westhrenen, 2010, a number of predictors emerged as explanatory predictors for the classification. They were determined based on a logistic regression study using the **S**tatistical **P**ackage for the **S**ocial **S**ciences SPSS statistical package. (http://www-01.ibm.com/software/analytics/spss/). A forward stepwise regression selection method is applied. Starting with a constant-only model at each step a predictor is selected with the largest statistical score (likelihood ratio based) and a significance less than 0.05. The selection and inclusion is stopped when the significance of the remaining predictors is more than 0.05. Should during the inclusion a predictor obtain a significance of more than 0.10 then this predictor is excluded from the further steps of the evaluation. Forward stepwise regression selects the predictors purely on statistical criteria. The regression is capable to identify groups of predictors which individually contribute only weakly to moderately to the explanatory power but as a group contribute significantly.

In De Valk and van Westrhenen, 2010 the 2009 data set was used to determine the explanatory predictors using a collocation area that consisted out of a circle with a radius of 15 km around the ARP. The predictors identified were:

- the highest occurring radar contour number. The occurring contours in the collocation area are numbered from 1 till 17, with 1 relating to the 14 dBz contour (rain rate 0.25 mm/hr, see table 3.1) and the next numbers relate in steps of 2.5 dBz till ~ 55 dBz(>100 mm/hr). A high contour number relates to a high precipitation rate and is most likely related to convective precipitation.
- the number of radar contours with 14 dBZ (0.25 mm/hr) occurring in the collocation area. A patchy rain pattern with many separated rainy areas could be related to (small) Cb. This is of course dependent on the size of the collocation area, in relation to the pixel size used.
- the average of the cloud top temperature, determined from satellite data. The cloud is defined here as those pixels with a brightness temperature below 268.15 K. A cold cloud top could be related to Cb. To exclude Cirrus here an additional pre-check on Cirrus occurrence is performed, using the 12.0 µm and 10.8 µm difference.

For night time conditions only:

- The areal fraction of the collocation area where the brightness temperature difference between the 3.9 µm and the 10.8 µm channel is below zero is valid (T03.9µm -T10.8 µm <0). Several literature studies imply that this difference is related to precipitation, see for example Fig 4 from Lensky, I.T. and D. Rosenfeld 2003. In this article the precipitation occurs when the brightness temperature difference ranges from -1.5 K to 4K. Within this 2014 study the confinement of the brightness temperature difference to this range caused a deterioration of the results. It was therefore decided to keep the difference as described above. The use of an areal fraction is nowhere described, and is therefore not confirmed as a precipitation indicator by literature studies. The consideration of an areal fraction of this temperature difference is a unique method, and only applicable for Cb classification in fixed defined areas.

For day time conditions only

- The difference between the maximum and minimum occurring value in the HRV channel within the collocation area. The occurrence of HRV difference range as indicator is linked to illumination of convective clouds with high reflective sides and tops and dark shadow sides. Especially in the winter with a lower solar elevation angle the difference becomes more apparent.

For the 2010 data set another statistical package was applied R, http://www.r-project.org/ opposed to the SPSS package. The availability of this package in a linux/unix environment enabled scripting of the research software and therefore facilitated a faultless transfer of the resulting coefficients into the developed software. Using the logistic regression method “StepPlr” from R, the earlier identified predictors used in the operational algorithm, version 2010, and other predictors partly suggested in the literature were considered. StepPlr is an L2 penalized logistic regression (http://cran.r-project.org/web/packages/stepPlr/index.html) with a stepwise variable selection. Similar to the development of the SPSS based algorithm in De Valk and van Westrhenen, 2010, the goal was a limited number of predictors combined with an optimum score in AIC.

The 2007 data set and predictors used in the SPSS study were re-evaluated with the R package. It was confirmed that the results using SPSS or R were exactly identical for a test set.

For the 2014 version of the software a number of satellite predictors, identified in the literature as having a high correlation to Cb occurrence were evaluated. A selection of potential predictors based on satellite observations by Mecikalsky (2007) were considered, 6.2-10.8 µm 8.7-10.8 µm and 7.3 -6.2 µm. These were also considered for the 2010 version but were rejected as explanatory predictors as they did not contribute to the Cb classification. The predictors were added to the input for the statistical package StepPlr of R. Similar to the 2010 study none of them emerged as an explanatory predictor. Most likely a possible cause for this difference with the conclusions of Mecikalsky et al is their focus on strong convection where in this study also weaker convection is considered. The weaker and moderate convection has a higher occurrence frequency than strong convection in the Dutch FIR. This maybe another reason that the added predictors derived from literature had no significant explanatory impact.

The operational algorithm has weaknesses reported in the feed-back by forecasters in the discrimination between heavy frontal rain and Cb. The additional information from NWP on instability was introduced and expected to mitigate this weakness. A number of instability NWP parameters like the convective available potential energy CAPE, level of neutral buoyancy, LNB, lifting condensation level, LCL, Convection inhibition, CIN, were evaluated as potential contributing predictors. They were included in the R analyses. The KNMI operational model HIRLAM supplied the instability information. The instability parameters used as predictors had a marginal positive impact on the classification. The improvement however was not significant. Apparently the used HIRLAM version is not capable to provide information which contributes significantly to Cb classification. This is in accordance with the results of Petersen, 2013 which indicates that convection is still not adequately represented by NWP models to forecast the exact location and timing of convection.

One should be aware that future NWP can improve upon the description and modelling of convection. Then the added value of NWP can become significant. So the explanatory contribution of NWP based predictors need to be re-analysed in the future improvements of the algorithm.

Due to the marginal positive impact of these NWP based parameters on the Cb classification, they were at present disqualified as potential predictors. Neglecting NWP information as required input to the algorithm simplifies the dependencies of the algorithm.

The probability of Cb occurrence at the previous evaluation time was considered as a potential predictor. The theoretical background was that once the atmospheric instability is beneficial for Cb formation Cb's are likely to appear at consecutive times. Likewise they most likely will not appear at consecutive times when the atmosphere is stable. Similar to the NWP parameters the predictor impact was slightly positive but restricted to a limited number of stations, mostly at sea. The

increase in AIC score when considered together with the predictors from the 2010 report was negligible. Hence like the NWP parameters the previous Cb evaluation was not considered as potential contributing predictor. Like neglecting NWP the removal of the previous evaluation makes the algorithm implementation simpler.

Probably the Cb occurrence within the aerodromes is not consecutively triggered, by orography or other means. Also the time difference between the METAR reports is relatively large, 30 minutes. These factors probably disqualify the Cb classification at the previous evaluation time as a contributing predictor.

From the application of the R-package on the 2010 data set emerged nearly the same variables as explanatory predictors, as in De Valk and van Westrhenen, 2010. Nearly because R offers an additional functionality compared to the earlier used SPSS package, it evaluates combinations of predictors.

A difference between the operational algorithm described in De Valk and van Westrhenen, 2010 and the 2014-version algorithm is the emerging of the contrast in the radar observation between the maximum and minimum (non-zero) precipitation intensity within the collocation area as a predictor. The predictor representing the number of radar contours with 14 dBZ (0.25 mm/hr) from the 2010 algorithm version did not re-appear in the 2014 version as a predictor. Most likely the former predictor, contrast in radar reflectivity, has a higher explanatory impact than the latter one, thus replacing the latter in the list of predictors. The removal of number of radar contours also excludes the dependency on pixel size and its' relation to the collocation area.

From the R evaluation also combined products resulted as explanatory predictors:

- the highest occurring radar contour number times the contrast in the radar observation between the maximum and minimum (non-zero) precipitation intensity. This appeared as an explanatory predictor for summer night over sea.
- the average of the cloud top temperature times the areal fraction where the brightness temperature difference between the 3.9 μm and the 10.8 μm channel is below zero is valid (T03.9-T10.8 μm<0). This was applicable for winter and summer night
- the highest occurring radar contour number times the average of the cloud top temperature. This appeared as an explanatory predictor for winter day over land.

Note that two combined products show combinations of one observations source, either radar or satellite. Only the last one combines satellite and radar observations. For this combination the difference in area coverage due to the slanted view of the satellite may require attention.

In a limited number of cases the decrease of AIC score when using the most optimal set of predictors was not significant when compared to a less optimal predictor set. In those cases the choice for predictors was dominated by the strive for uniformity in the applied predictor sets. Uniformity limits the complexity of algorithm development and maintenance.

Clutter in the radar data.

During the evaluation very high rain intensities were noticed in the radar data up to 1300 mm/hr. This high radar observations are related to false reflections also known as clutter. Clutter can occur when large horizontal temperature gradients occur in the atmosphere. Especially above the sea it occurs frequently in spring and fall. Clutter impacted the summer results predominantly and the winter results only marginally.

Clutter occurrence did not impact the performance of the operational algorithm as this was only applied on land stations.

A rudimentary clutter removal was implemented. It flags all the cases with a maximum rain intensity of higher as 40 mm/hr as non-Cb. In Appendix 8 the impact of clutter on the performance is discussed.

This clutter removal did impact the predictor coefficients, and not the predictor selection.

The applied predictors and their coefficients are given in appendices 6.

Performance

	METAR #	Day	Night	Day land	Night land	Day sea	Night sea
2010 summer	207532	8645	5705	5271	2926	3374	2779
2010 winter	202878	4855	11156	1746	3688	3109	7468
2013 summer	17424	1801	810	1061	431	740	379
2013 winter	13980	688	1246	364	612	324	634

Table 4.1 Number of Cb occurrences, per season, per surface type. The number in the second column indicates the number of used METARs. In 2013 only a limited set of days and stations are considered, hence a lower number of METAR's.

Two data sets of Cb classification done by forecasters were available for algorithm development and evaluation, one for 2010 and one for 2013. The 2010 data set consists out of classification every 30 minutes for a full year, for 26 stations. The 2013 consists out of every 30 minutes classifications for the 7 to 10 wettest days for each month for 8 stations.

The Cb evaluation results for 2010 and 2013 are summarized in table 4.1. It shows in the summer a higher Cb occurrence number during the day versus the night and over land versus the sea. In the winter the number of Cb in the night is higher than during the day. The day-night differences in occurrence number between the seasons are partially attributable to the difference in day-night time length for 2013 land and sea and for 2010 land and winter time over sea. In 2010 winter over the sea there is a high Cb occurrence rate during the night, while in the summer over sea the day and night occurrence rates differ less.

In the 2013 data set the numbers are lower as a limited part of the year and stations is considered. Still they show the same qualitative performance and relative relations as the occurrence rates of 2010.

The 2010 set is used to obtain an optimized probabilistic equation based on the predictors with the highest explanatory relation to the classification. The latter algorithm version is referred to as the 2014 algorithm. In 2011 an operational algorithm was implemented. It was based on a manual classification for 4 stations, throughout 2009 every 30 minutes, De Valk and van Westrhenen, 2010.

Both the operational algorithm and the 2014 algorithm are applied to the 2013 data set. The 2013 data set served as an independent set.

In this section we present the results of the 2014 algorithm applied on the 2010 dependent data set. The discussion on the performance of both the operational algorithm and the 2014 algorithm applied to the 2013 data set finalise this section. The application of the 2014 algorithm includes a crude clutter removal. The clutter removal classifies cases with a maximum rain intensity > 40 mm/hr as non Cb.

The results are presented in a consistent manner to enable comparison between the various cases. For each station 6 tiles (2 columns 3 rows) are given for each season. The left columns give the results for the day and the right columns for the night. Per page two stations are shown in alphabetic order under the condition that both stations have the same surface, either land or sea. Only the latter graph of each season contains the combination of a land station EHWO and an island/sea station EHVL.

Caption for the Figures on the next pages.

The top figure gives the averaged HKS score in red as function of the probability threshold from 0.05 till 0.5, in steps of 0.05. The average score is the result of bootstrapping on the dependent data set for the 2010 data set. In the evaluation of the 2013 case the bootstrapping is done on the independent 2013 data set. The median value is given in black. The grey vertical lines indicate the 95 percentiles.

The blue lines and dots in the top figure indicate the SEDI score also as function of the probability threshold from 0.05 till 0.5.

The middle figure from the top is the Detection (POD) and False Alarm Ratio (FAR) diagram. The upper left corner corresponds to a high POD and a low FAR. The curved dashed lines give the CSI scores in intervals of 0.1, starting in the upper left corner with 1 and decreasing to 0 in the lower right corner. The red diagonal from upper left to bottom right indicates the bias is 1 line. Bootstrapping on the dependent (2010) or independent (2013) data set resulted in average score, Red line with dots for probability threshold from 0.05 (upper right) to 0.5 (lower left) in steps of 0.05, ***black line and dots*** *denotes the median for the same probabilities as the red line, occasionally the red and black line may overlap, dark grey denotes 66 percentile of all bootstrapped cases, and light grey denotes the 95 percentile. A single blue dot in the POD-FAR diagram represents an approximation, explained below, of the previous 2007 algorithm, which is based on radar observations only.*

The bottom figure is the attribute diagram as a function of the averaged predicted probability, in black dots. The perfect reliability line is the diagonal. The horizontal line above the lower axis, relates to the climatological Cb occurrence at the station, different for each station and season. The no skill line lies halfway the diagonal and the climatological Cb line. The dark and grey shading denotes the same percentiles as for the middle figure. For climatology only the 95 percentile grey shading is shown.

Figure 3a – m: Summer results for 26 stations for the updated 2014 version on the 2010 dependent set from page 16 onwards

Figure 4a – m Winter results for 26 stations for the updated 2014 version on the 2010 dependent set from page 29 onwards

Figure 5 Summer results for 8 stations for the operational algorithm applied to the 2013 independent set from page 42 onwards

Figure 6 Winter results for 8 stations for the operational algorithm applied to the 2013 independent set from page 46 onwards

Figure 7 Summer results for 8 stations for the updated 2014 version applied to the 2013 independent set from page 50 onwards

Figure 8 Winter results for 8 stations for the updated 2014 version applied to the 2013 independent set from page 54 onwards

The text of this chapter continues on page 58.

Figure 3a. Summer 2010 data set. The probability equation is derived on the dependent 2010 data set . The caption is given above.

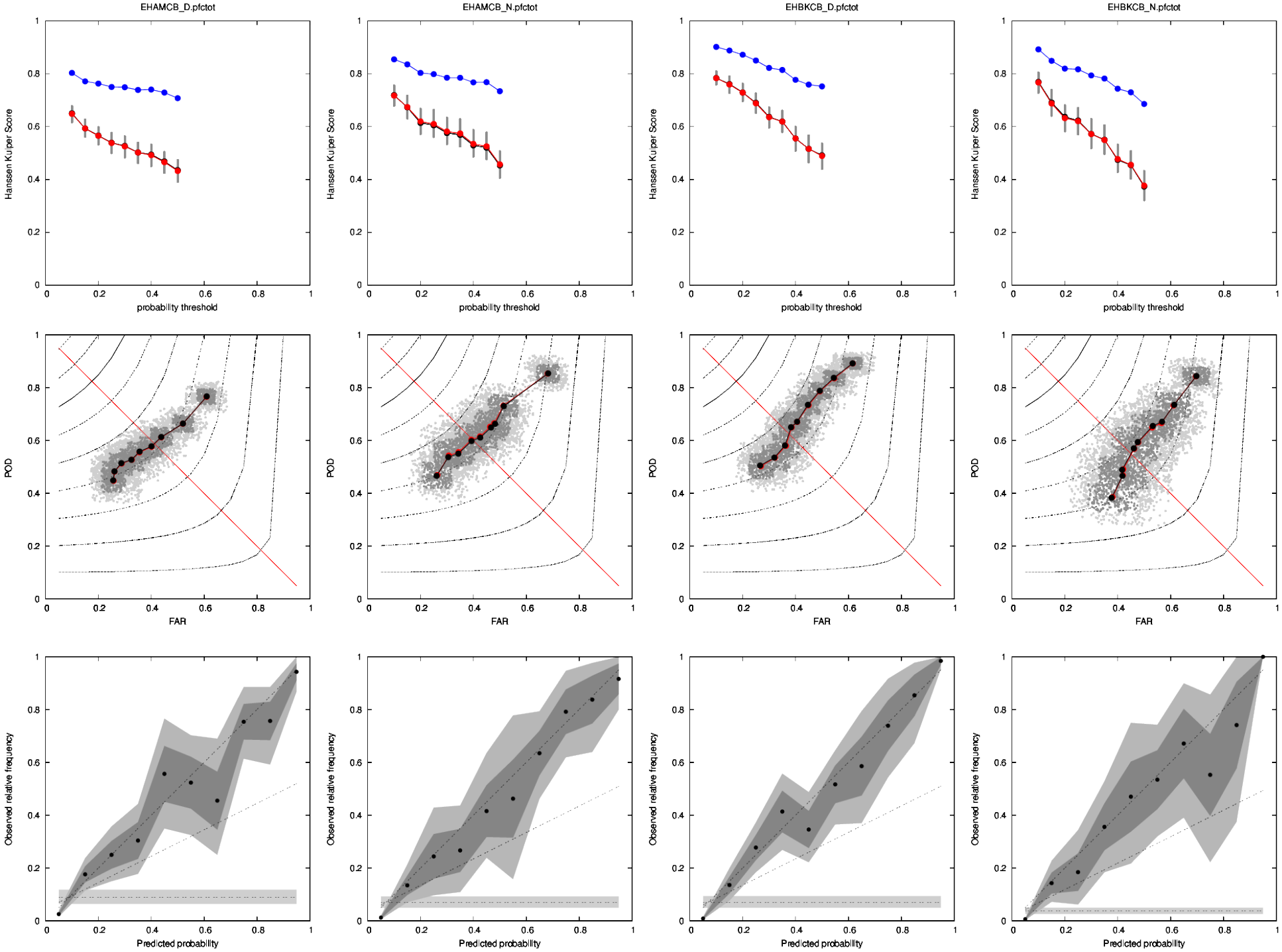

Figure 3b. Summer 2010 data set. The probability equation is derived on the dependent 2010 data set . The caption is given above.

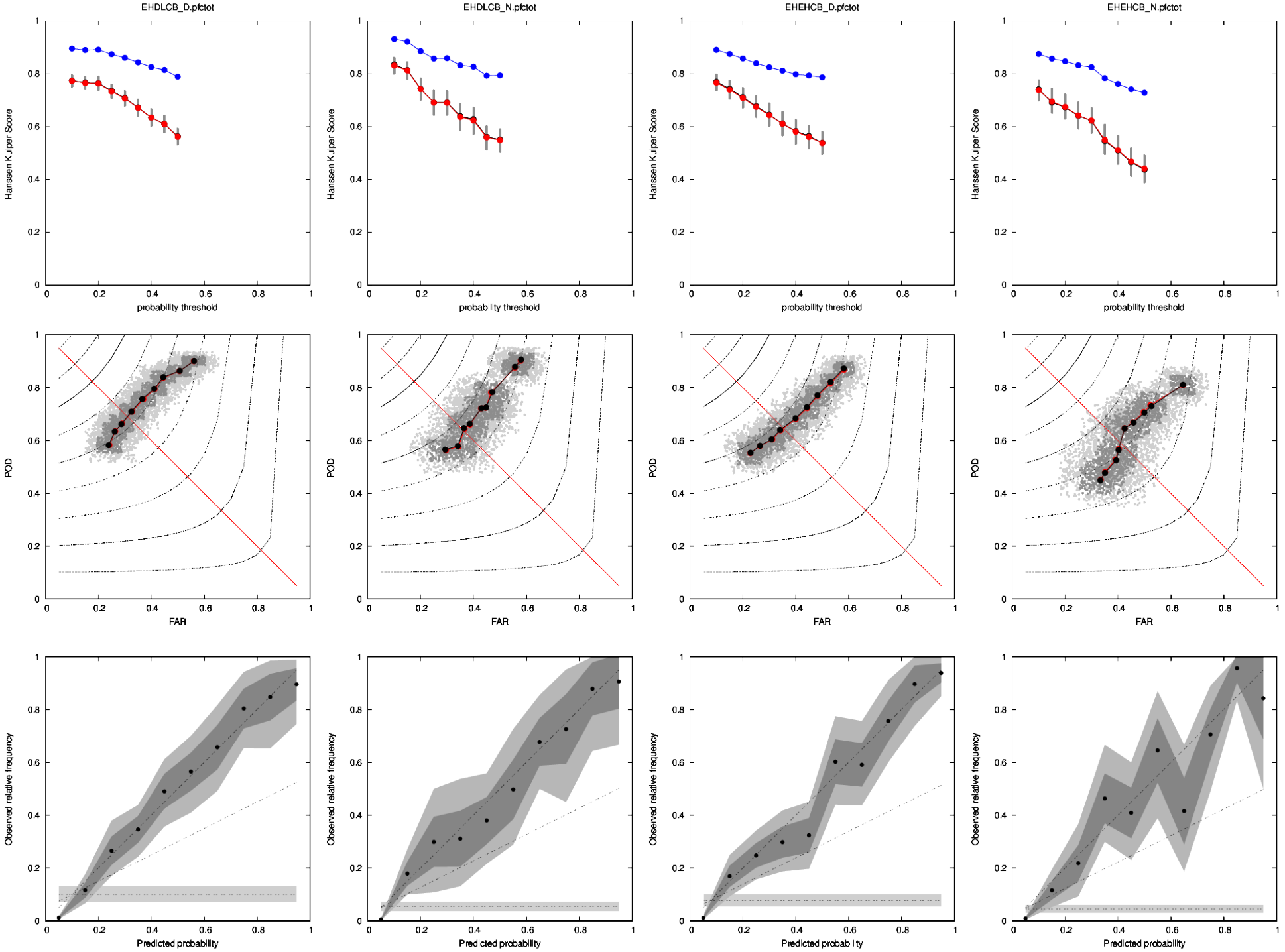

Figure 3c. Summer 2010 data set. The probability equation is derived on the dependent 2010 data set . The caption is given above.

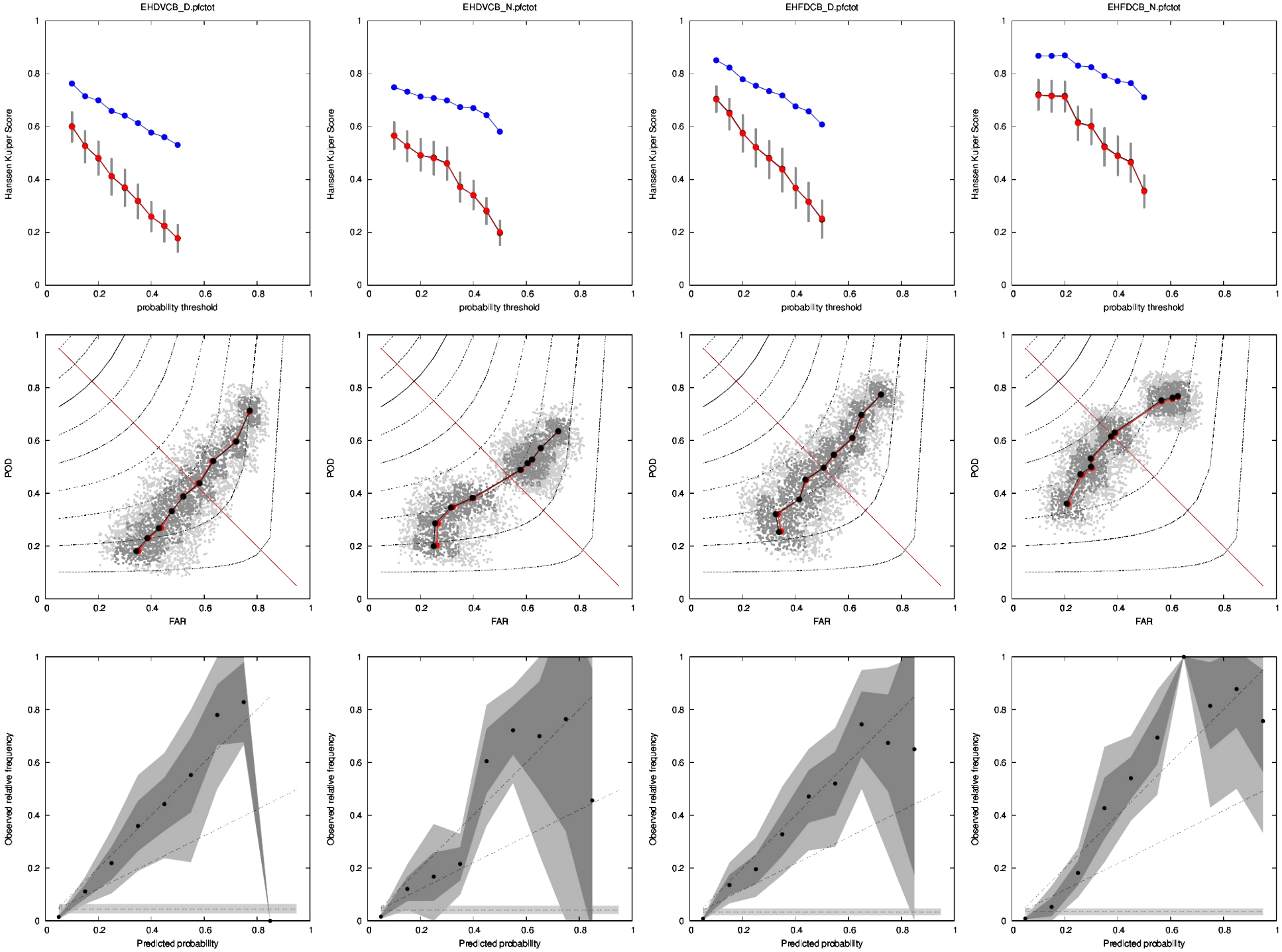

Figure 3d. Summer 2010 data set. The probability equation is derived on the dependent 2010 data set . The caption is given above.

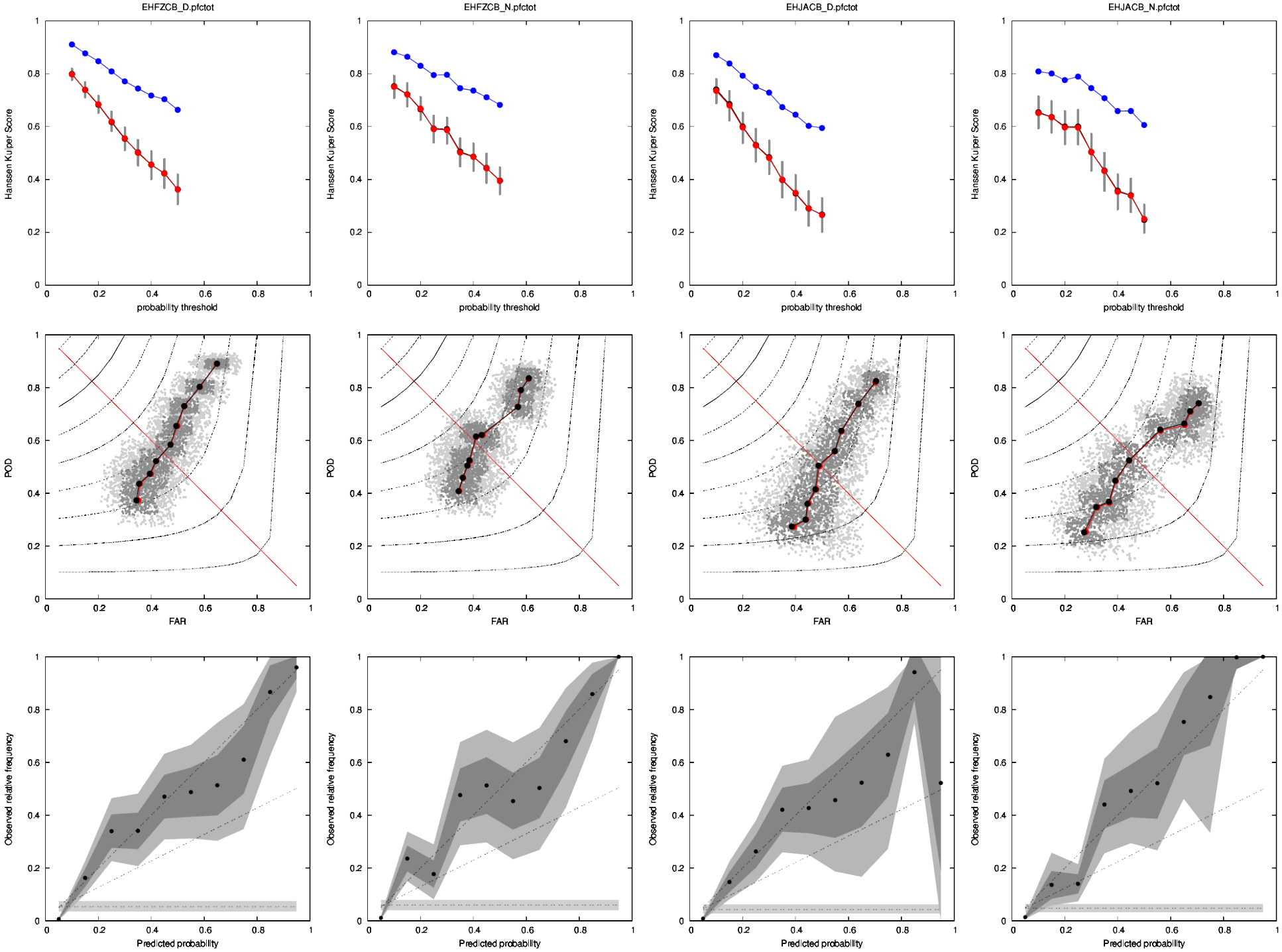

Figure 3e. Summer 2010 data set. The probability equation is derived on the dependent 2010 data set . The caption is given above.

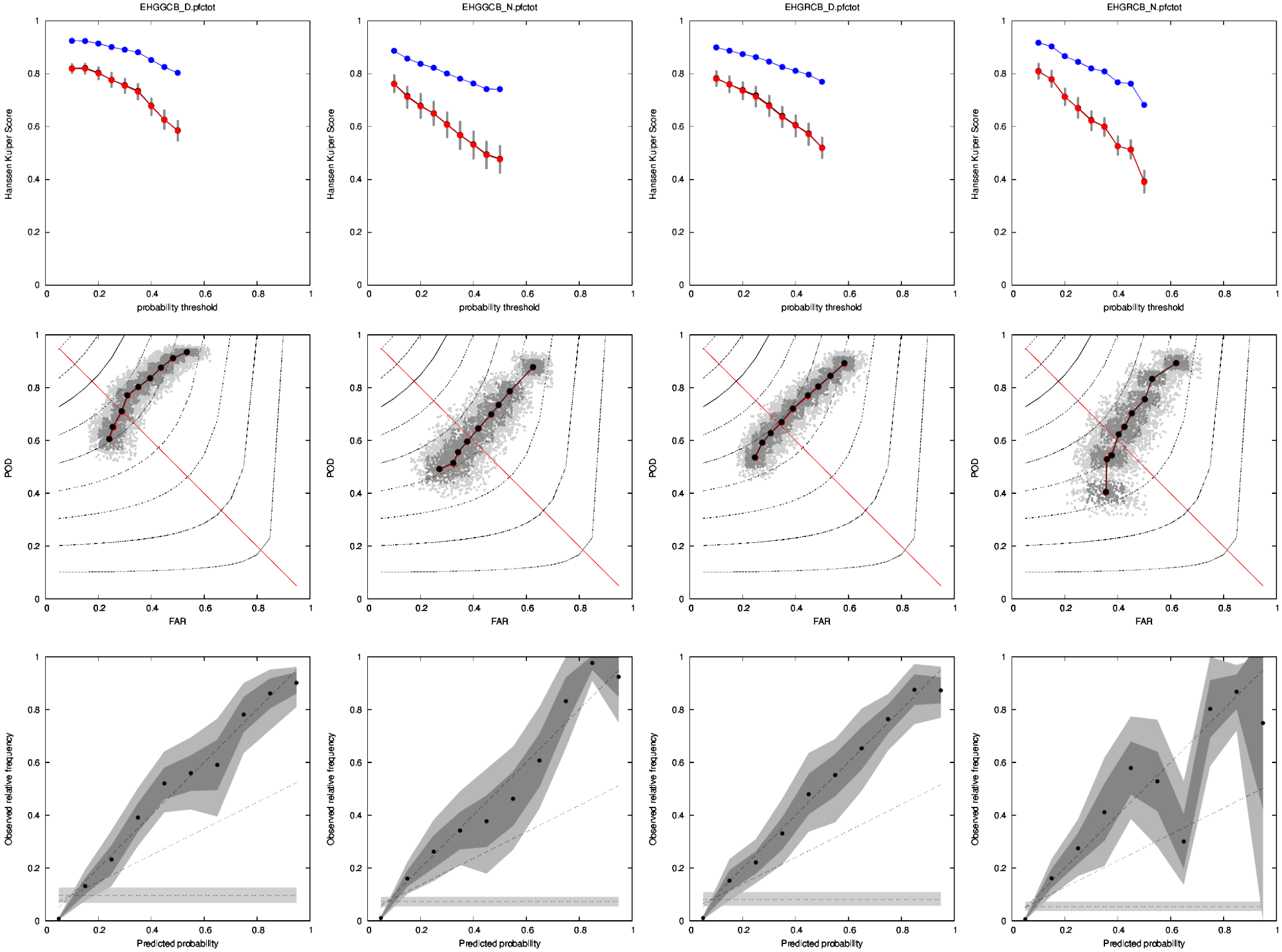

Figure 3f. Summer 2010 data set. The probability equation is derived on the dependent 2010 data set . The caption is given above.

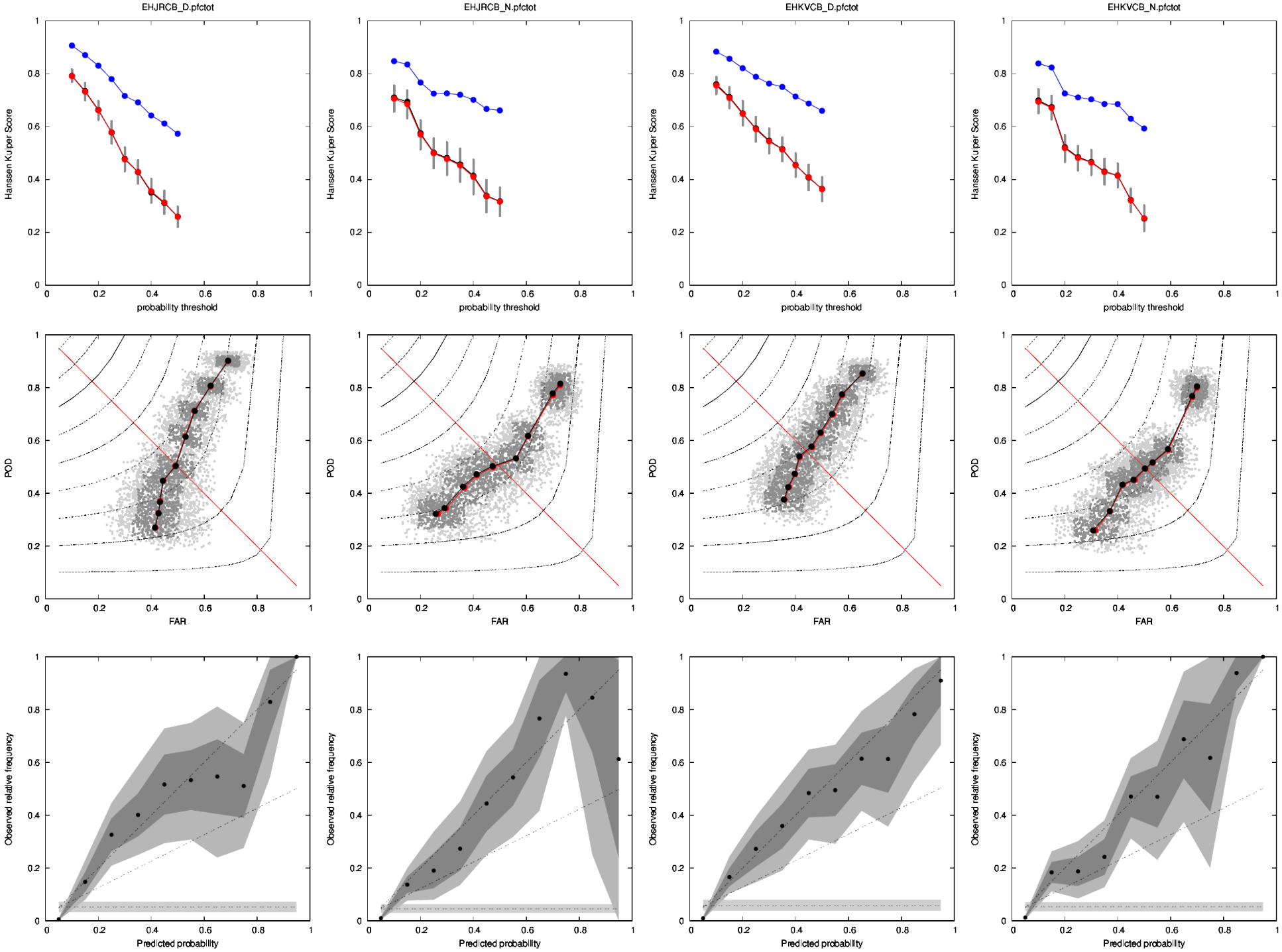

Figure 3g. Summer 2010 data set. The probability equation is derived on the dependent 2010 data set . The caption is given above.

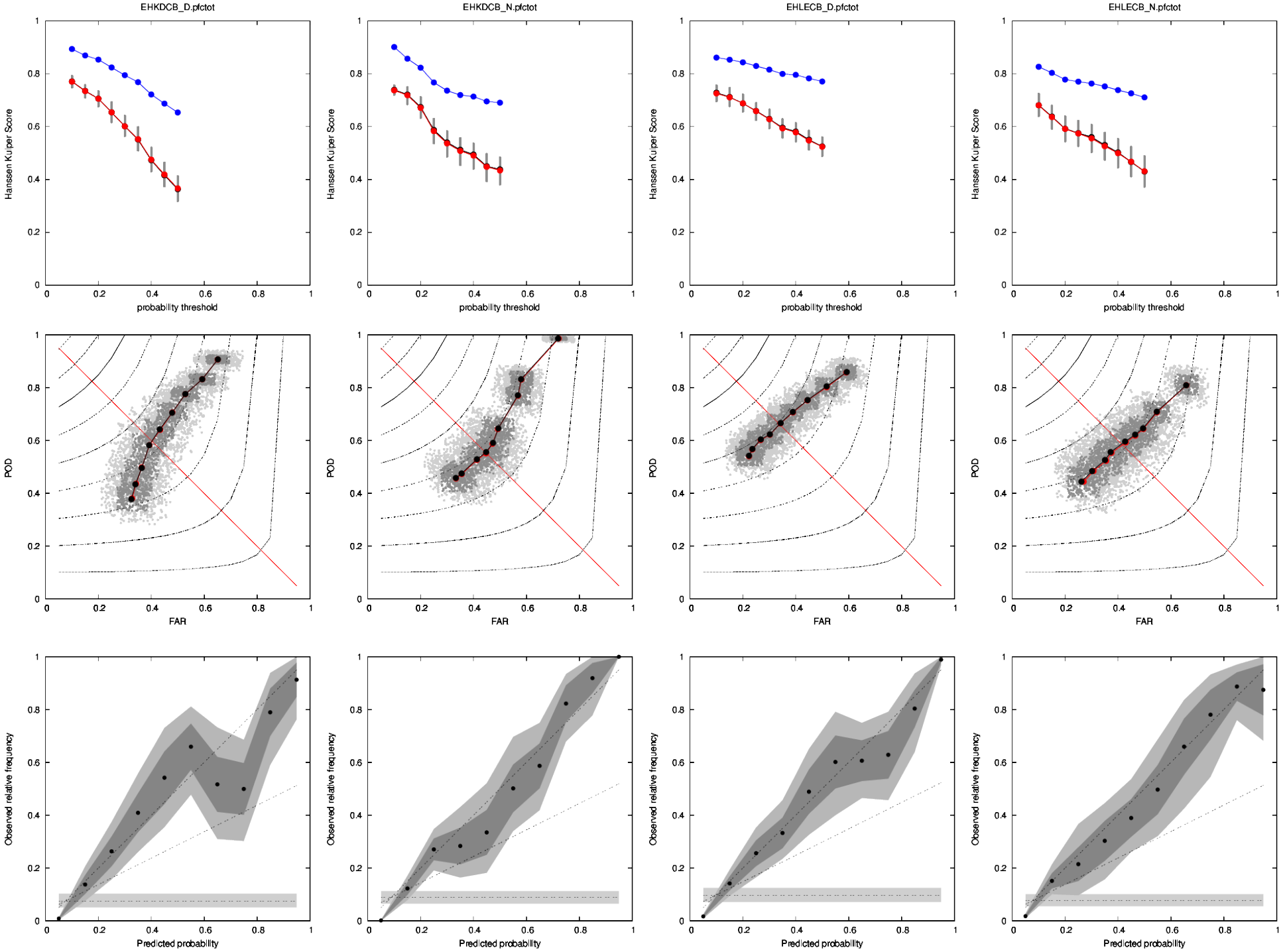

Figure 3h. Summer 2010 data set. The probability equation is derived on the dependent 2010 data set . The caption is given above.

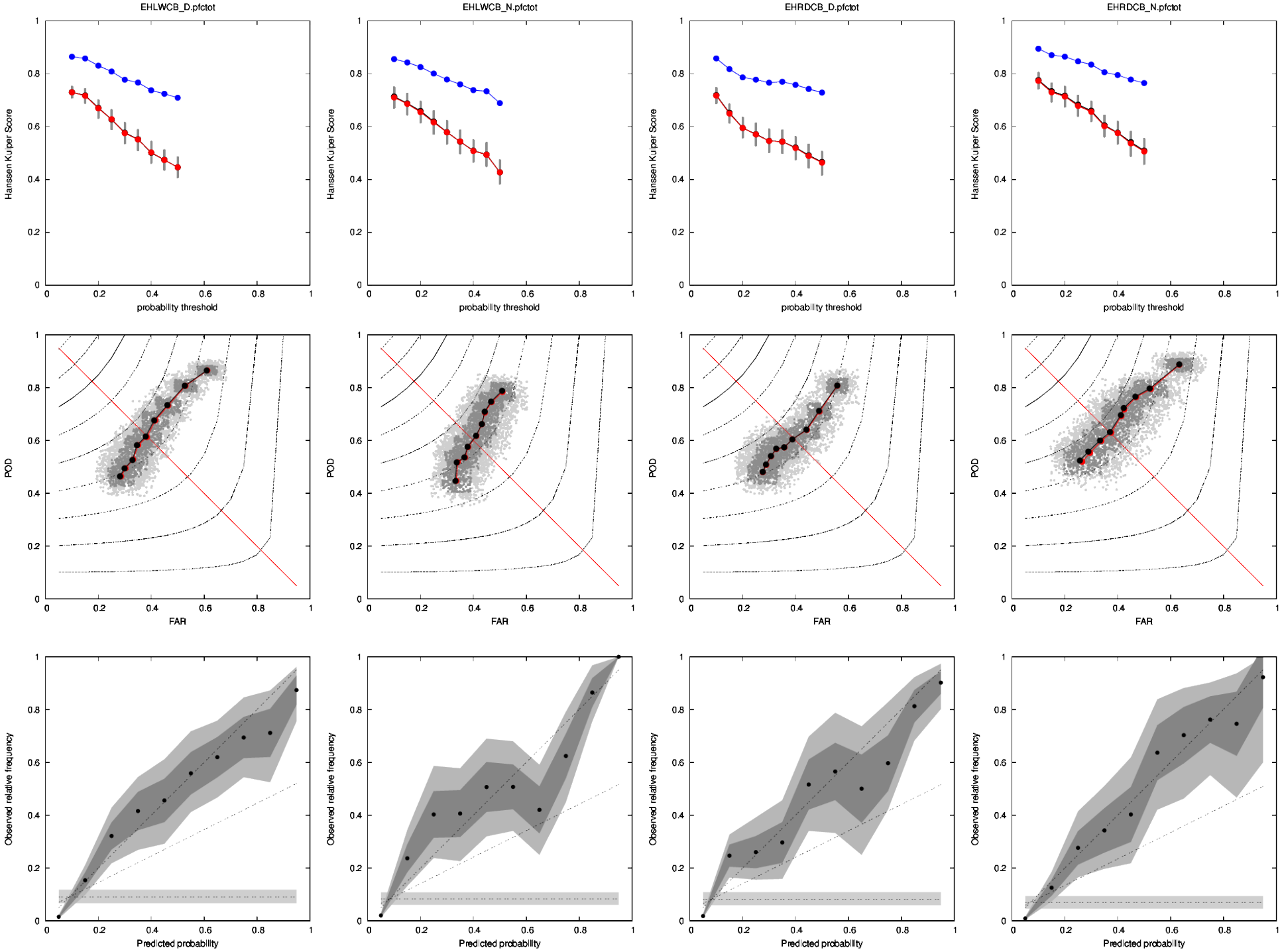

Figure 3i. Summer 2010 data set. The probability equation is derived on the dependent 2010 data set . The caption is given above.

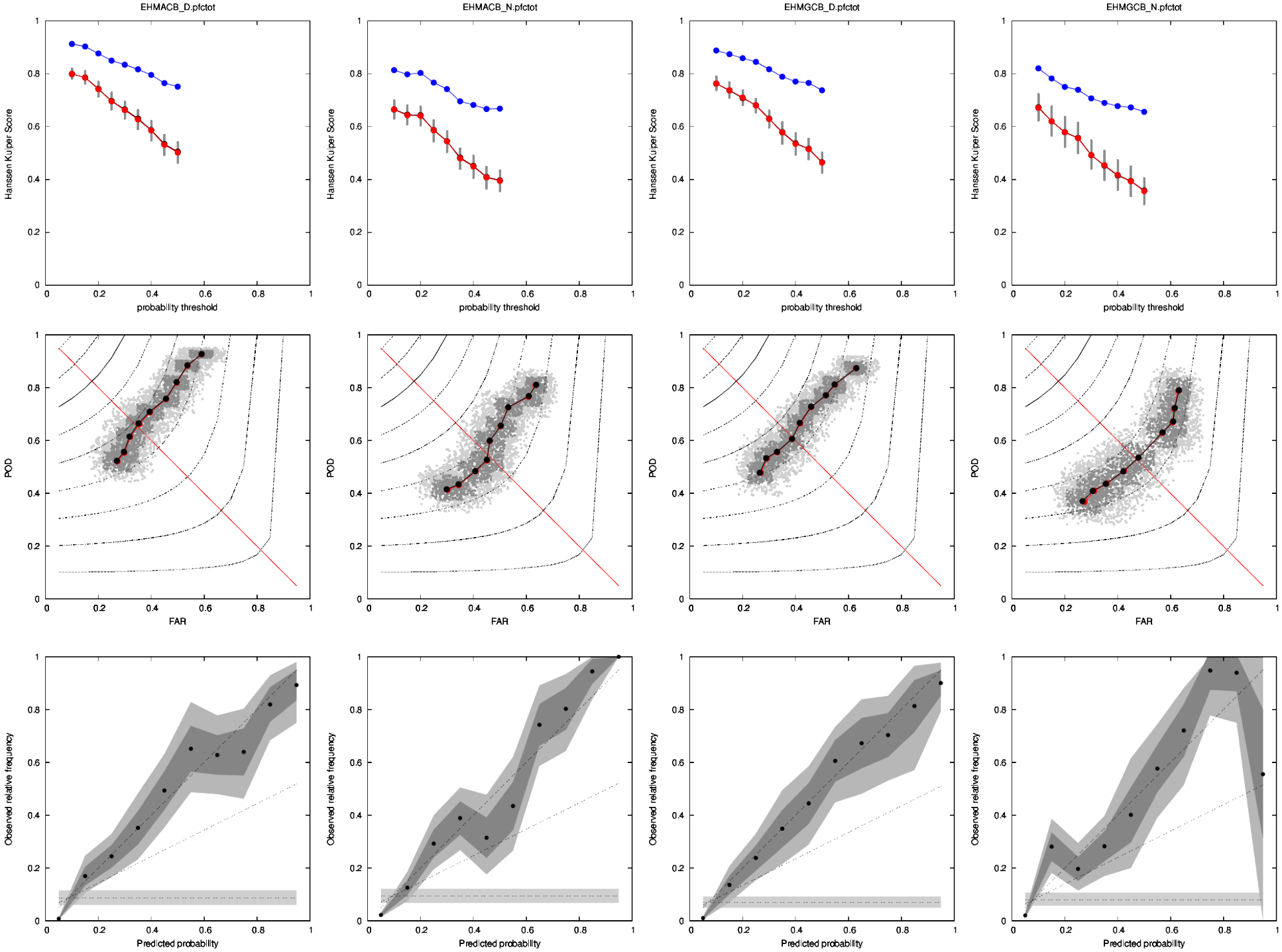

Figure 3j. Summer 2010 data set. The probability equation is derived on the dependent 2010 data set . The caption is given above.

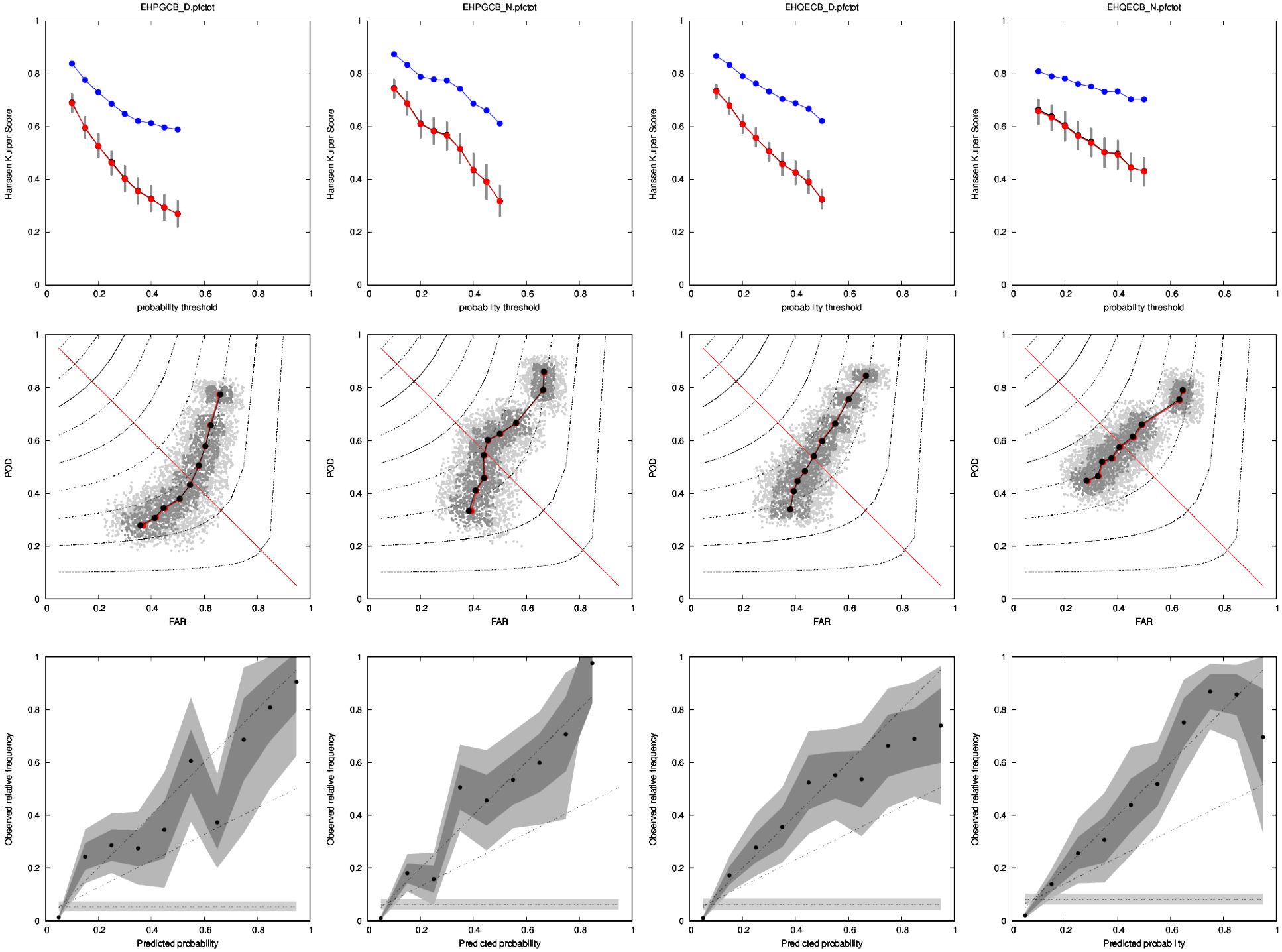

Figure 3k. Summer 2010 data set. The probability equation is derived on the dependent 2010 data set . The caption is given above.

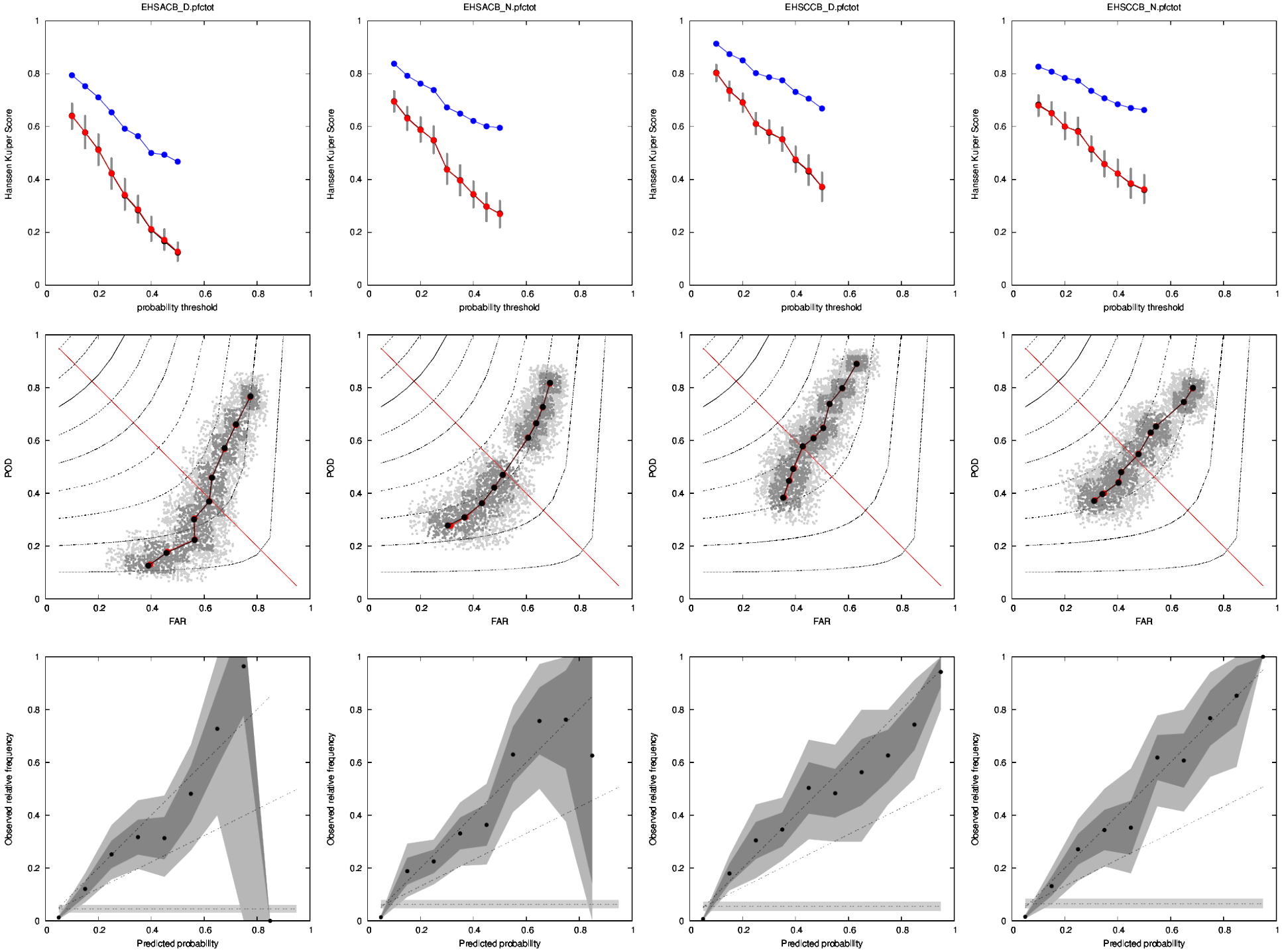

Figure 3l. Summer 2010 data set. The probability equation is derived on the dependent 2010 data set . The caption is given above.

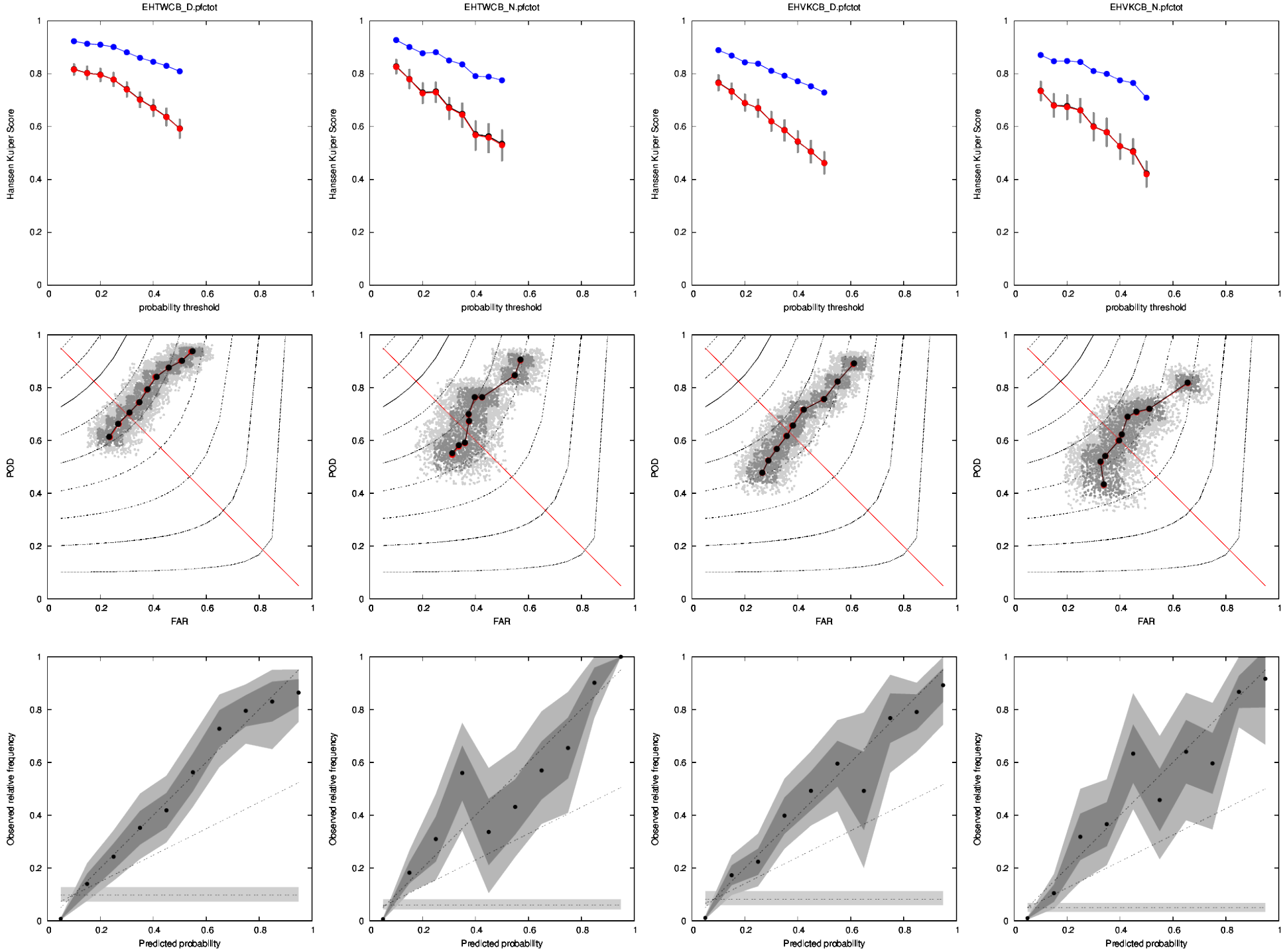

Figure 3m. Summer 2010 data set. The probability equation is derived on the dependent 2010 data set . The caption is given above.

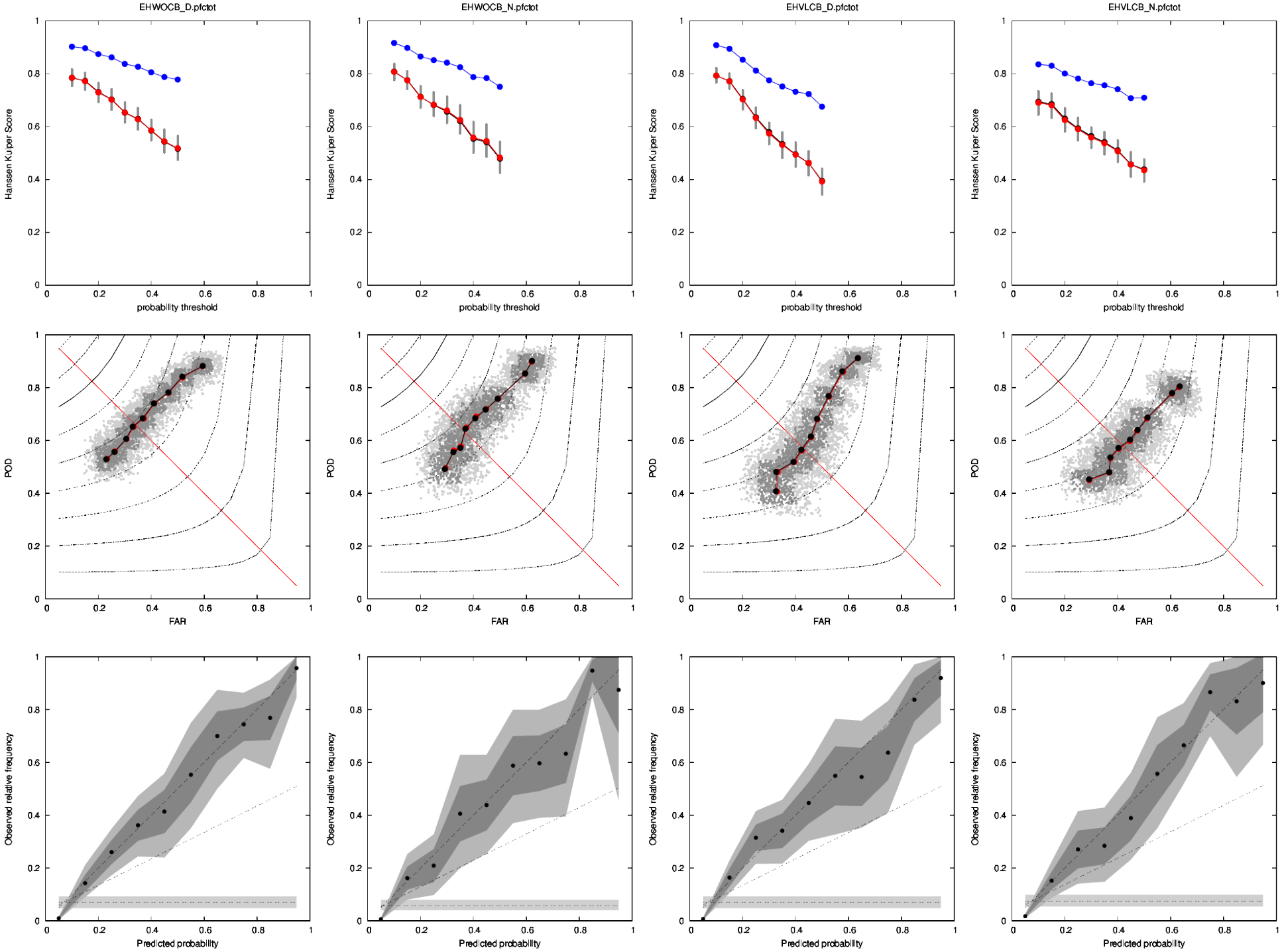

Figure 4a. Winter 2010 data set. The probability equation is derived on the dependent 2010 data set. The caption is given above.

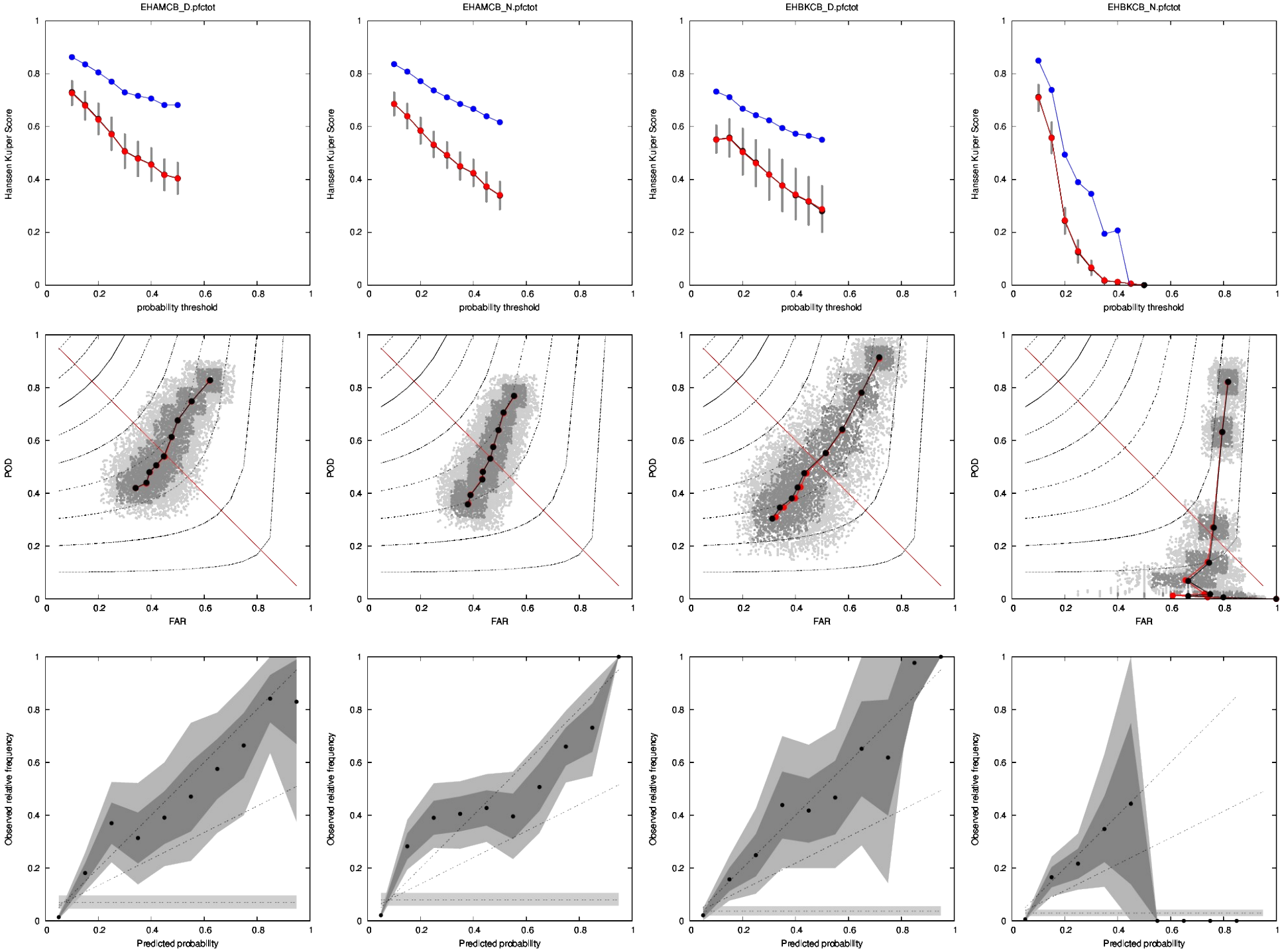

Figure 4b. Winter 2010 data set. The probability equation is derived on the dependent 2010 data set. The caption is given above.

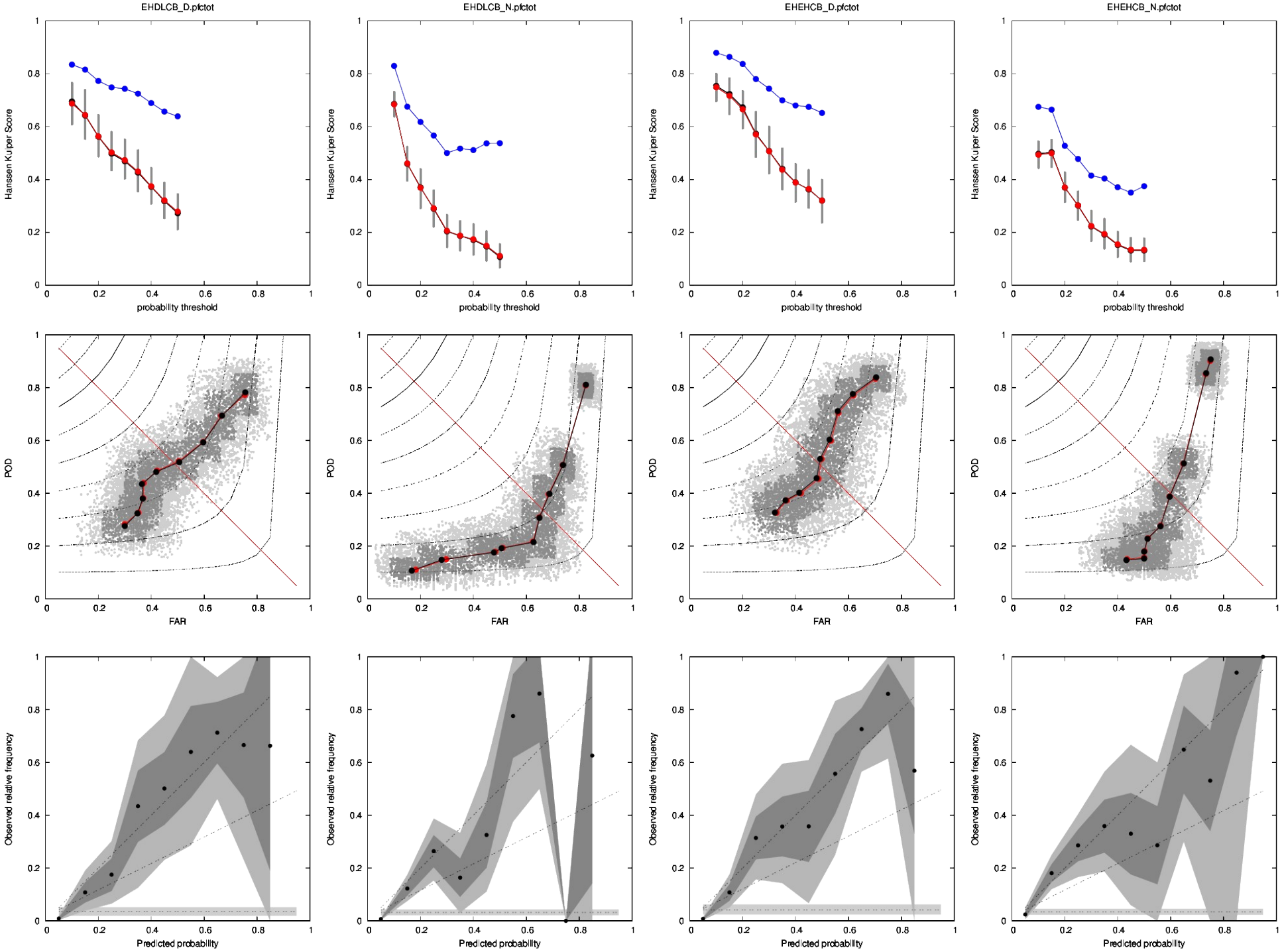

Figure 4c. Winter 2010 data set. The probability equation is derived on the dependent 2010 data set. The caption is given above.

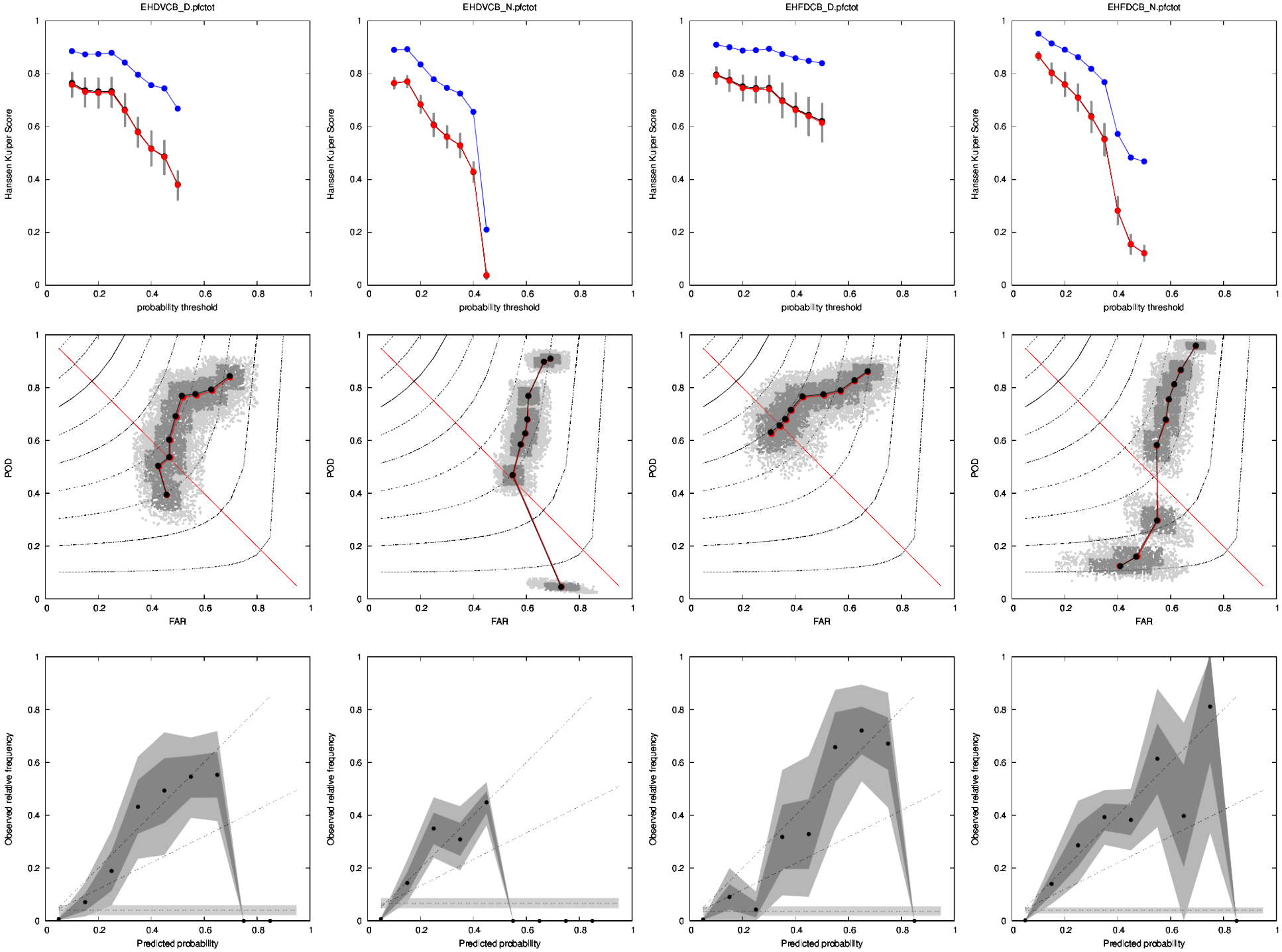

Figure 4d. Winter 2010 data set. The probability equation is derived on the dependent 2010 data set. The caption is given above.

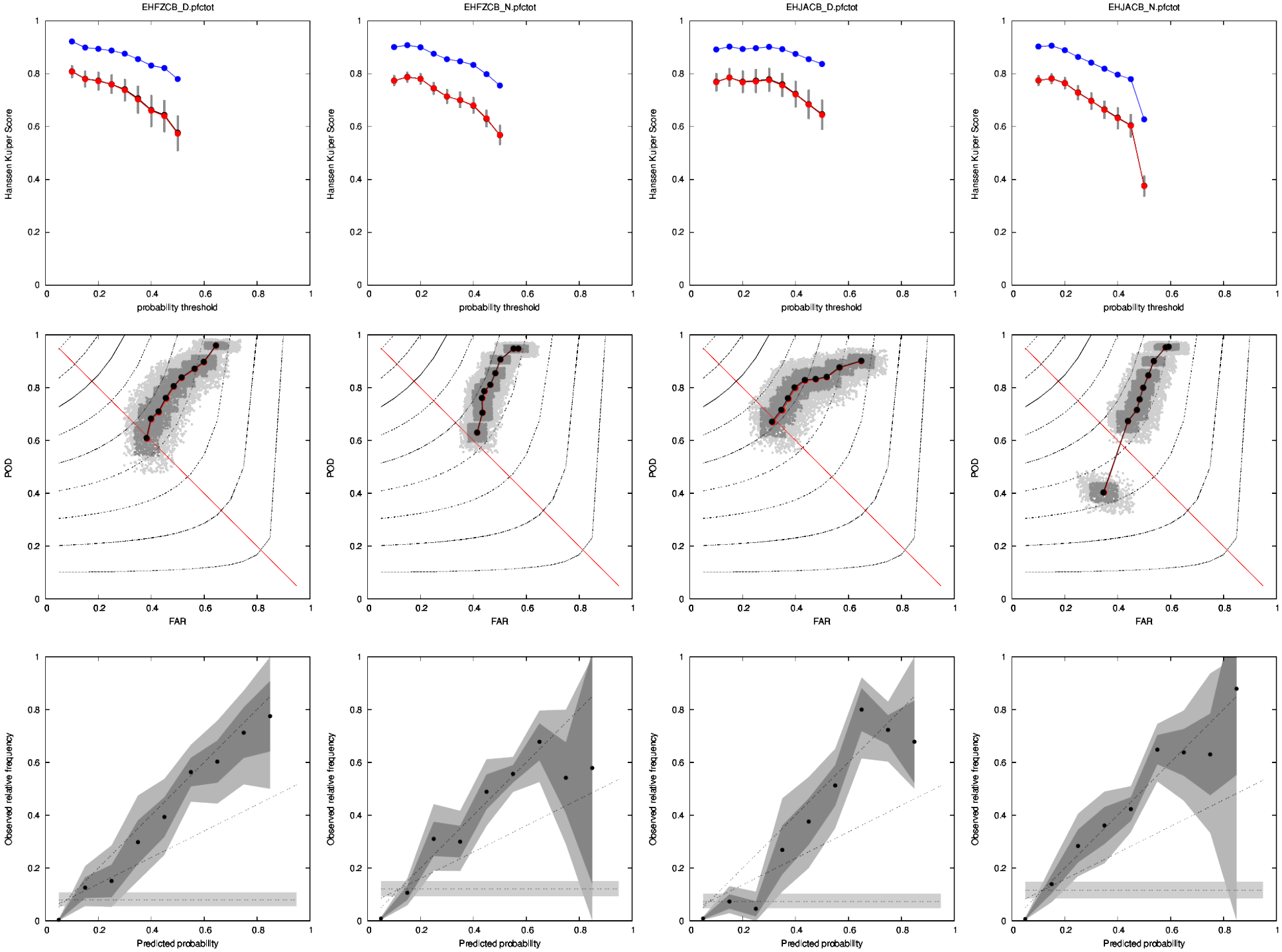

Figure 4e. Winter 2010 data set. The probability equation is derived on the dependent 2010 data set. The caption is given above.

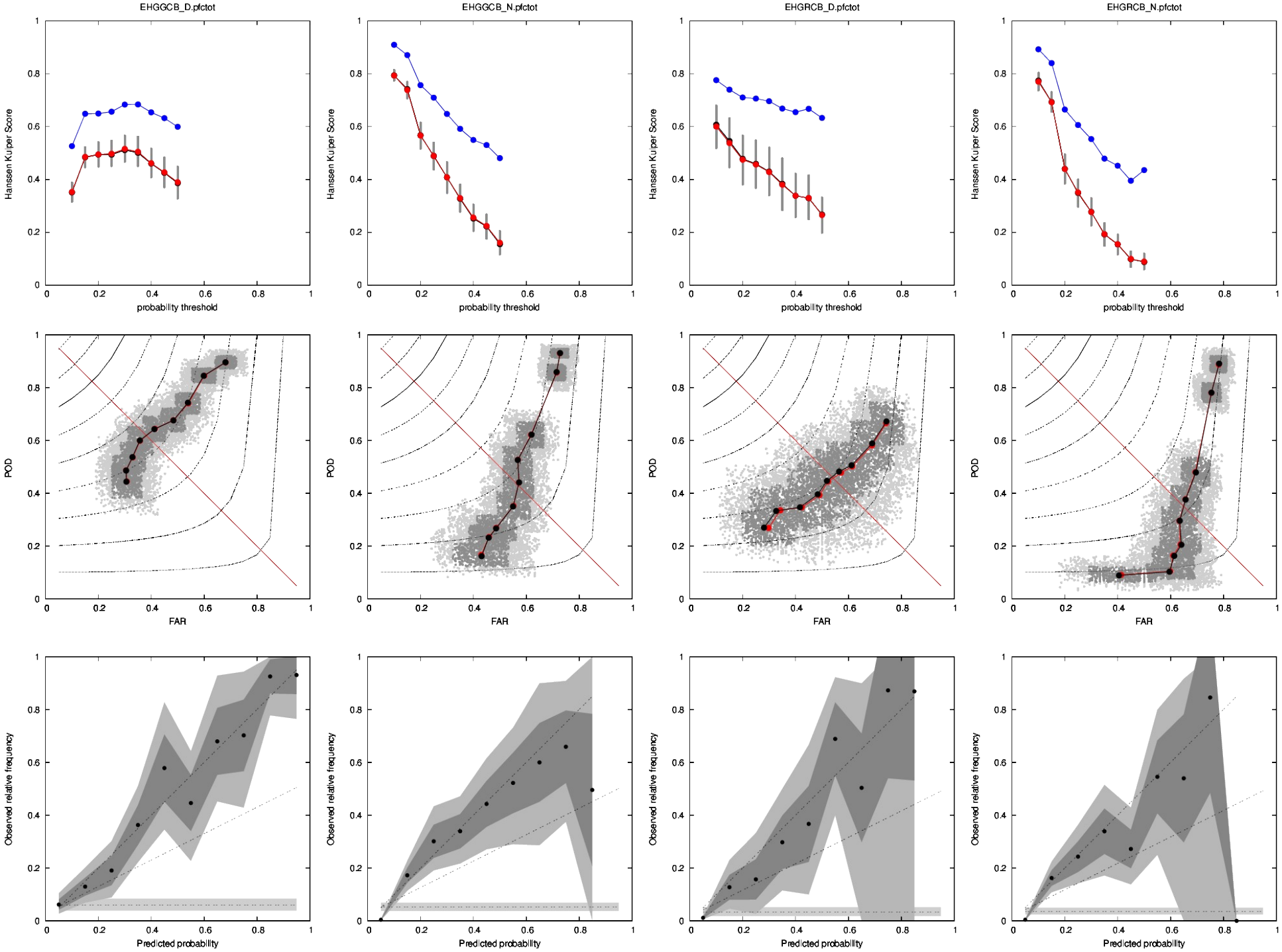

Figure 4f. Winter 2010 data set. The probability equation is derived on the dependent 2010 data set. The caption is given above.

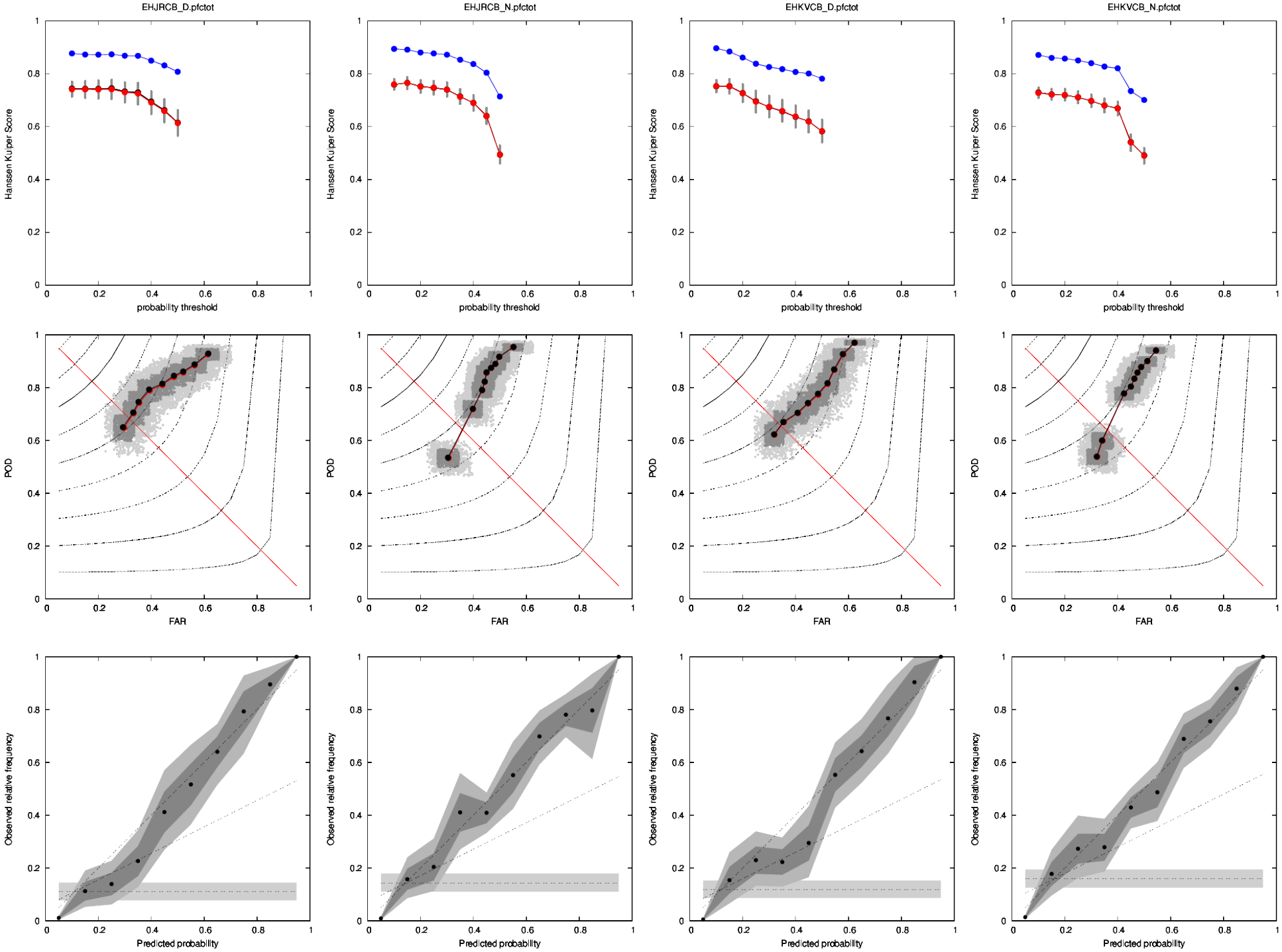

Figure 4g. Winter 2010 data set. The probability equation is derived on the dependent 2010 data set. The caption is given above.

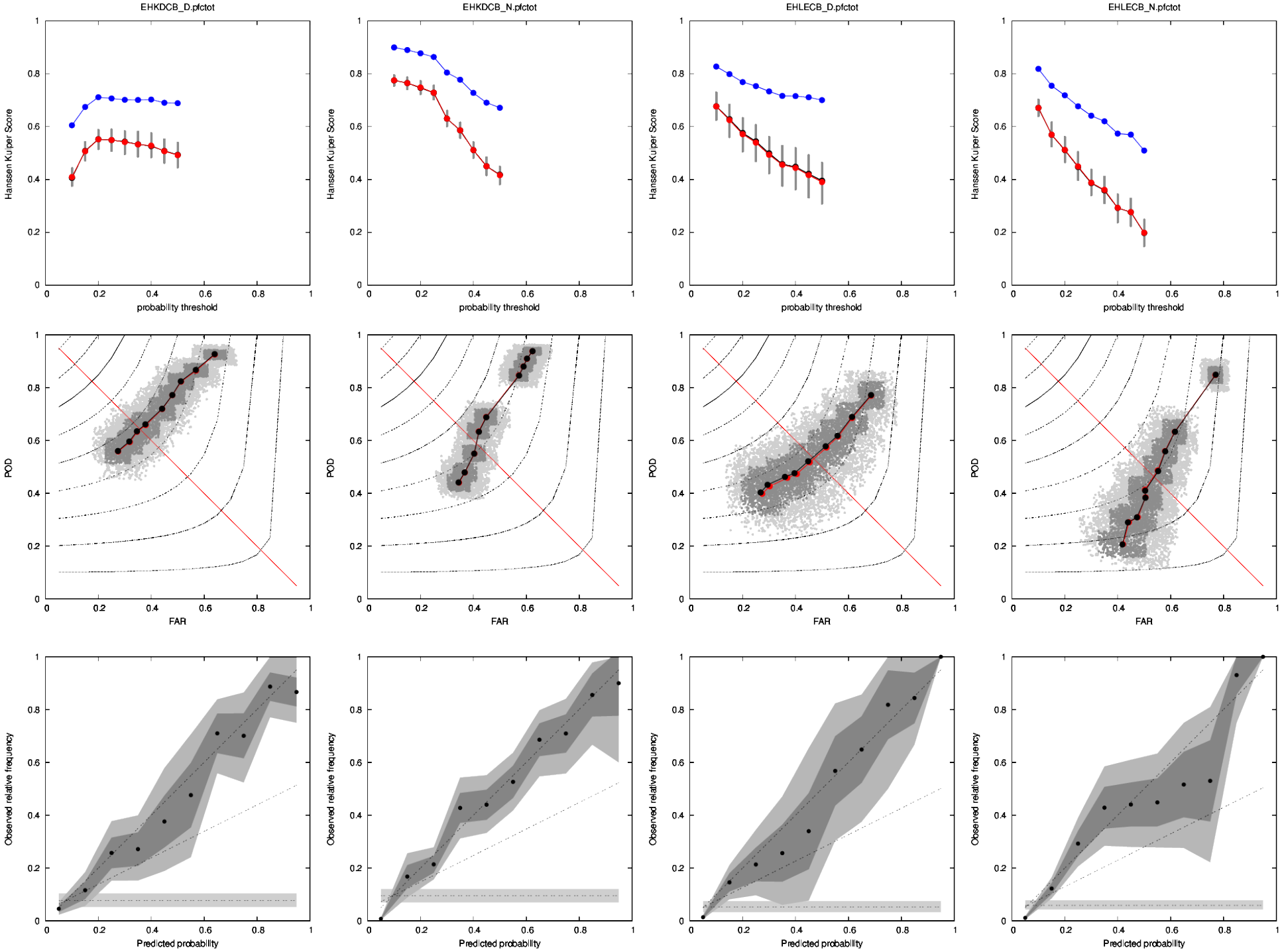

Figure 4h. Winter 2010 data set. The probability equation is derived on the dependent 2010 data set. The caption is given above.

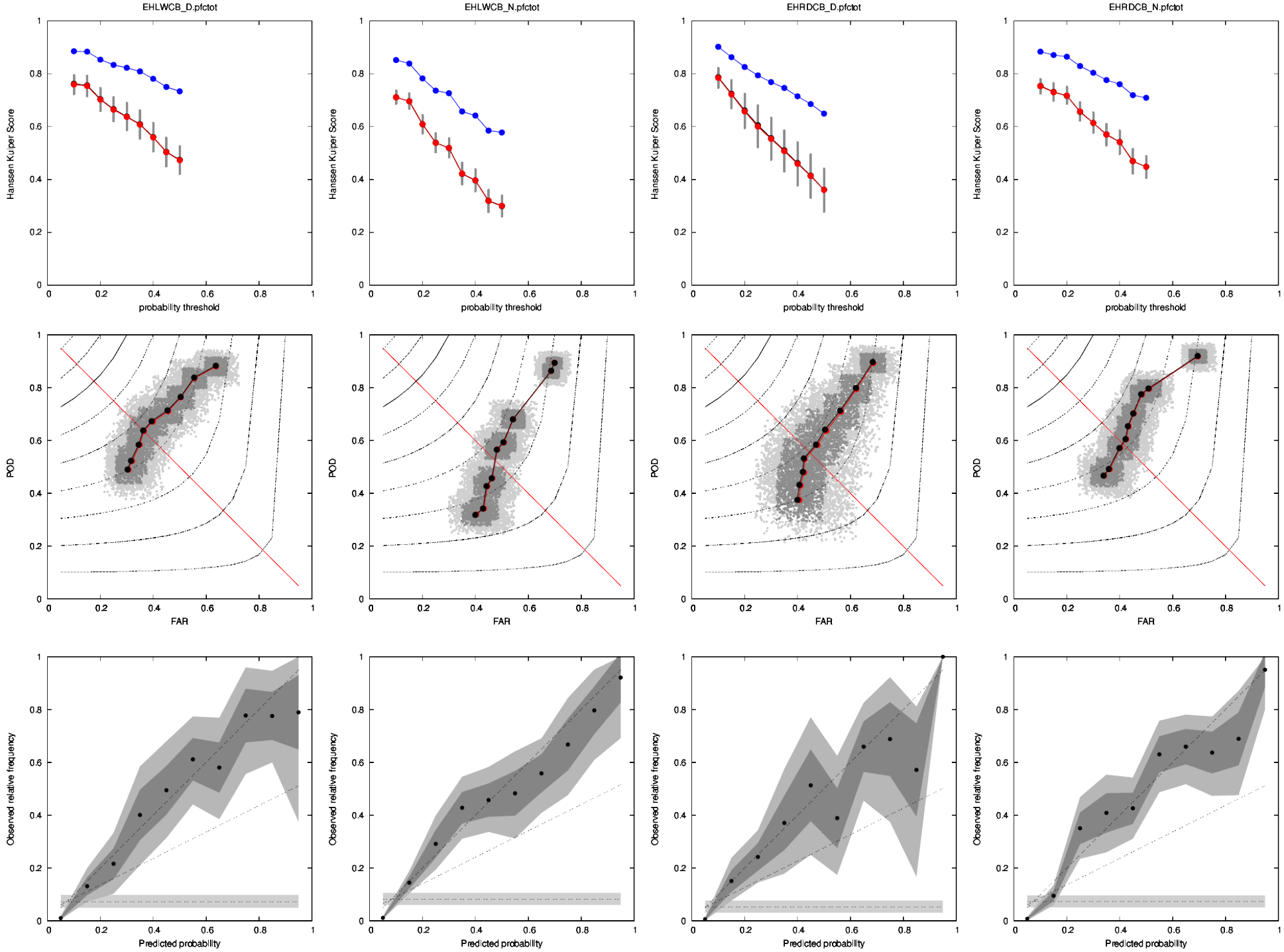

Figure 4i. Winter 2010 data set. The probability equation is derived on the dependent 2010 data set. The caption is given above.

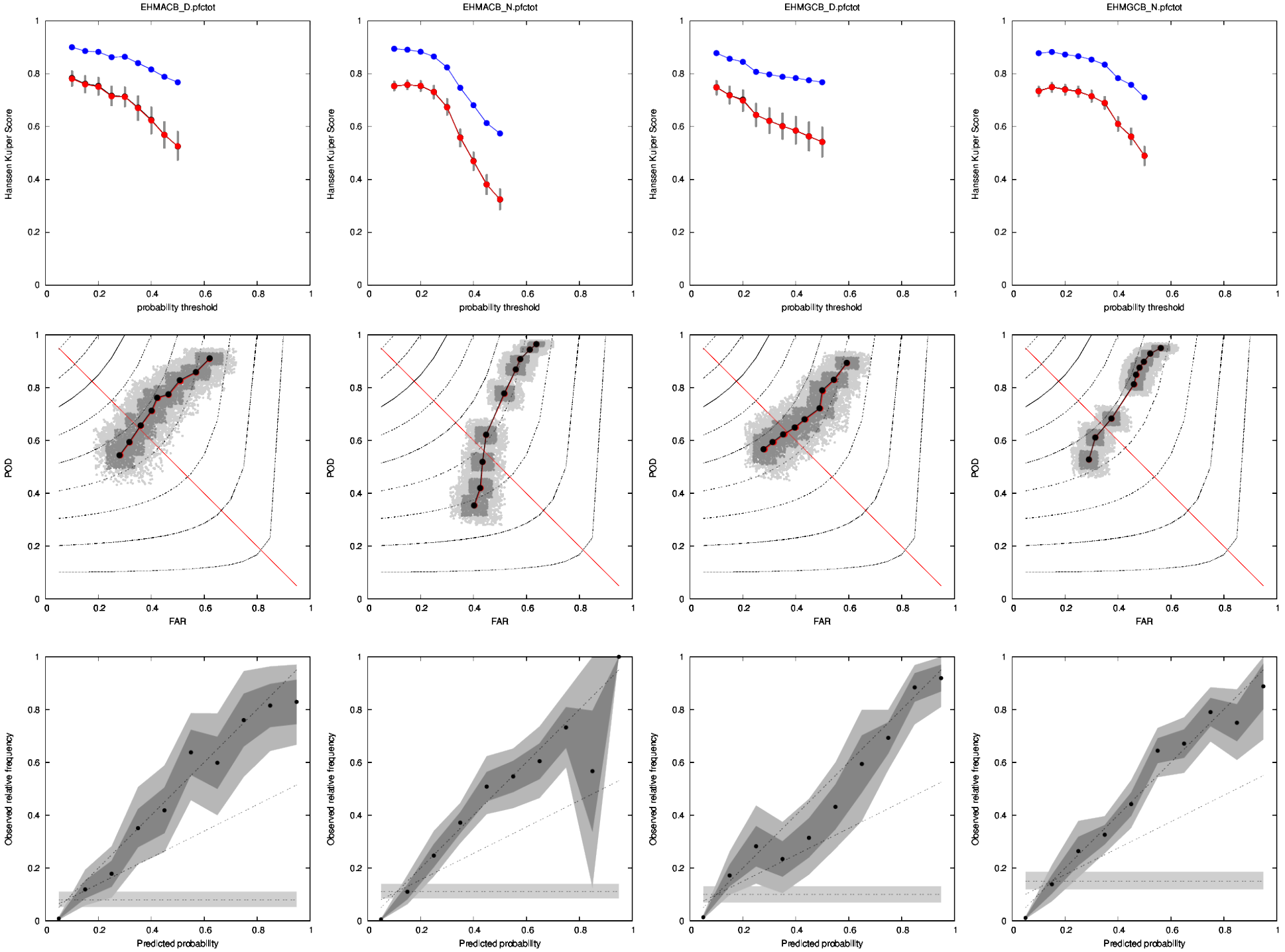

Figure 4j. Winter 2010 data set. The probability equation is derived on the dependent 2010 data set. The caption is given above.

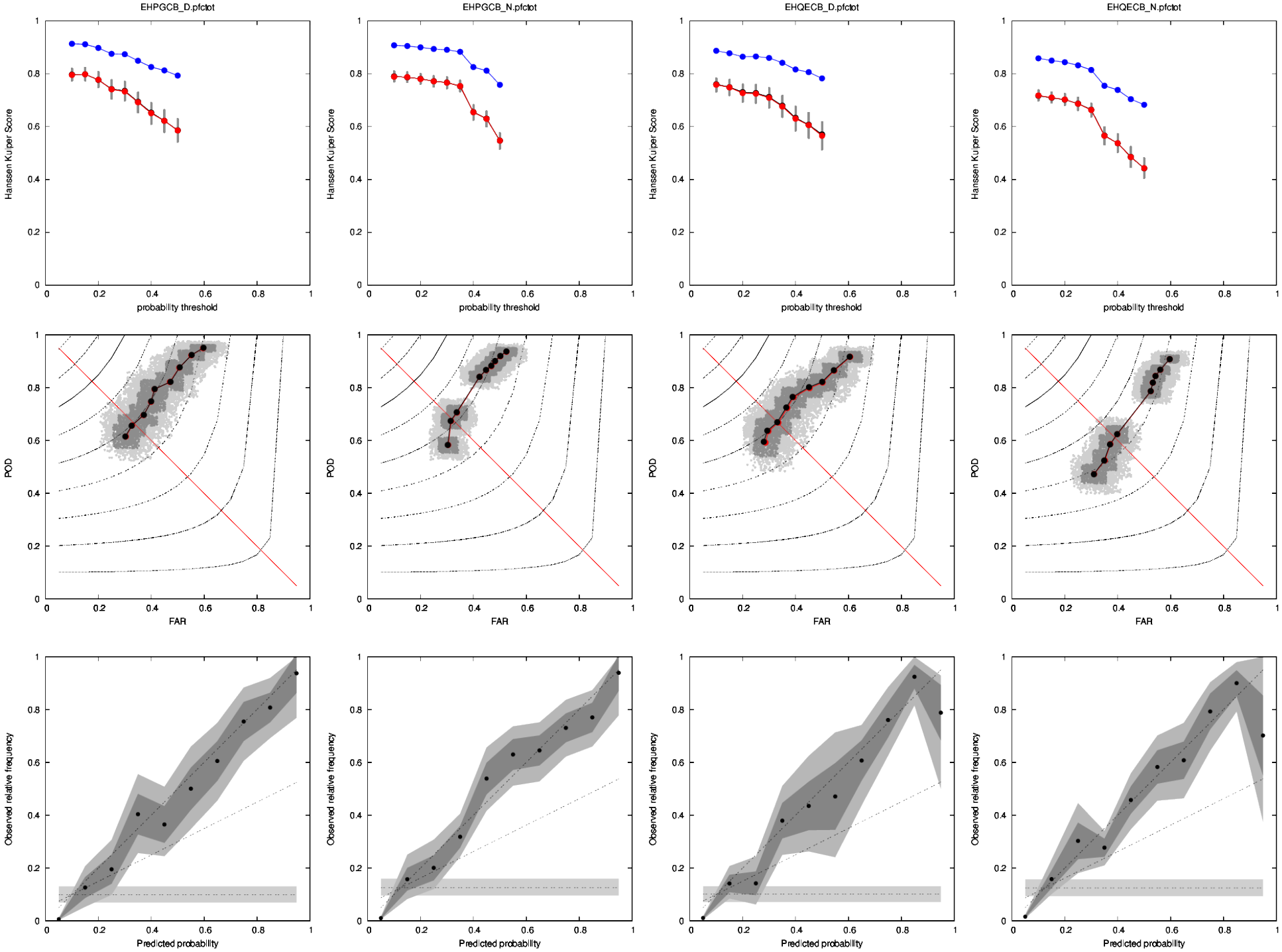

Figure 4k. Winter 2010 data set. The probability equation is derived on the dependent 2010 data set. The caption is given above.

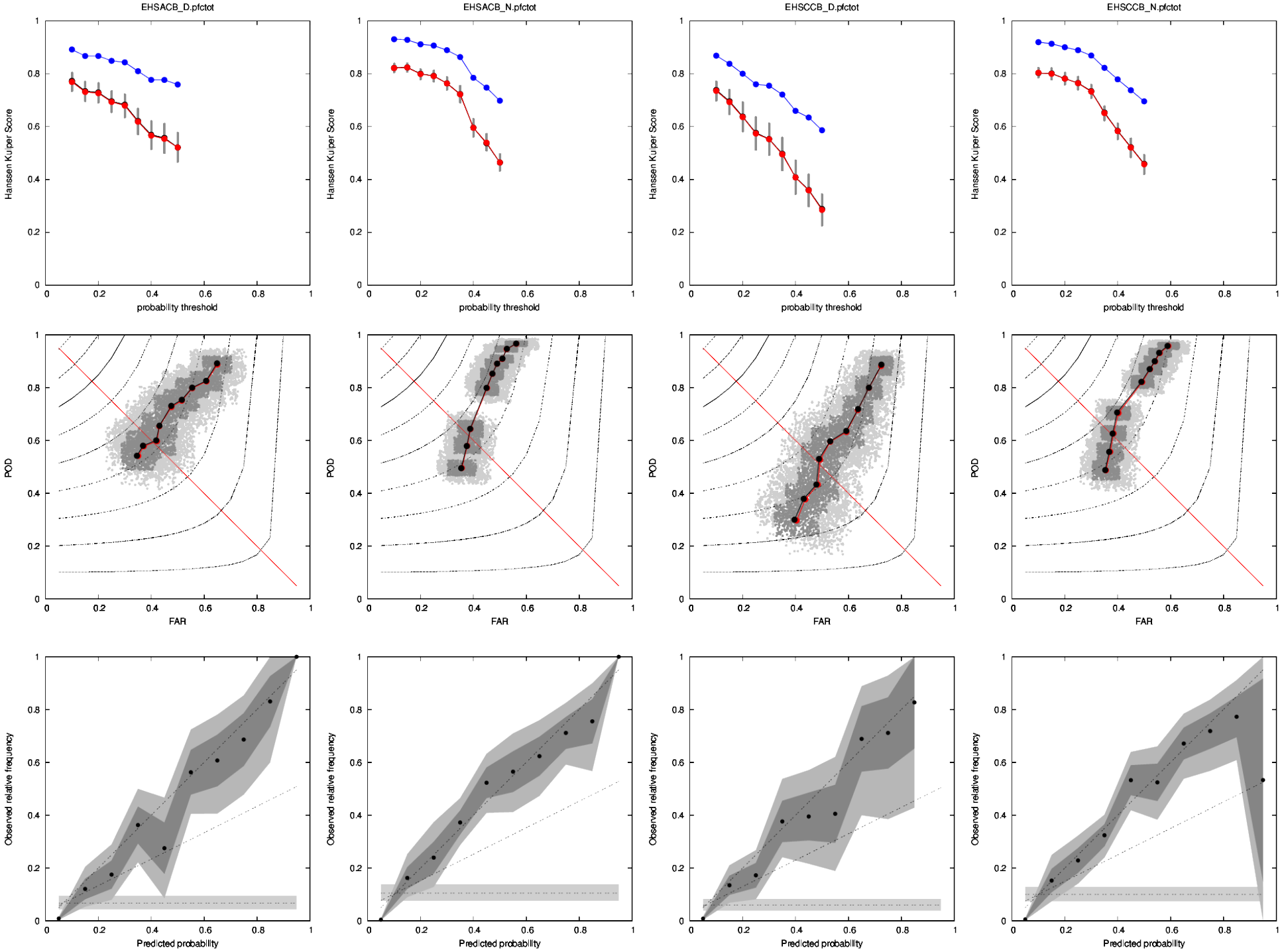

Figure 4l. Winter 2010 data set. The probability equation is derived on the dependent 2010 data set. The caption is given above.

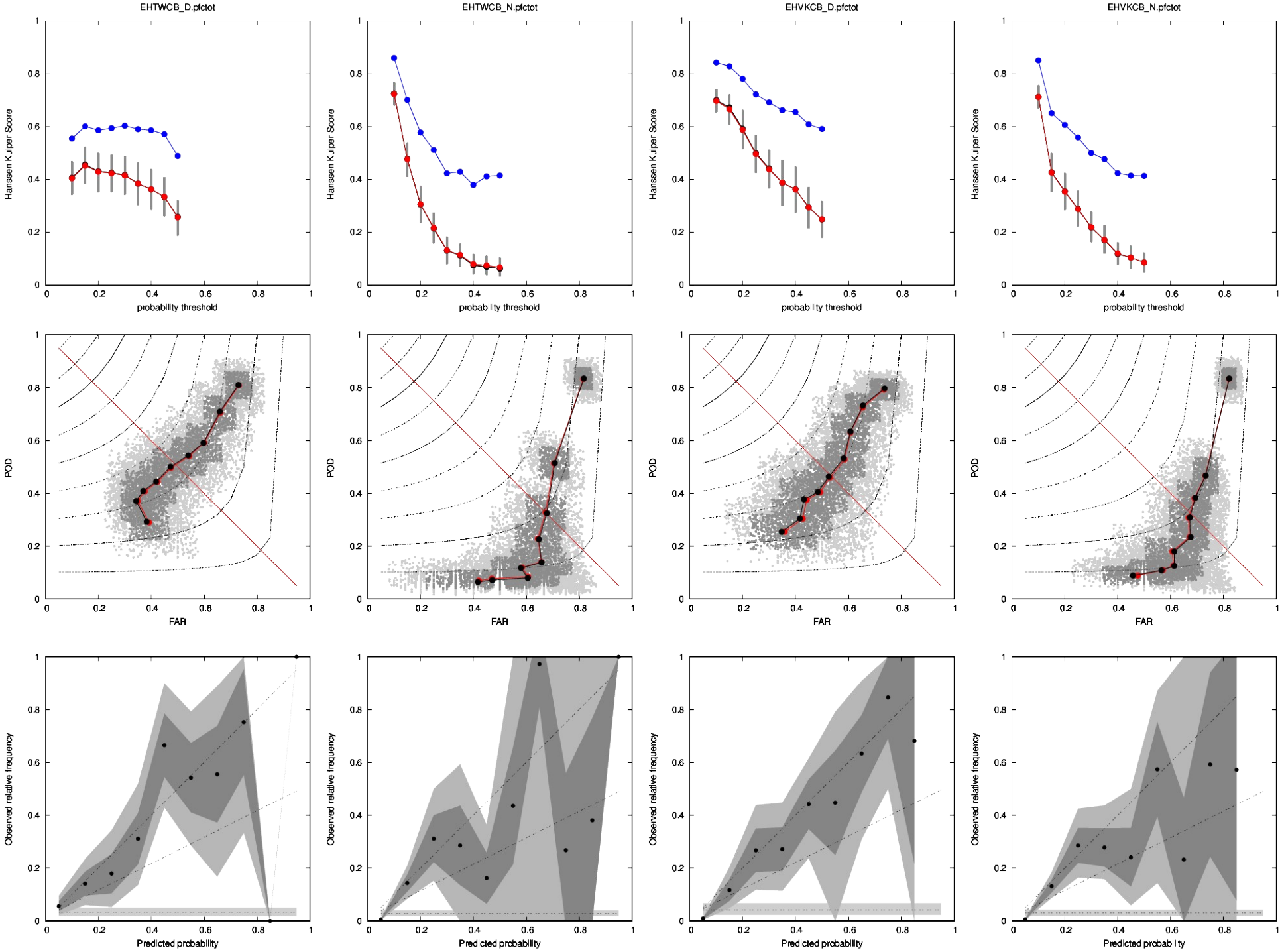

Figure 4m. Winter 2010 data set. The probability equation is derived on the dependent 2010 data set. The caption is given above.

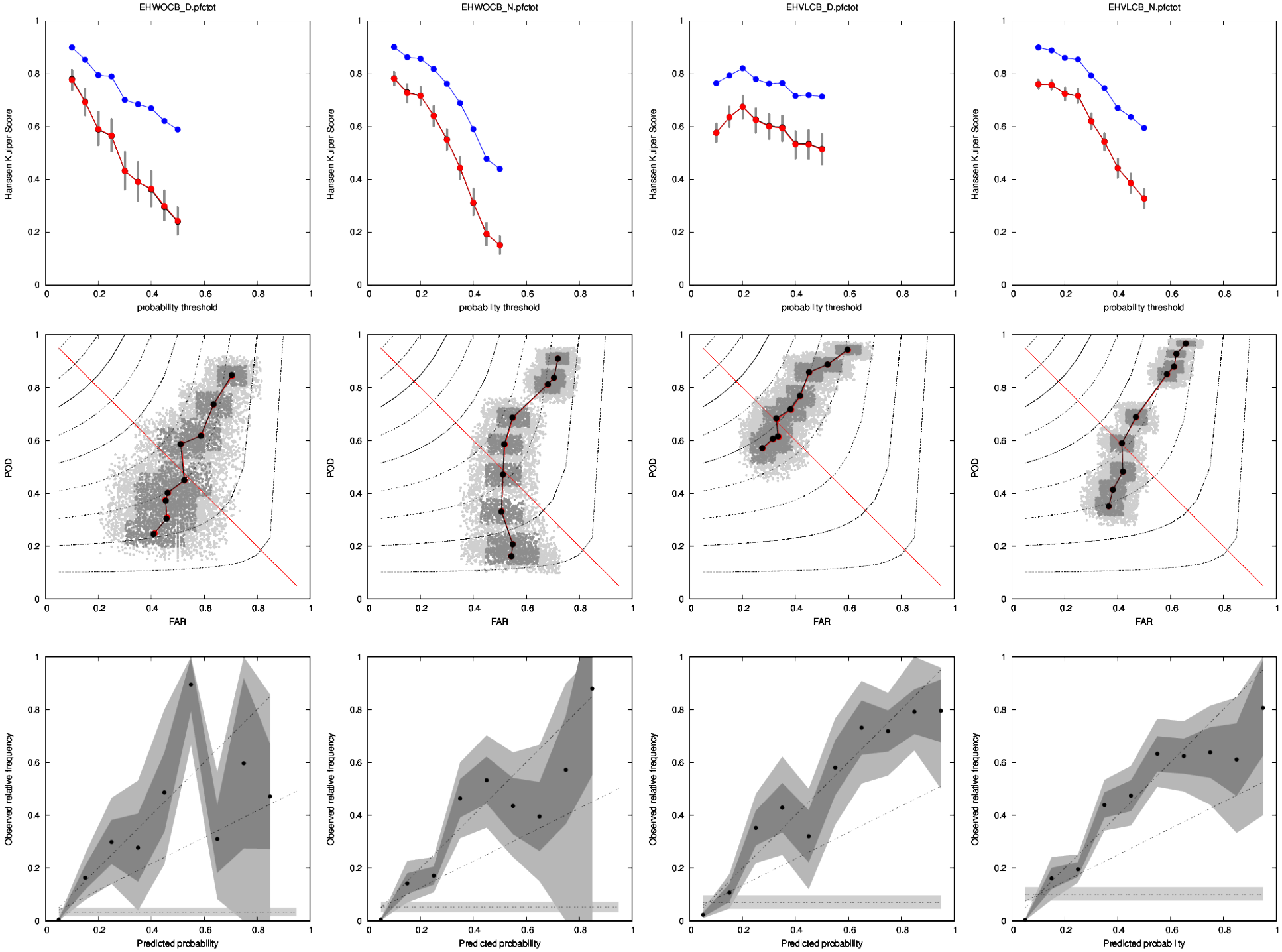

Figure 5a. The probability equation of the operational algorithm applied to the Summer 2013 data set. Caption as above, note the blue dot

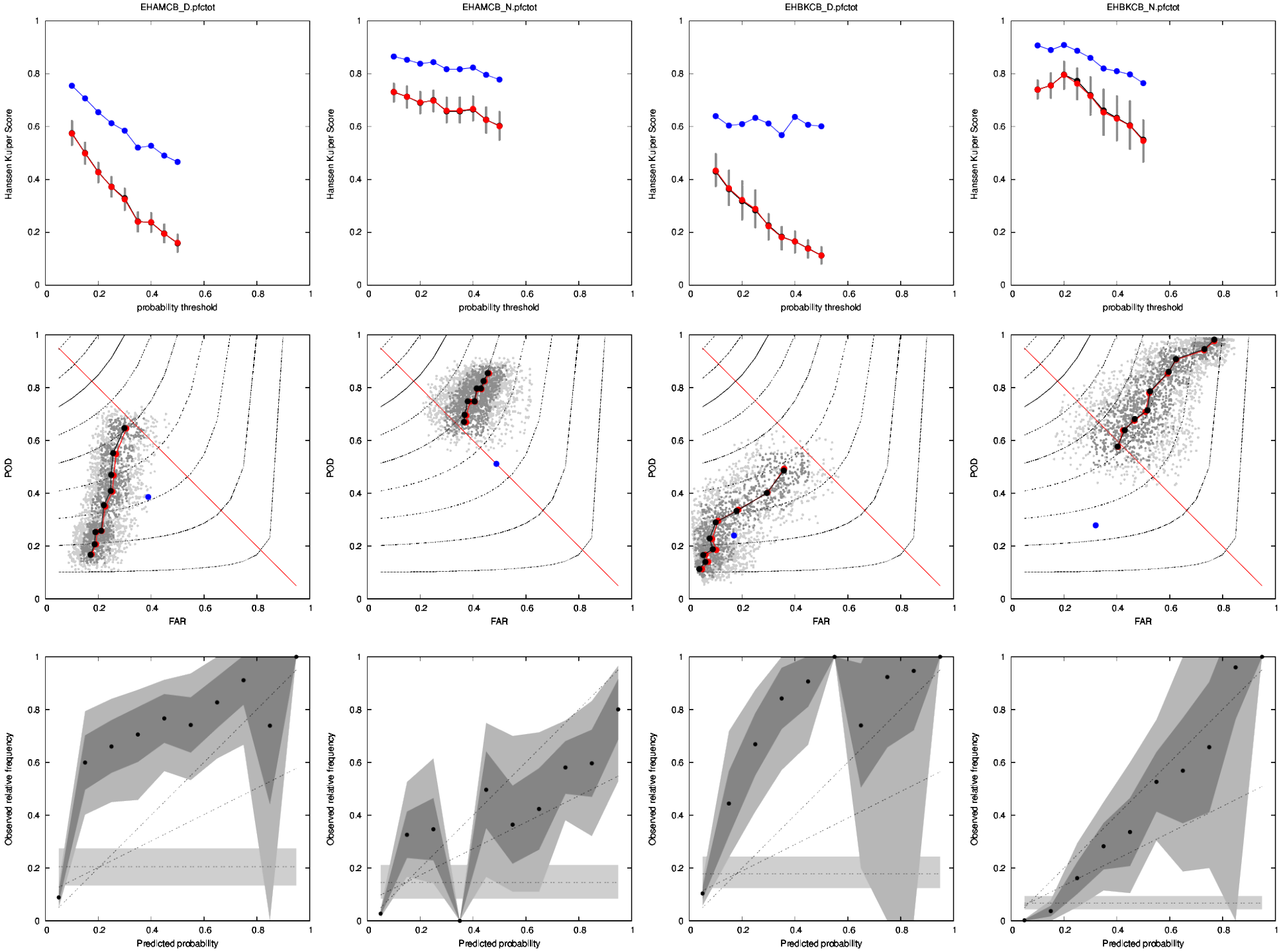

Figure 5b. The probability equation of the operational algorithm applied to the Summer 2013 data set. Caption as above, note the blue dot

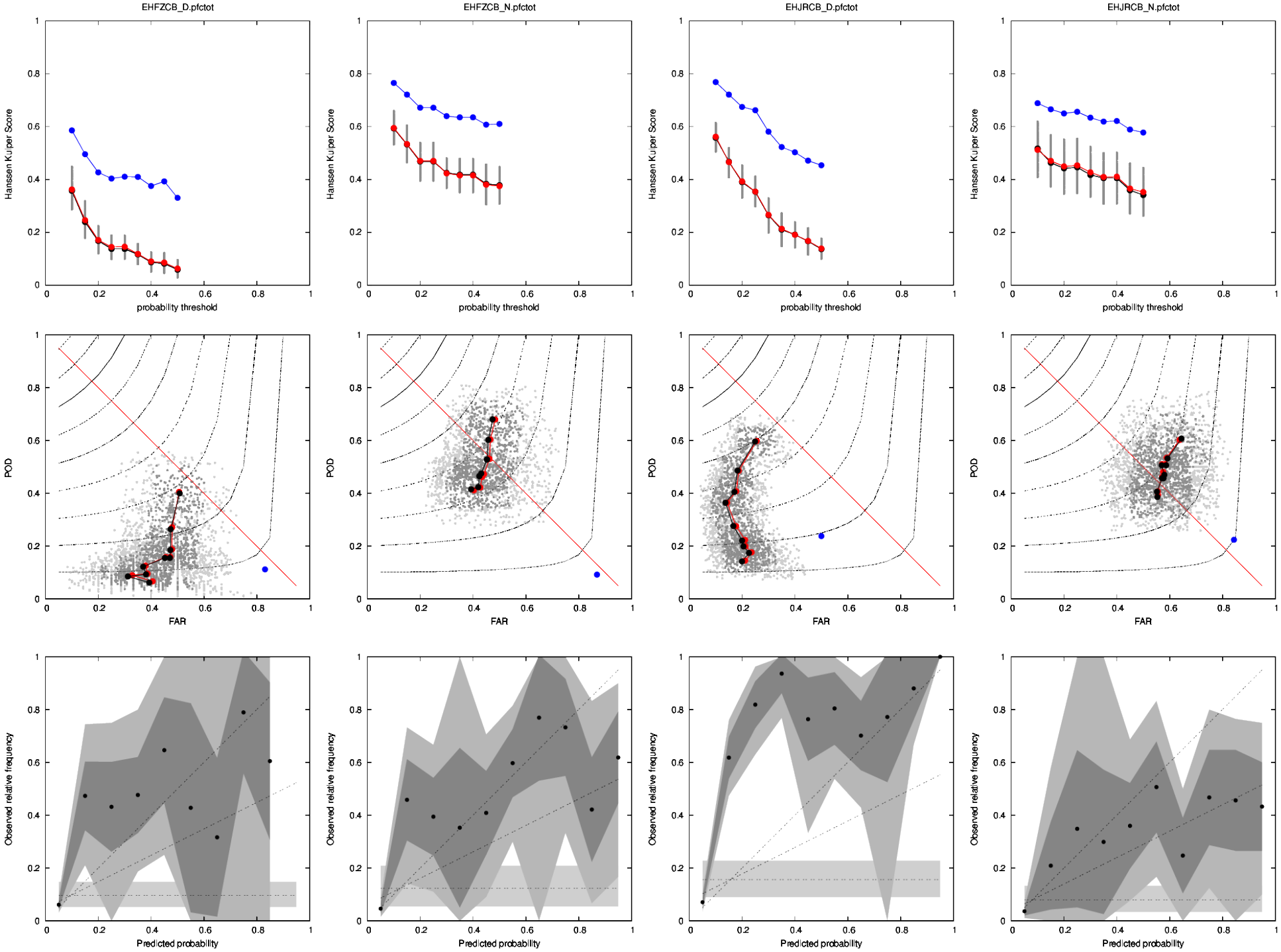

Figure 5c. The probability equation of the operational algorithm applied to the Summer 2013 data set. Caption as above, note the blue dot

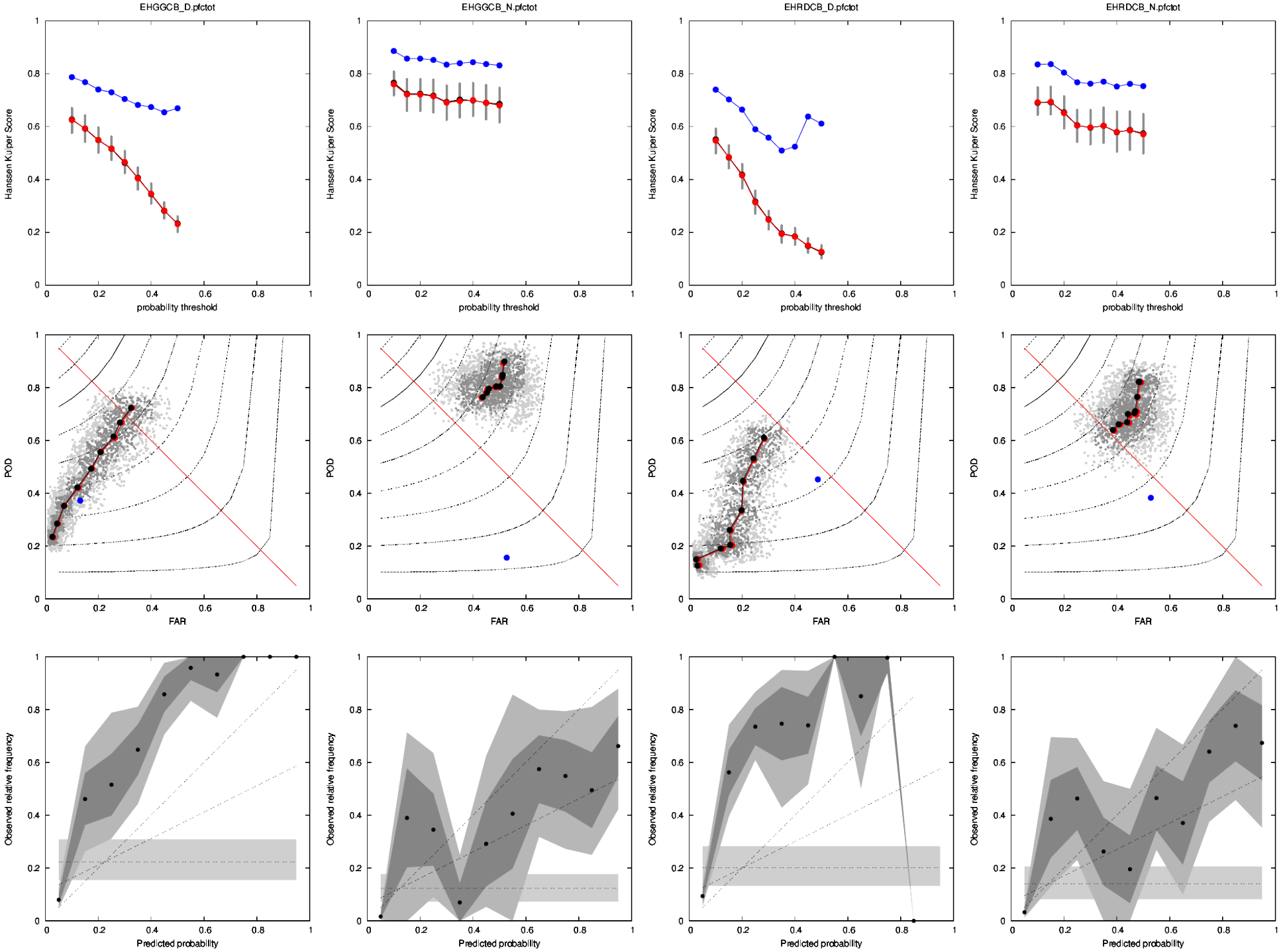

Figure 5d. The probability equation of the operational algorithm applied to the Summer 2013 data set. Caption as above, note the blue dot

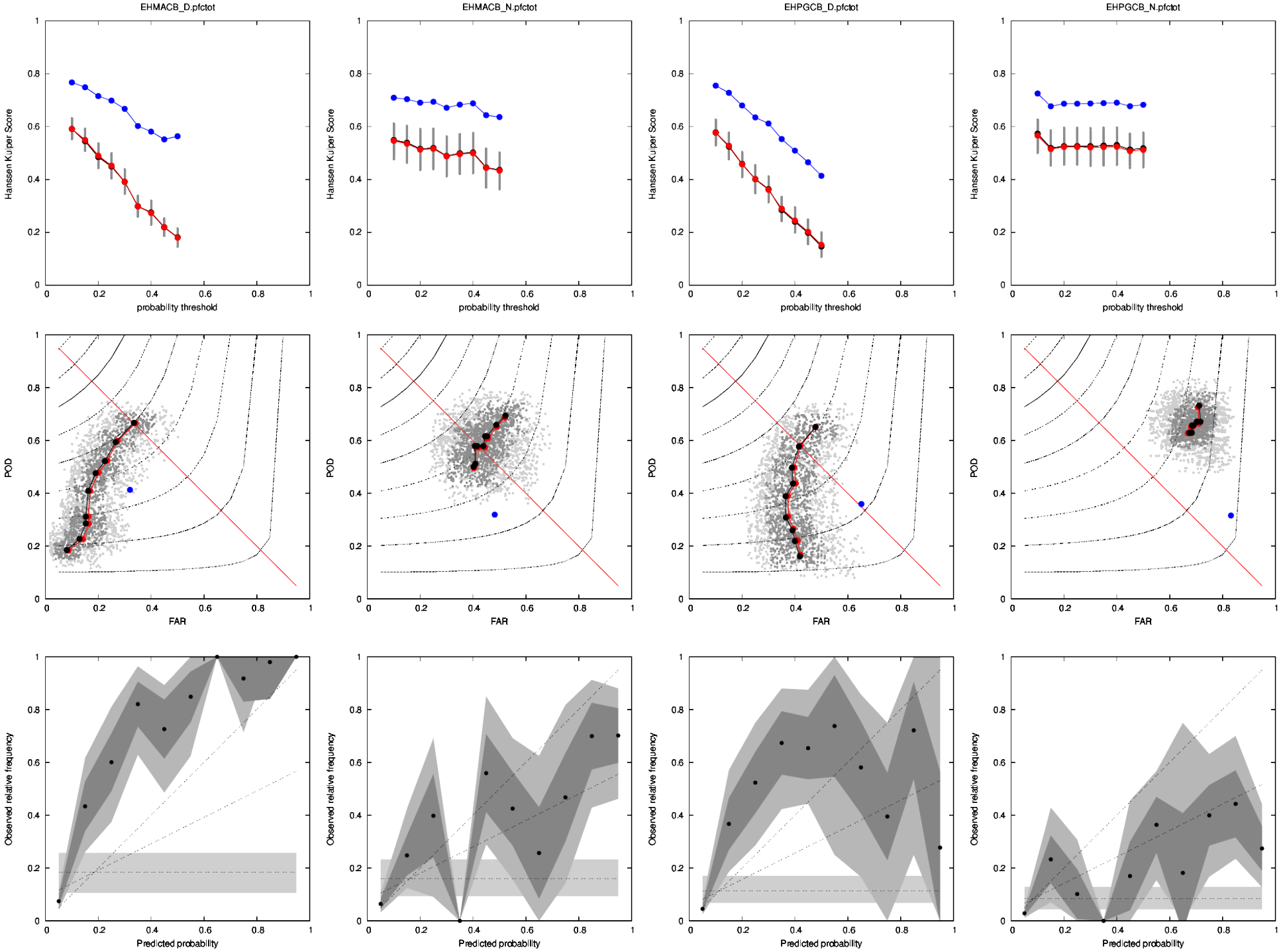

Figure 6a. The probability equation of the operational algorithm applied to the Winter 2013 data set. Caption as above, note the blue dot

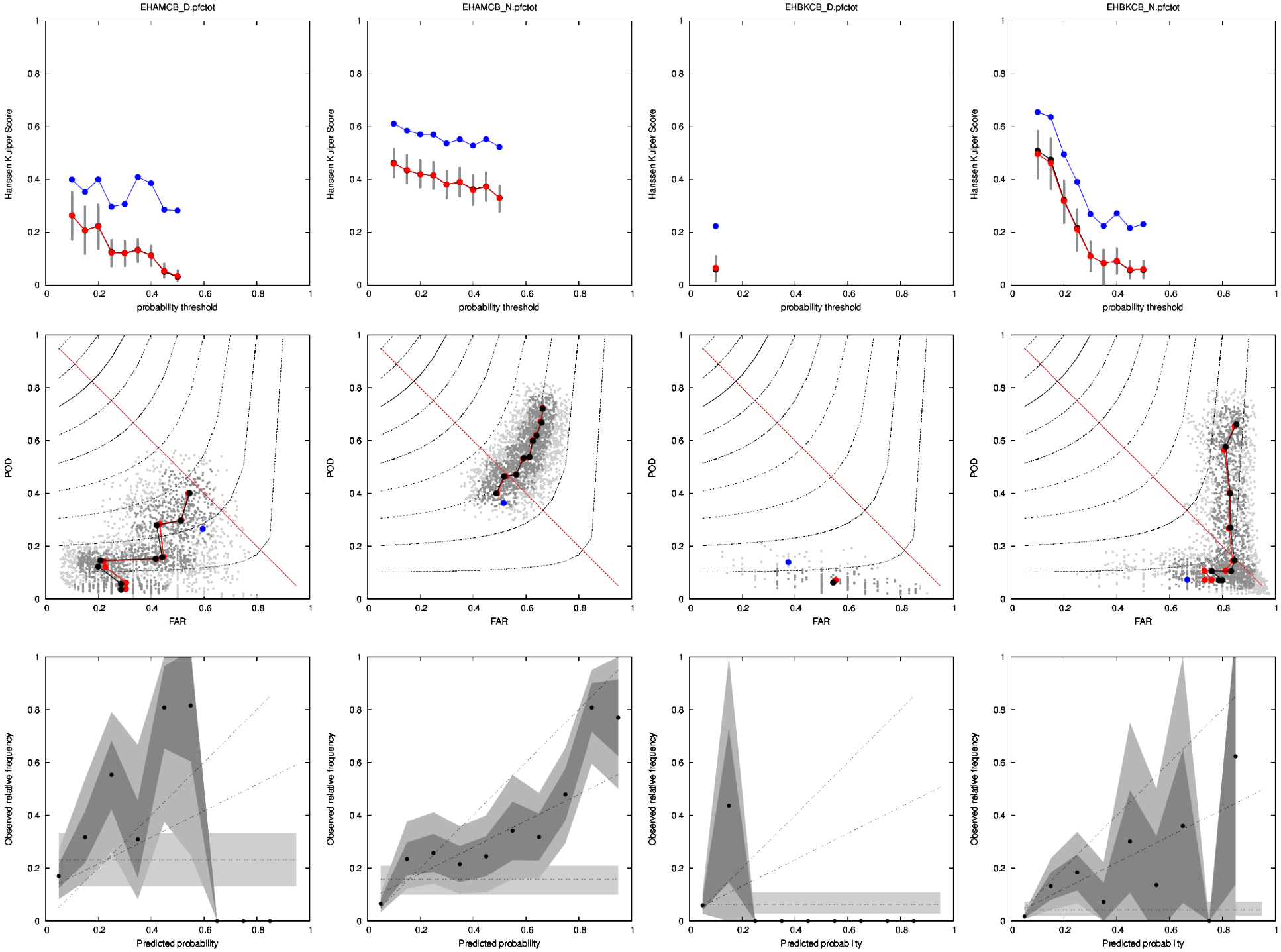

Figure 6b. The probability equation of the operational algorithm applied to the Winter 2013 data set. Caption as above, note the blue dot

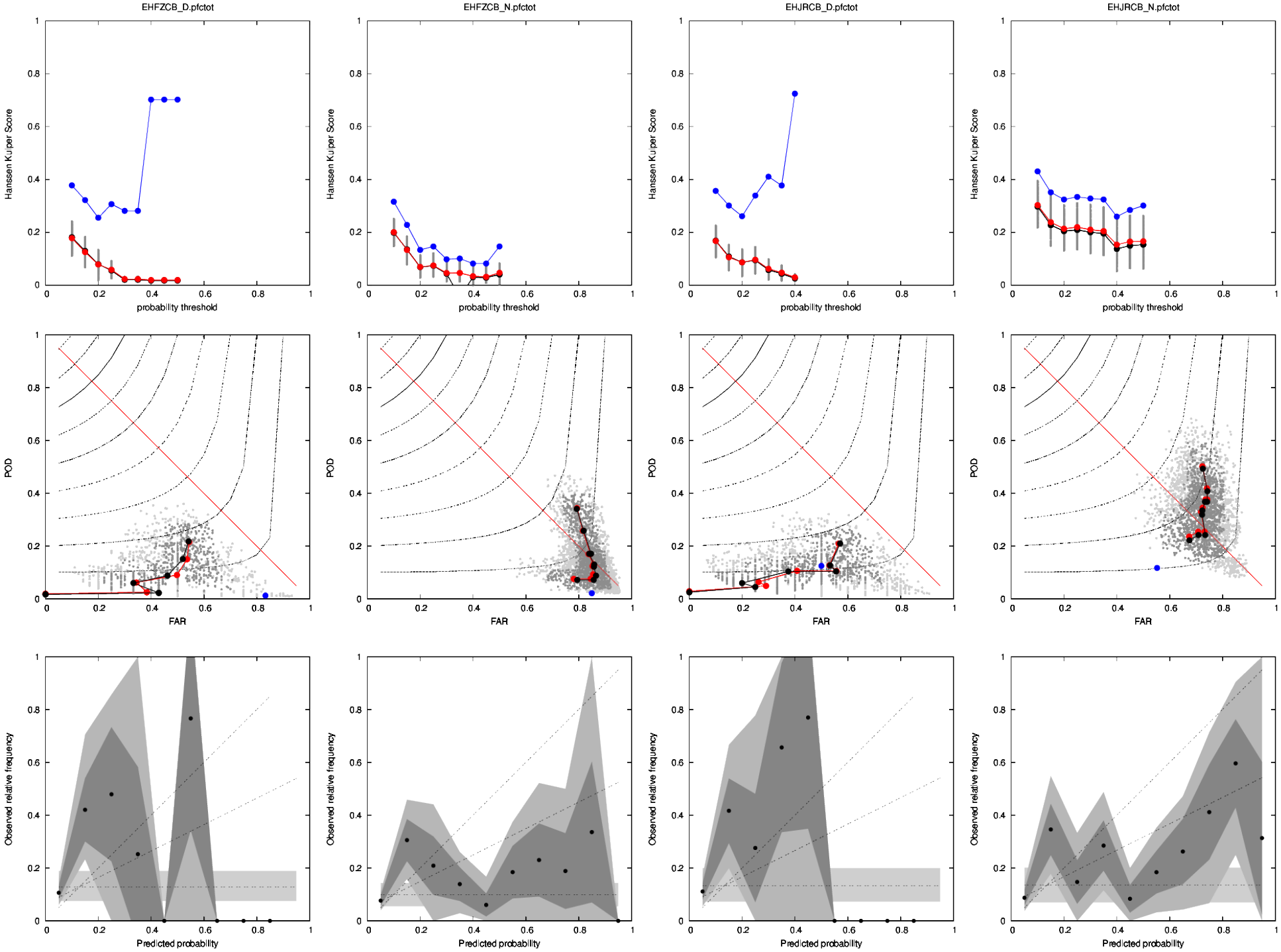

Figure 6c. The probability equation of the operational algorithm applied to the Winter 2013 data set. Caption as above, note the blue dot

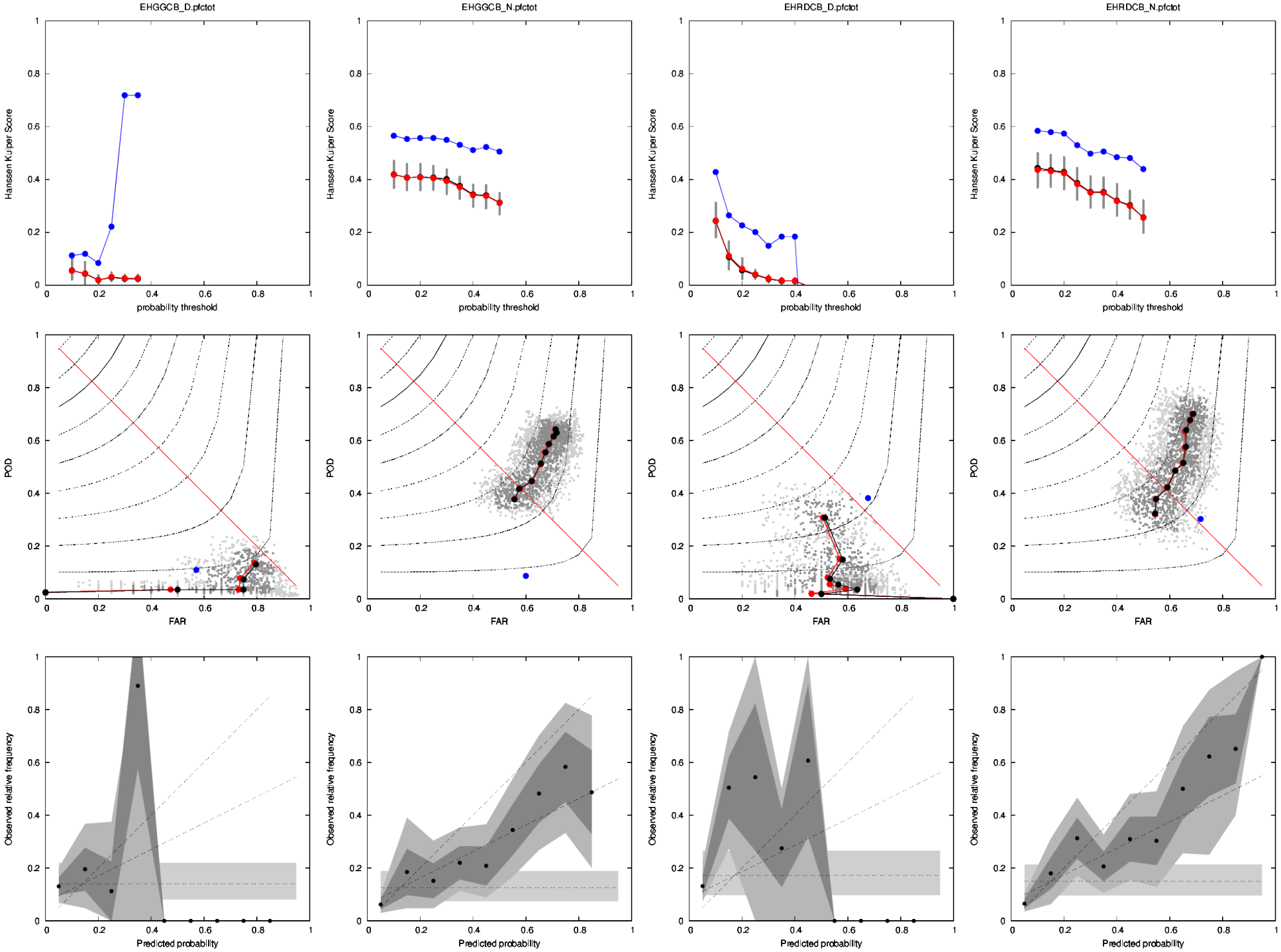

Figure 6d. The probability equation of the operational algorithm applied to the Winter 2013 data set. Caption as above, note the blue dot

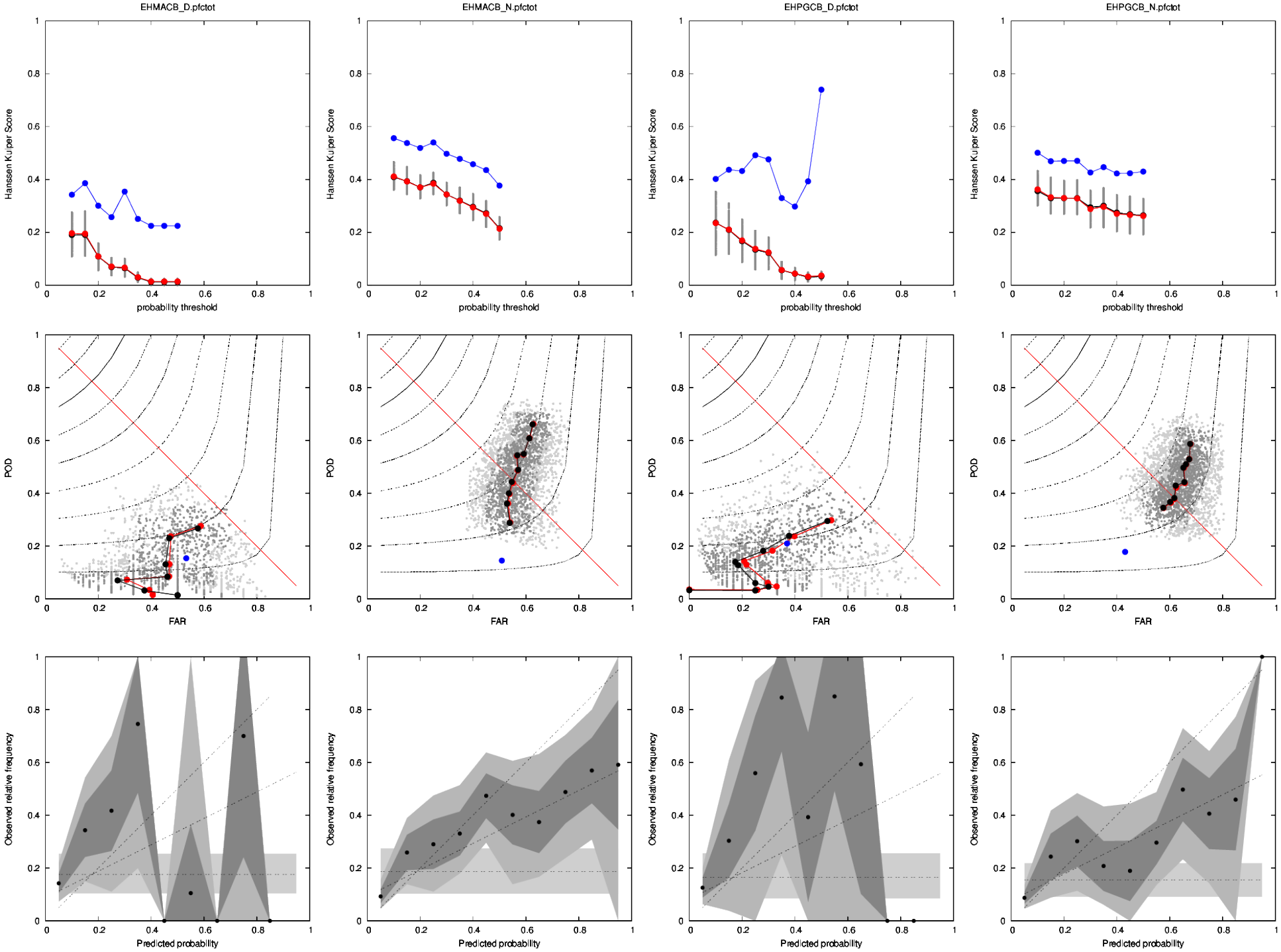

Figure 7a. Summer 2013 data set. The probability equation is derived on the independent 2010 data set . The caption is given above.

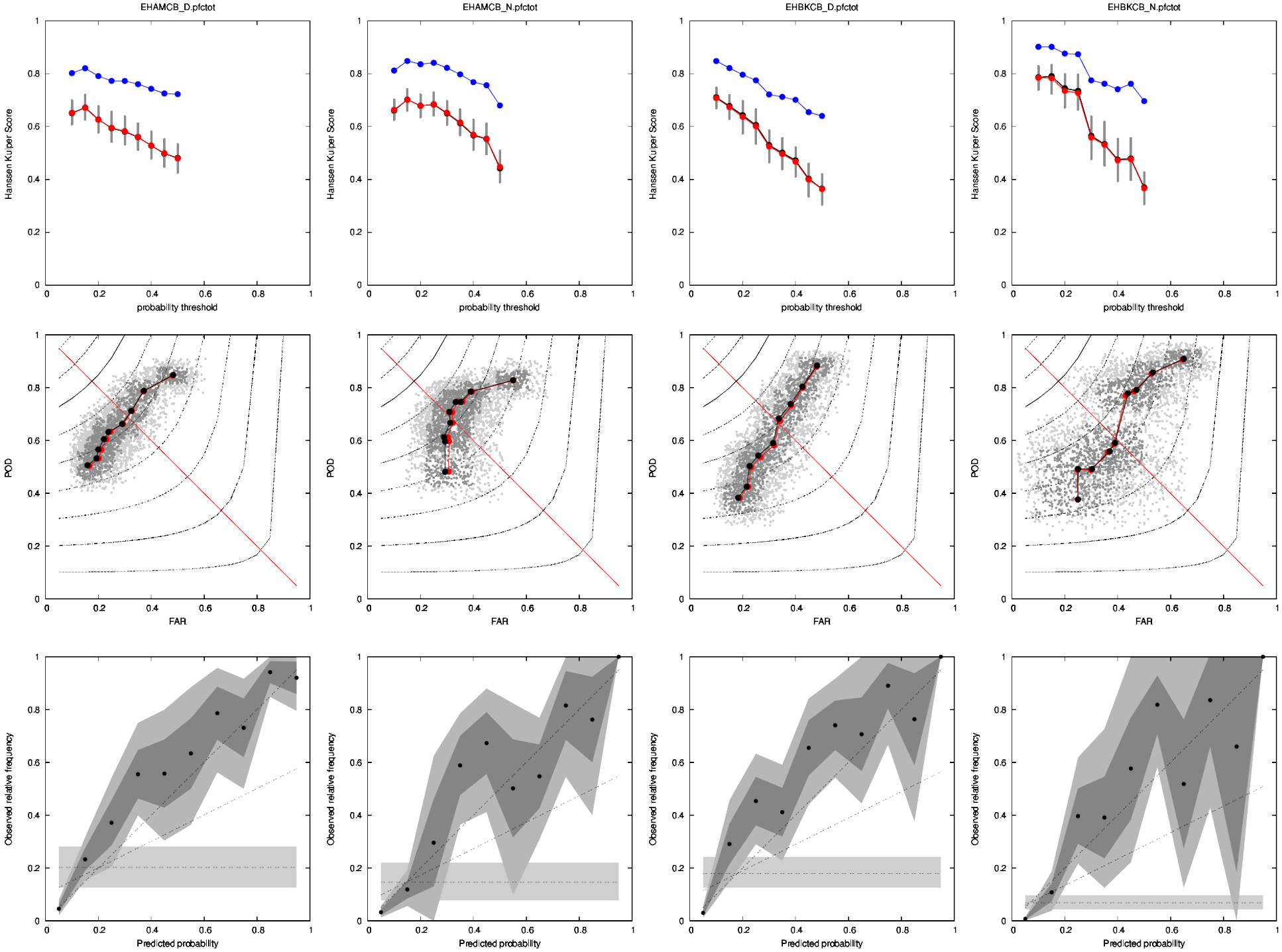

Figure 7b. Summer 2013 data set. The probability equation is derived on the independent 2010 data set . The caption is given above.

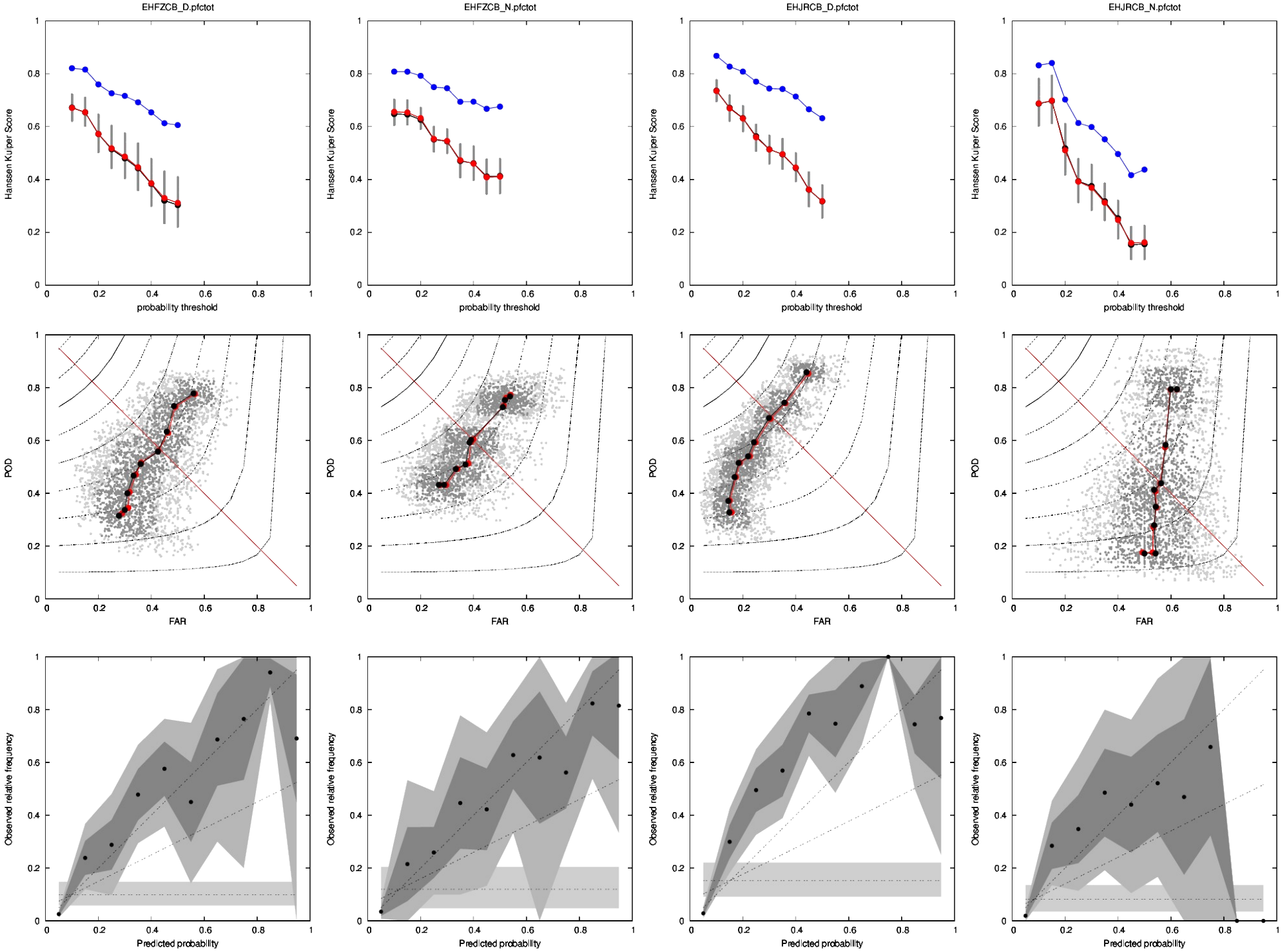

Figure 7c. Summer 2013 data set. The probability equation is derived on the independent 2010 data set . The caption is given above.

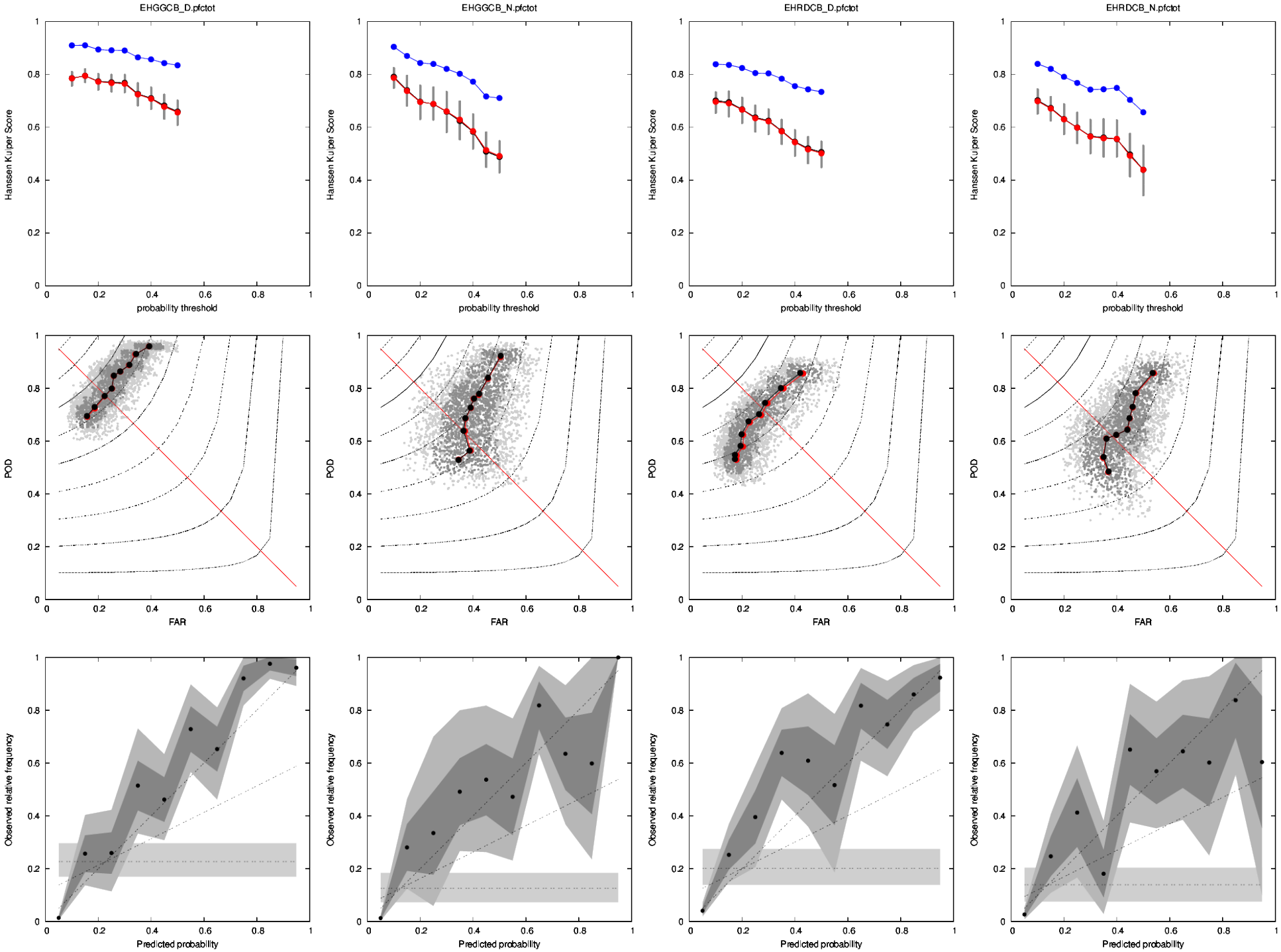
EHGGCB_D.pfctot
EHGGCB_N.pfctot
EHRDCB_D.pfctot
EHRDCB_N.pfctot
Hanssen Kuiper Score
probability threshold
POD
FAR
Observed relative frequency
Predicted probability

Figure 7d. Summer 2013 data set. The probability equation is derived on the independent 2010 data set . The caption is given above.

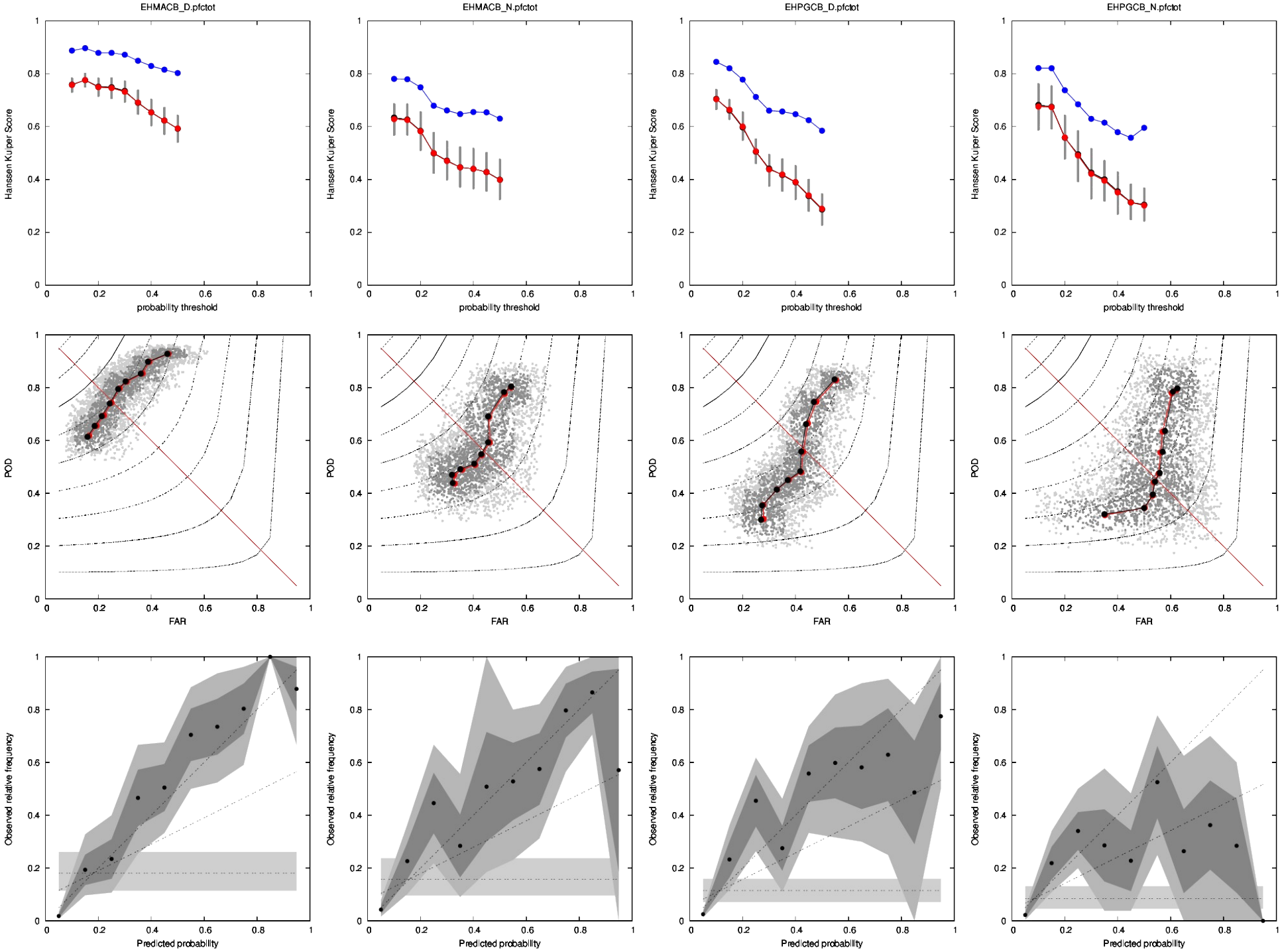

Figure 8a. Winter 2013 data set. The probability equation is derived on the independent 2010 data set. The caption is given above.

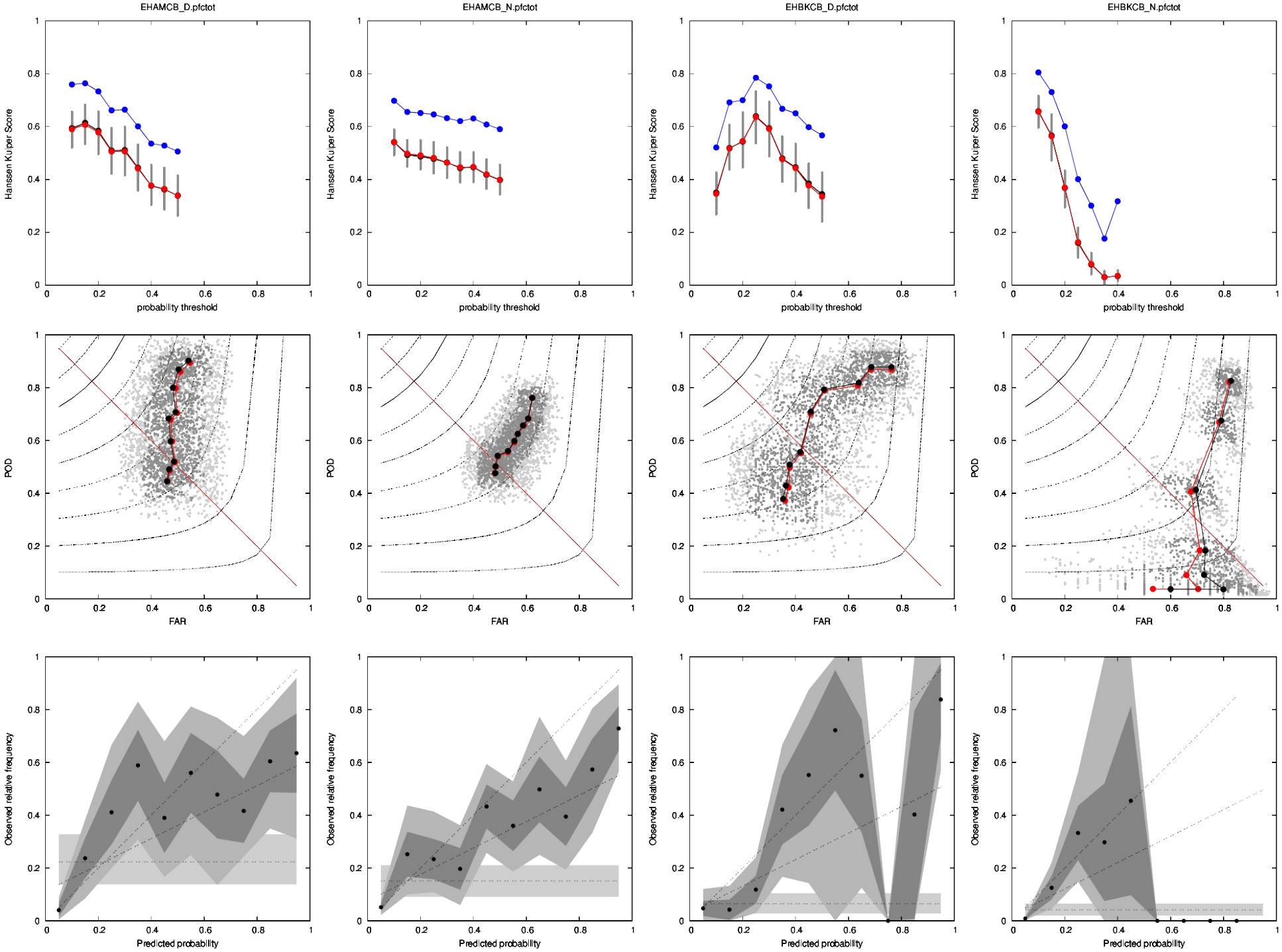

Figure 8b. Winter 2013 data set. The probability equation is derived on the independent 2010 data set. The caption is given above.

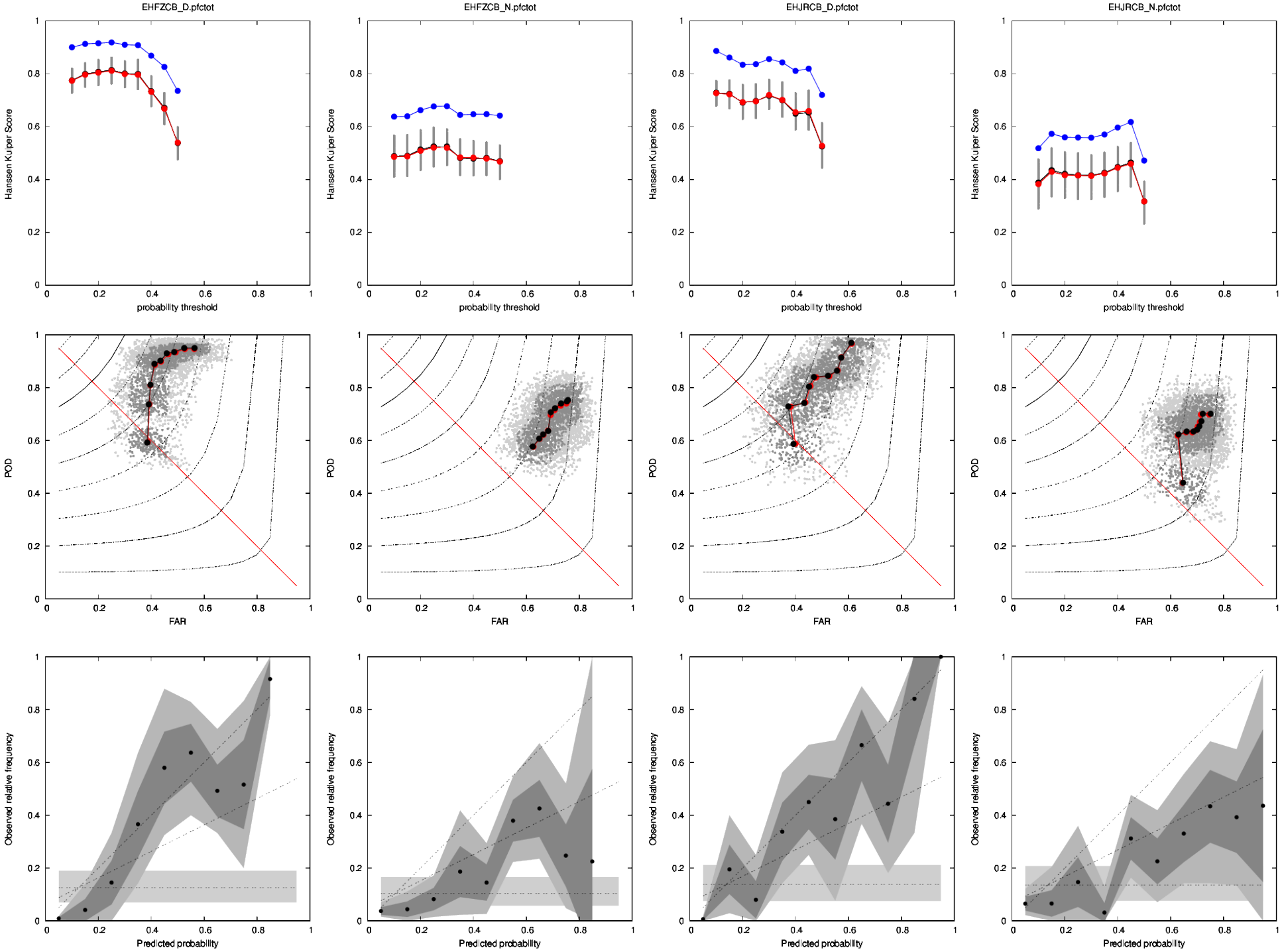

Figure 8c. Winter 2013 data set. The probability equation is derived on the independent 2010 data set. The caption is given above.

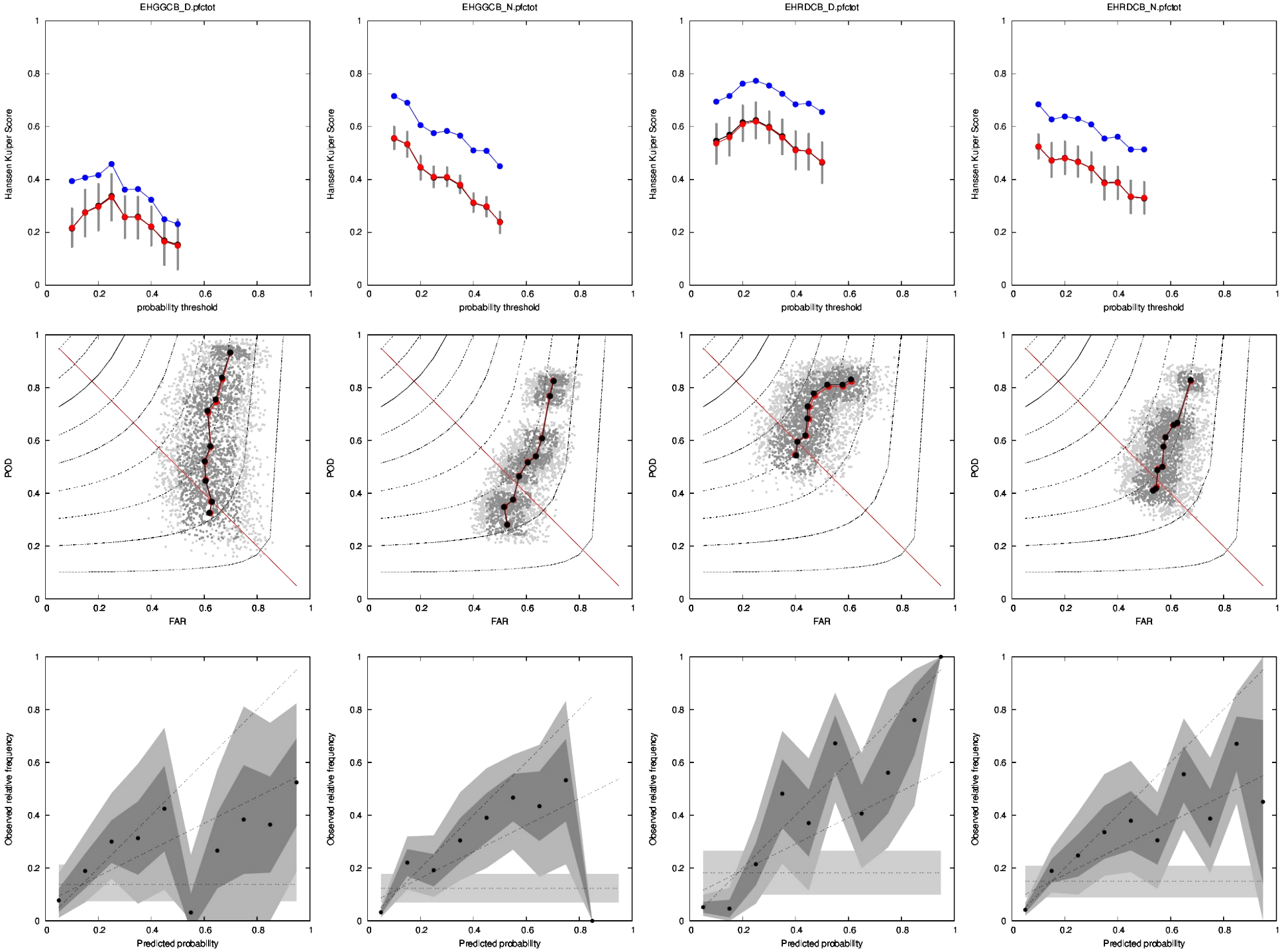

Figure 8d. Winter 2013 data set. The probability equation is derived on the independent 2010 data set. The caption is given above.

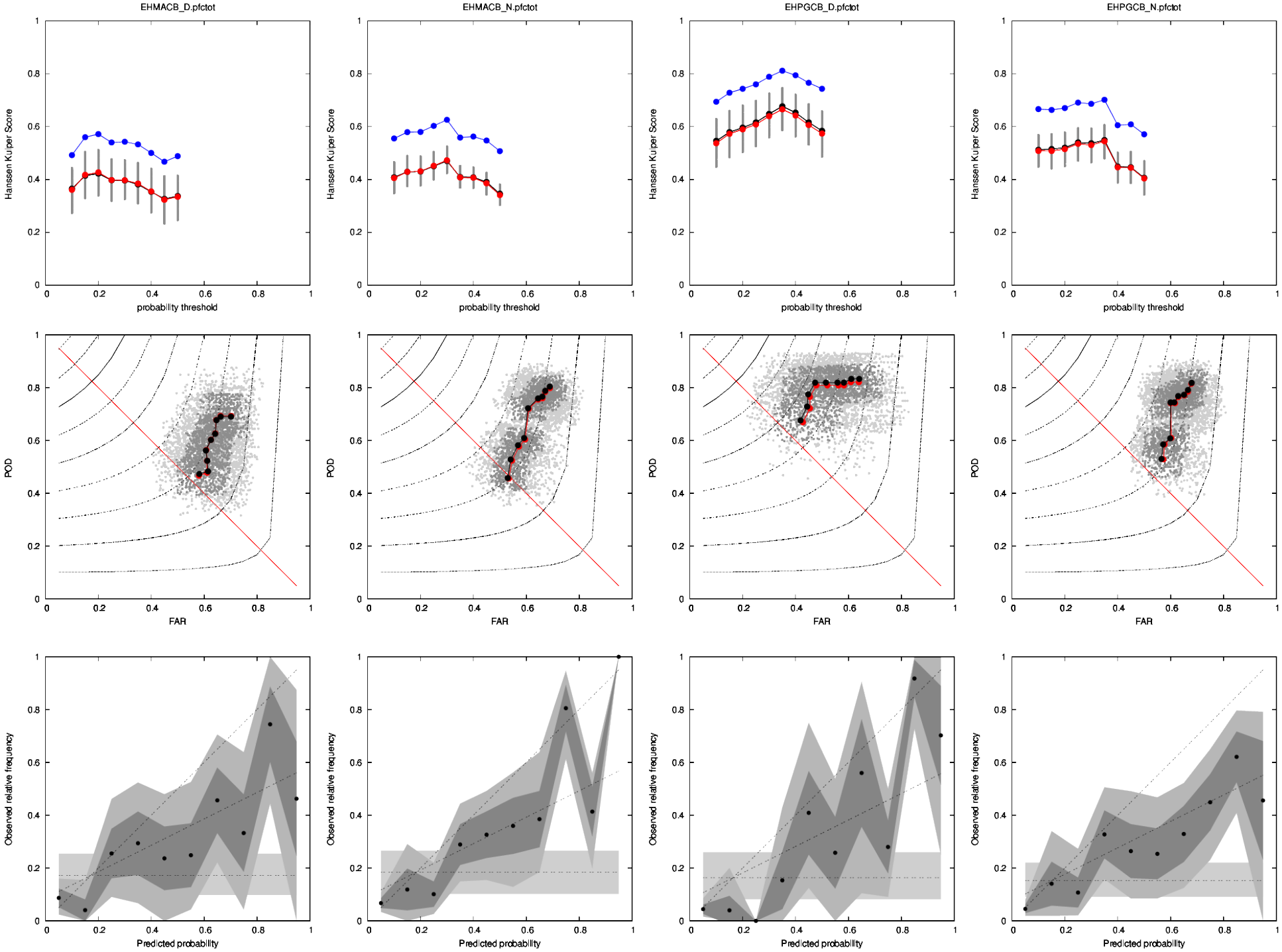

Dependent set 2010

Based on the figures 3 and 4 for the dependent 2010 data set we conclude that generally

- Evaluation requires the interpretation of all diagrams to come to a balanced conclusion, E.g. a high SEDI score does not imply a low FAR value, see for example the winter night at EHBK.
- The SEDI score is always higher than HKS, except for rare cases. SEDI rarely becomes less than 0.6.
- Day time performance is better compared to night time performance. Here the HRV satellite information appears a valuable contributor to the classification of Cb.
- Summer performance is better compared to winter performance. The higher precipitation rate in summer versus the winter cases contributes here to the classification performance.
- Performance over sea is worse compared to performance over land. Partially attributable to the remoteness of some of the sea stations to the radar locations.
- Winter performance over sea appears better compared to summer performance over sea. Possibly attributable to the triggering of convection in the winter season over relatively warm sea water, especially in the autumn.
- Winter performance over land is worse compared to summer performance over land. Possibly attributable to the relative low Cb occurrence frequency in winter time over land especially during the night. The difficulty in discrimination between Cb precipitation and heavy frontal precipitation by the algorithm could be another cause. The remoteness of land stations to the radar sites hampers the classification performance in the winter night.

In tables in the appendix 1 the Brier skill scores (BSS) are summarized per season for all stations in 2010.

The BSS values confirm the general conclusions. They are included here as they can serve as reference for a comparison to the dependent set.

Another way of representing the results is shown in table 4.2. In Table 4.2 the performance for the application of the 2014 algorithm on the 2010 data set is summarised in POD and FAR values for the highest achievable CSI and a BIAS close to 1. They are based on Figures 3 for, summer and Figure 4 for winter. The results are classified in five categories ranging form good in dark green to poor in red. The colours are explained in the table caption.

These results in colour coding are given in a geographical context, in figure 9. In this figure also the radar coverage is shown. Two circles are drawn around each radar site. The inner circle shows the area where the radar signal is good and where the psuedocappi height is at a constant level. In the outer circle the radar signal is weaker and therefore more perceptible for atmospheric disturbances. Furthermore the psuedo-cappi height increases with the distance to the radar site. Within the outer circle the radar signal still can contain significant information.

The classification results are in agreement with above conclusions.

2010	Sd **pod**	Sd far	Sn **pod**	Sn far	Wd **pod**	Wd far	Wn **pod**	Wn far
EHAM	65	30	62	40	50	45	50	45
EHBK	62	35	60	40	50	45	20	70
EHDL	70	30	62	35	50	50	30	65
EHDV	40	55	45	55	50	50	45	55
EHEH	65	35	60	40	50	50	30	55
EHFD	50	50	60	40	65	35	45	50
EHFZ	55	45	60	40	60	40	60	40
EHGG	70	25	60	35	60	40	40	55
EHGR	65	30	60	35	40	55	30	65
EHJA	50	45	50	45	65	30	60	40
EHJR	50	50	50	45	70	35	60	40
EHKD	60	40	50	45	60	35	60	40
EHKV	55	45	50	50	65	35	65	35
EHLE	65	35	60	40	50	45	45	55
EHLW	60	35	60	40	60	35	55	45
EHMA	65	35	55	45	65	35	60	40
EHMG	60	40	50	50	60	35	65	35
EHPG	40	55	55	40	65	35	70	30
EHQE	50	45	55	40	65	30	60	40
EHRD	60	40	65	35	55	45	55	40
EHSA	35	60	45	50	60	40	60	40
EHSC	55	40	50	45	50	50	60	40
EHTW	70	30	60	35	45	50	30	65
EHVK	65	35	60	35	45	55	30	65
EHVL	55	45	55	40	65	35	60	40
EHWO	65	35	65	30	40	50	45	50

Green	POD > 60 FAR <40
light green	(POD > 55 and FAR <45) or (POD>60 and POD-FAR >20)
yellow	POD > 50 FAR <50
orange	POD > 45 FAR < 55
red	FAR >60 or POD < 40

Table 4.2. Performance of the 2014 algorithm on the dependent 2010 evaluated data set. Sd Summer day Sn Summer night Wd Winter day Wn Winter night.

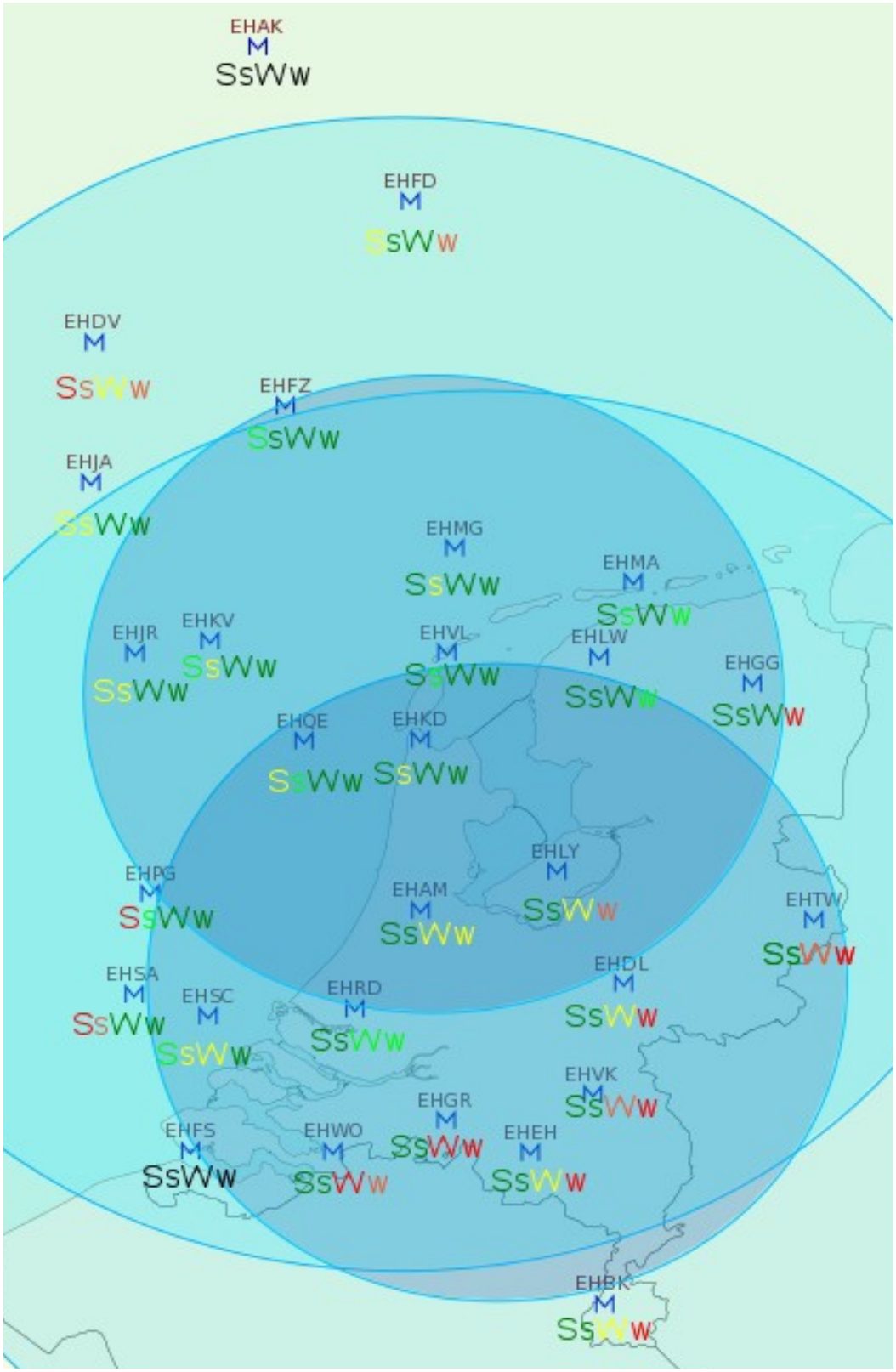

Figure 9. Performance evaluation table 2010 projected on geographical map S: Summer day s: summer night W winter day w winter night. Colour coding as given in table 4.2 above. The outer circles represent the maximum radar coverage of the two radars. This coverage can be distorted by atmospheric phenomena. The inner circle depicts the coverage of the relative higher quality radar data, less sensible to atmospheric distortion. EHFS and EHAK were not evaluated, hence that their non relevant scores are given in black.

Independent set 2013

In the next set of figures the Cb probabilistic equations from the operational algorithm and the 2014 algorithm are applied to the 2013 data set. Please note that the 2013 evaluated set focusses on the 7 to 10 wettest days of each month. This focus causes a relative high Cb climatological occurrence frequency in the attribute diagrams.

We split the comparison in a winter and summer part, as there is a clear difference in performance by both the operational and the 2014 algorithm.

When the operational algorithm was implemented in 2010 it was reported that the winter classifications would be a challenge partly due to the significant lower occurrence frequency of Cb in winter. The results of the operational algorithm shown in figure 6 confirms this. The SEDI scores can become low, the POD FAR diagrams show poor figures and the results in the attribute diagram are also poor. The Cb classification performance during the winter day is very poor. The performance is similar to the 2007 algorithm performance based on radar observations only. For reference purposes an approximation of the 2007 algorithm is added in the POD FAR diagram indicated by the added blue dot. It is an approximation because the exact calculation method was not reproduced here. The approximation classifies a Cb occurrence when the maximum radar reflectivity is over 33 dBZ ~ 4.2 mm/hr. In the 2007 algorithm this is only valid when the reflectivity over 33 dBZ occurs in three adjoining pixels. The approximation only considers the maximum occurring value in one pixel and therefore can overestimate both the POD and the FAR.

The BSS in the appendix 1 underline the above conclusions on poor performance with low and even negative values. Note that the sea stations are added for reference purposes only, as they are not a part of the operational algorithm. Their probabilistic equations were set equal to the probabilistic equation of EHAM, a station most close to the coast.

The application of the 2014 algorithm, shown in Figure 8, on the 2013 winter data set led to improved results in comparison to the results of the operational algorithm. Higher SEDI, improved POD and FAR scores, improved performance in the attribute diagrams, and higher Brier skill scores. The Brier skill scores from the dependent set are comparable to the scores of the 2014 algorithm applied on 2013 data set.

The improvement in performance of the 2014 algorithm for the winter day results is significant and for the winter night it is marginal compared to the operational results. The latter marginal improvement shows that the night time predictor equation set was also sufficiently adequate in the operational algorithm, and that the winter night remains the most challenging season to classify Cb occurrence correctly.

For the summer season the performance of the operational algorithm, shown in Figure 5, are in agreement with the predicted POD and FAR as reported in De Valk and van Westhrenen, 2010. When the operational algorithm performance is compared to the 2007 algorithm performance the former is always better than the latter, both for day and night. However the attribute diagrams for the operational algorithm show frequently an underestimation in predicted probability during the day and an overestimation in predicted probability during the night.

Figure 7 shows that the 2014 algorithm can even improve on the adequate operational algorithm performance in the summer, shown in Figure 5. This can be concluded from the improvement in SEDI, POD, FAR the attribute diagrams when comparing figure 7 and 5 for each station and the brier scores shown in table 3 and 5 in the appendix.

Like in the winter night the summer night performance comparison shows only a marginal improvement between the operational and 2014 algorithms.

Remarkable is the performance of the operational algorithm over sea in the summer Figure 5b and 5d. Except for the station FZ during the day and the station PG at night the performance of the operational and the 2014 algorithm appear very similar. Considering that the probabilistic equation of the sea stations within the operational application is based on EHAM, a land station, this is an

unexpected good performance.

The 2014 algorithm performance in the night over sea is relatively poor compared to the performance during the day over sea. The remoteness of stations to radars appears to deteriorate the classification performance.

These latter two conclusions are in line with the conclusions on the performance of the 2014 algorithm applied to the dependent 2010 data set. Also the other conclusions with regard to difference in day versus night performance, land surface versus sea surface, and summer versus winter performance are valid for the 2014 algorithm application to the 2013 data set.

The conclusions on the 2013 data set are drawn on the wettest days of each month. Therefore the conclusions may be biased to significant precipitation events. The conclusions however appear to be in line with the conclusions on the dependent evaluation of 2010.

Another way of representing the results is shown in table 4.3 till 4.5. In Table 4.3 the performance for the application of the 2007 algorithm on the 2013 evaluated data set is summarised in POD and FAR values for the highest achievable CSI and a BIAS close to 1. They are based on the blue dots in Figure 5 and 6. The results are classified in five categories ranging form good, green to poor red. The colours are identical to the table caption of 4.2.

In table 4.3 the application results of the operational 2011 algorithm on the 2013 data set is shown, derived also from figure 5 and 6. In table 4.4 the application results of the 2014 updated algorithm on the 2013 data set is shown, derived also from figure 7 and 8. From the change in performance between the various tables one can deduce the improvement in achieved performance. But also that there is room for improvement. The winter night especially remains a challenge to achieve a good classification.

These results in colour coding can also be displayed in a geographical context, see figure 10. In this figure also the radar coverage is displayed. The results underline the above conclusions.

2013	Sd **pod**	Sd far	Sn **pod**	Sn far	Wd **pod**	Wd far	Wn **pod**	Wn far
EHAM	**40**	40	**50**	50	**25**	60	**35**	55
EHBK	**25**	15	**25**	30	**15**	35	**5**	65
EHGG	**35**	10	**15**	55	**10**	55	**10**	60
EHRD	**45**	50	**35**	55	**35**	70	**30**	70
EHFZ	**10**	80	**10**	85	**0**	80	**5**	85
EHJR	**20**	50	**20**	85	**10**	50	**10**	55
EHMA	**40**	30	**30**	50	**10**	45	**15**	50
EHPG	**35**	65	**30**	80	**20**	35	**15**	45

Table 4.3 2007 algorithm applied to independent 2013 data set

2013	Sd **pod**	Sd far	Sn **pod**	Sn far	Wd **pod**	Wd far	Wn **pod**	Wn far
EHAM	**65**	30	**65**	35	**35**	55	**45**	50
EHBK	**45**	35	**55**	40	**10**	50	**10**	85
EHGG	**70**	30	**70**	45	**10**	80	**35**	60
EHRD	**60**	25	**60**	35	**30**	50	**40**	60

Table 4.4 Operational algorithm applied to independent 2013 data set

2013	Sd **pod**	Sd far	Sn **pod**	Sn far	Wd **pod**	Wd far	Wn **pod**	Wn far
EHAM	**63**	23	**72**	32	**70**	45	**50**	50
EHBK	**65**	30	**60**	40	**70**	45	**40**	70
EHGG	**80**	25	**70**	40	**45**	60	**45**	55
EHRD	**70**	30	**60**	40	**60**	40	**45**	55
EHFZ	**55**	45	**60**	35	**60**	40	**60**	60
EHJR	**70**	30	**50**	55	**70**	40	**65**	60
EHMA	**70**	25	**70**	45	**45**	55	**45**	55
EHPG	**50**	40	**45**	55	**65**	40	**50**	55

Table 4.5 2014 updated algorithm applied to independent 2013 data set.

These results in colour coding can also be displayed in a geographical context, see figure 10. In this figure also the radar coverage is displayed. The results underline the above conclusions.

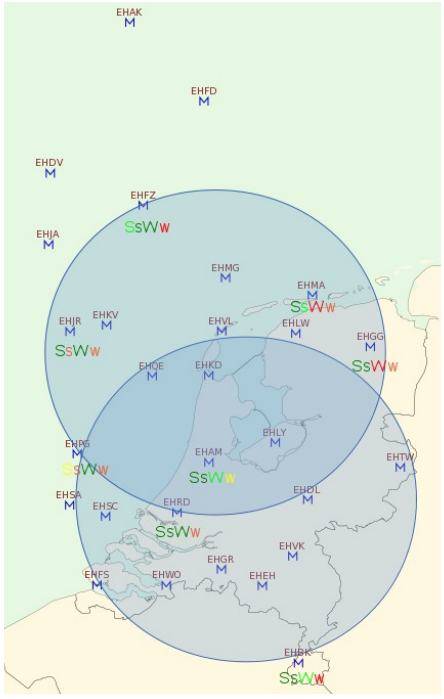

Figure 10. Caption as Figure 9. Performance of the algorithm on the 2013 limited data set. Of 8 stations. Only the inner radar coverage circles are shown.

5 Conclusions

Convective clouds form a serious treat for aviation. To maximize safe flying conditions ICAO regulations require the observation of these clouds in the vicinity of aerodromes. These observations are globally predominantly done by human observers. At KNMI an automated detection method of convective clouds, henceforward referred to as automated Cb-Tcu detection algorithm, is implemented operationally in 2011.

An automated Cb-Tcu detection algorithm based on the synergy between radar and satellite observations is further developed, based on the operational 2011 version applied at KNMI. The algorithm uses logistic regression to determine the probability of Cb-Tcu occurrence. Within logistic regression a forward stepwise approach is applied. The predictors having the highest explanatory relation to the Cb occurrence were from the radar observations:

- the highest radar contour occurring in collocation area with a 15 km radii around the ARP,
- the difference between maximum and minimum (non-zero) precipitation intensity,

and from the satellite observations:

- the reflection contrast within the collocation area of the high resolution visible channel,
- the averaged cloud top temperature,
- the areal fraction where the brightness temperature in the 3.9 um channel is lower than the brightness temperature in the 10.8 um channel.

For night time also combinations of the explanatory predictors contributed to the classification.

Two data sets with manual Cb classification were available for algorithm development and evaluation, one for 2010 and one for 2013. The 2010 data set consists for 26 METAR stations out of classification every 30 minutes for a full year and the 2013 consists for 8 METAR stations out of every 30 minutes classifications for the 7 to 10 wettest days for each month.

The further developed version of the operational classification algorithm, referred to as Cb-2014 is optimised using the 2010 data set. Both the Cb-2014 and the operational algorithm are then applied to the data set derived for 2013.

In Figures 5 to 8 the results are shown. The results are presented in three diagrams summarising the performance of the algorithm. From these diagrams the following conclusions can be drawn:

- The SEDI score in summer is high SEDI rarely becomes less than 0.6. In the winter lower SEDI scores occur.

- day time performance is better compared to night time performance. Here the HRV satellite information appears a valuable contributor to the classification of Cb.

- summer performance is better compared to winter performance. In summer the Cb's have a higher precipitation rate and are therefore better detectable by radar. They also have higher cloud tops which increase their detectability both in the HRV and brightness temperature channels.

- performance over sea is worse compared to performance over land. Partially attributable

to the remoteness of some of the sea stations to radar.

- winter performance over sea appears better compared to summer performance over sea. Possibly attributable to the triggering of convection over relatively warm sea water in the fall which is considered as a part of the winter season.

- winter performance over land is worse compared to summer performance over land. Partially attributable to the low Cb occurrence frequency over land in winter time especially during the night. Other causes maybe the shallowness of winter convection hampering a correct radar detection at remote places and the limited discrimination ability of the algorithm to distinguish between intense frontal precipitation and convective rain. The remoteness of land stations to the radar sites hampers a correct classification performance in the winter night.

In Table 4.5 the performance for the application of the 2014 algorithm on the 2013 is summarised in POD and FAR values for the highest achievable CSI and a BIAS close to 1. They are based on Figure 7 for summer and Figure 8 for winter.

This performance can be compared to the METAR performance obtained by human observers when compared to the supervised data set generated by the forecaster. For 2010 EHAM the observer scores were for

summer day POD 43 percent, FAR 4 percent,
summer night POD 42 percent, FAR 6 percent,
winter day POD 49 FAR 11,
winter night POD 44, FAR 11 respectively.

Outlook

The present performance is good. The maximum information extraction from radar and satellite observations appears to be achieved. This is based on the satellite and radar observations as provided at the time of writing. Improvements in observations will contribute to the performance.

A good clutter removal is important to reduce the number of False Alarms over sea. Here only a rudimentary clutter filter has been applied. A more sophisticated clutter removal method will increase the performance. The improvement will be predominantly for the sea stations.

Regurlarly satellite information has a significant latency. A version which in those cases uses solely radar observations for its classification should be evaluated versus the operational version.

An additional improvement is expected when the present algorithm is applied to a combination of radar and satellite observations with 5 minutes update frequency. As the algorithm is also used for the ACTUALs, this frequency accommodates the ACTUAL information generation and demand more optimal.

The implementation of the Rapid Scan Service could be done in a next project. The only caveat is the none-operational status of Rapid Scan Service of MSG-SEVIRI. It is available 80 percent of the time. The remaining 20 percent could be supplied by the normal operational service. This however requires a high level scheduling method of the classification algorithm, taking into account the various sources of information flows.

Please note that the introduction of a (new) high resolution radar or new satellite information would require a research-update and a new supervised Cb-classification.

As there was a requirement to discriminate between Cb and Tcu we can suggest a sub-optimal solution. The solution is sub-optimal because it is and probably never will be validated. When a classification for Cb is done, the coverage is determined by calculating the areal coverage within the area of interest with a radar rain intensity above a threshold.

Here we could introduce a radar precipitation threshold T_Cb. When the threshold T_Cb is not achieved within the area of study, the cloud is automatically classified as Tcu.

References

Carbajal Henken, C., Schmeits, M., Wolters, E. and Roebeling, R. ,2009,Detection of Cb and Tcu clouds using MSG-SEVIRI cloud physical properties and weather radar observations. KNMI WR 2009-04

De Valk, P. and van Westhrenen, R., 2010, Probability of Cb and Tcu occurrence based upon radar and satellite observations, KNMI WR 2010-4 http://www.knmi.nl/bibliotheek/knmipubWR/WR2010-04.pdf.

De Valk, P. and van Westhrenen, R., 2011, The implementation of automated Cb-Tcu detection, http://www.knmi.nl/bibliotheek/knmipubIR/IR2011-05.pdf

Holleman, I. Introduction to Radar internal webpage at KNMI. http://info.knmi.nl/~beekhuis/index.html

Lensky, I.T. and D. Rosenfeld 2003 “A night-Rain delineation algorithm for infrared satellites data based on microphysical considerations.”J appl meteorology 42 1218.

Mecikalski, John R. and Bedka, Kristopher M.. Forecasting convective initiation by monitoring the evolution of moving cumulus in daytime GOES imagery. Monthly Weather Review, Volume 134, Issue 1, 2006, pp.49-78.

Mecicalski (2007) -based Convective Initiation Nowcasting System Improvements Expected from the MTG FCI Meteosat Third Generation Capability, EUM/CO/07/4600000405/JKG Technical Report http://www.eumetsat.int/groups/pps/documents/document/pdf_mtg_rep35.pdf

Petterssen S., 2008 Introduction to meteorology. 3rd edn. New York: McGraw-Hill.

Ralph Peterson, 2013 Improve very-short-range forecasts of the pre-convective environment using clear air SEVIRI products, Vienna 2013 EUMETSAT data user conference.

Sokol Z. and Pesice, P. 2009, Comparing nowcastings of three severe convective events by statistical and NWP models, Atmospheric Research Vol. 93. p397-407.

Schmeits, M.J., C.J. Kok, D.H.P. Vogelezang and R.M. van Westrhenen, 2008, *Probabilistic forecasts of (severe) thunderstorms for the purpose of issuing a weather alarm in the Netherlands* Weather and Forecasting, 2008, 23, 6, 1253-1267,

A. S. Thom, D.H. McIntosh 1969, Essentials of Meteorology Wykeham series

Wilks, D.S., (1995) Statistical Method in the atmospheric sciences, academic press, New york

T. Zinner, H. Mannstein and A. Tafferner (2008) Cb-TRAM: Tracking and monitoring severe convection from onset over rapid development to mature phase using multi-channel Meteosat-8 SEVIRI data, Meteorology and Atmospheric Physics,Volume 101, Numbers 3-4 / October

SPSS *www.spss.com/nl/*

http://www.meteorologie.eu.org/RDT/doc/SAF-NWC-CDOP-MFT-SCI-ATBD-11_v1.3.pdf

Appendix 1 Brier skill scores for all cases

ARP	Summer	Std dev	Winter	Std dev
EHAM	0..391	0.037	0.361	0.066
EHBK	0.466	0.045	0.358	0.080
EHDL	0.508	0.049	0.303	0.068
EHDV	0.231	0.049	0.334	0.064
EHEH	0.478	0.047	0.331	0.079
EHFD	0.307	0.064	0.445	0.070
EHFZ	0.388	0.055	0.420	0.057
EHGG	0.545	0.043	0.430	0.046
EHGR	0.478	0.040	0.258	0.097
EHJA	0.306	0.074	0.470	0.058
EHJR	0.315	0.062	0.483	0.048
EHKD	0.388	0.052	0.466	0.049
EHKV	0.359	0.063	0.433	0.044
EKLE	0.481	0.045	0.352	0.070
EHLW	0.410	0.044	0.421	0.052
EHMA	0.465	0.048	0.454	0.059
EHMG	0.432	0.043	0.450	0.053
EHPG	0.272	0.058	0.485	0.053
EHQE	0.322	0.058	0.475	0.049
EHRD	0.446	0.047	0.345	0.085
EHSA	0.210	0.047	0.400	0.072
EHSC	0.387	0.048	0.299	0.071
EHTW	0.530	0.047	0.319	0.063
EHVK	0.440	0.045	0.287	0.086
EHVL	0.397	0.058	0.485	0.056
EHWO	0.488	0.042	0.277	0.059

Table 1: Brier skill scores averaged for 500 cases with standard deviation for day time 2010.

ARP	Summer	Std dev	Winter	Std dev
EHAM	0.413	0.055	0.326	0.055
EHBK	0.344	0.079	0.134	0.039
EHDL	0.476	0.066	0.189	0.050
EHDV	0.252	0.054	0.270	0.035
EHEH	0.393	0.066	0.246	0.047
EHFD	0.407	0.059	0.319	0.047
EHFZ	0.392	0.062	0.408	0.036
EHGG	0.445	0.052	0.265	0.046
EHGR	0.414	0.056	0.197	0.046
EHJA	0.312	0.063	0.386	0.039
EHJR	0.325	0.061	0.443	0.038
EHKD	0.377	0.052	0.399	0.038
EHKV	0.309	0.063	0.430	0.034
EKLE	0.388	0.060	0.259	0.051
EHLW	0.400	0.049	0.314	0.039
EHMA	0.361	0.047	0.358	0.034
EHMG	0.338	0.059	0.436	0.031
EHPG	0.333	0.057	0.470	0.036
EHQE	0.367	0.056	0.392	0.037
EHRD	0.446	0.066	0.385	0.044
EHSA	0.283	0.051	0.439	0.043
EHSC	0.334	0.052	0.426	0.043
EHTW	0.483	0.063	0.167	0.048
EHVK	0.407	0.059	0.162	0.050
EHVL	0.379	0.051	0.351	0.037
EHWO	0.449	0.057	0.277	0.059

Table 2: Brier scores averaged for 500 cases with standard deviation for night time 2010.

ARP	Summer	Std dev	Winter	Std dev
EHAM	0.439	0.055	0.165	0.124
EHBK	0.413	0.055	0.292	0.148
EHFZ	0.356	0.081	0.439	0.083
EHGG	0.603	0.041	0.132	0.200
EHJR	0.399	0.049	0.393	0.125
EHMA	0.551	0.054	-0.026	0.153
EHPG	0.290	0.062	0.256	0.199
EHRD	0.463	0.052	0.275	0.113

Table 3: Brier scores averaged for 400 cases with standard deviation for day time 2013. Application

of 2014 algorithm.

ARP	Summer	Std dev	Winter	Std dev
EHAM	0.433	0.055	0.154	0.091
EHBK	0.415	0.101	0.120	0.071
EHFZ	0.340	0.087	-0.027	0.168
EHGG	0.407	0.101	0.172	0.071
EHJR	0.229	0.099	-0.134	0.183
EHMA	0.325	0.073	0.080	0.109
EHPG	-0.116	0.210	0.052	0.145
EHRD	0.347	0.084	0.116	0.105

Table 4: Brier scores averaged for 400 cases with standard deviation for night time 2013.

ARP	Summer	Std dev	Winter	Std dev
EHAM	0.187	0.050	-0.055	0.080
EHBK	0.129	0.056	0.027	0.021
EHFZ	0.091	0.047	-0.039	0.043
EHGG	0.285	0.047	-0.079	0.043
EHJR	0.191	0.056	-0.020	0.045
EHMA	0.245	0.042	-0.081	0.067
EHPG	0.207	0.050	-0.019	0.073
EHRD	0.150	0.046	-0.049	0.053

Table 5: Brier scores averaged for 300 cases with standard deviation for day time 2013 applying the operational algorithm.

ARP	Summer	Std dev	Winter	Std dev
EHAM	0.364	0.136	0.123	0.085
EHBK	0.333	0.139	-0.013	0.141
EHFZ	0.161	0.130	-0.144	0.097
EHGG	0.252	0.221	0.054	0.107
EHJR	0.019	0.193	-0.105	0.119
EHMA	0.202	0.122	0.056	0.084
EHPG	-0.544	0.411	0.021	0.096
EHRD	0.313	0.127	0.093	0.090

Table 6: Brier scores averaged for 300 cases with standard deviation for night time 2013 applying the operational algorithm.

Appendix 2: Verification data.

The creation of the verification data set is a key activity for the development of the algorithm. This section de scribes the procedure to merge the forecaster classification with the algorithm results for validation and optimization purposes.

In a prescribed microsoft office excel (*xls) file format containing 48 METAR report times the forecasters report:

“C” as a positive Cb classification

“T” as a positive Tcu classification

“?” as a possible Convective cloud, but not Cb or Tcu

“-” No Convective clouds to report

The first column contains the METAR time. Each consecutive column in the xls file represents one aerodrome. The order of the aerodromes is from North to South, East to West.

In the latter column clutter can be reported. This is an indication that clutter within the radar observations disables a successful classification. The latter column can also contain other causes for a failed classification, like data lacking.

The excel file name contains date information

Procedure to prepare the data.

The basic assumption here is that the data treatment is further done on a Linux platform, hence all subsequent commands are linux bash shell commands.

1) copy the excell files to an associated month directory e.g.

/usr/people/valkde/projects/CbTcu/CbEvaluation2010/nov2010/

from where the result xls files produced by the forecaster are stored. Examples:

/net/bens01/WNcommon_cx4/sharebase/common/b/beekman/Cbalg/Maart\ 2010/

/net/bens01/WNcommon_cx4/sharebase/common/b/brinkhor/Cbalg/2010-02/

/net/bens01/WNcommon_cx4/sharebase/common/b/blom/CbAlg/

/net/bens01/WNcommon_cx4/sharebase/common/r/rijkhold/Cb\ alg/

2) Use openoffice.org or libreoffice to read the xls file, activate and copy the relevant information with cursor and mouse clicks and paste it in a *.txt file, which could be generated with “gedit” or “nedit” or “vi” (Remark: if the software is unknown use google to understand and find alternatives). The relevant information excludes the last column which indicates the occurrence of clutter.

The output has to consist out of ascii or txt files which contain no hidden characters.

3) Modify [give the correct month + date. Please note this consists of 2 actions, preferable in a “vi” text editor] the next awk.script and use it

/usr/people/valkde/projects/CbTcu/CbEvaluation2010/awk.script >> Cb012010

to convert to an Cb0?2010 file.

The latter file will consist of a date-time string and 26 columns representing the aerodromes in a fixed sequential order (North to South, East to West position).

Important: changing the order requires that the subsequent applied software has to be changed accordingly. This is also required when stations are removed or added.

Include example of heading of file

4) Modify [introduce the correct month] and use in the correct month directory the script

/usr/people/valkde/projects/CbTcu/CbEvaluation2010/noteawk01

to get a five column file per month per aerodrome containing a date-time string, Cb, Cb+Tcu+?, Tcu, Cb+Tcu . “0” denotes no-occurrence, “1” denotes an occurrence. Do this for each month., preferable with a script.

Example of an output line:

201306120900 0 1 0 0

201306121000 1 1 0 1

4a) concatenate the monthly METAR files with the next commands to a year file

Go to /usr/people/valkde/projects/CbTcu/CbEvaluation2010/nov2010/

Create a variable “list” .

Ensure that $list consists of a list of all aerodromes. And that these files for each month are located in “month” directories (01....11,12).

E.g. In c-shell(csh): “set list=`ls -1 EH*2010`”

```
foreach i ( $list )
  cat ../*/{$i}_Cb* >> {$i}_
  sort {$i}_ > {$i}2010
 end
```

This concludes the actions required to make the classifications file created by the forecaster to file format which can be merged with the software results.

Appendix 3: Input data for the evaluation software

The data from radar and satellite are combined and processed by an algorithm. The program reads the satellite and radar file and produces the predictor values, combined with the name of the aerodrome and the date-time string.

In the operational mode the program produces an xml file with a strict prescribed format. The xml file is distributed to the various stations and is used in the local environment in combination with the local available observations to come to a classification. The subsequent steps to come to a classification and the requirement on the availability demands a strict timeliness of processing and sending and receiving the classification.

In the research mode a more elaborate output can be produced, allowing for evaluation and optimization. The research output consist of approximately 100 predictors. For additional research evaluation some 20 predictors are considered.

The next scripts combine the METAR files produced by the forecaster with the algorithm output. They also remove the non contributing predictors and make a distinction between day and night using a threshold on the signal of the satellite HRV channel.

/usr/people/valkde/projects/CbTcu/CbEvaluation2010/prepareSPSS2.ksh
/usr/people/valkde/projects/CbTcu/CbEvaluation2010/extract2.ksh

An awk command splits the data set in a summer and winter season.

```
awk '$1>201305000000&&$1<201310000000{print $0}' EHMACb_D for summer _S
awk '$1<201305000000||$1>201310000000{print $0}' EHMACb_D for winter _W
```

In the operational mode 3 to 5 predictors are actually used from the circa 30 extracted from the algorithm output .

Appendix 4. Program description functionality

The algorithm and scripts to produce a Cb classification processes the next steps. The input is the time stamp for the next METAR or ACTUAL. The time stamp is used to collect the most recent available radar and satellite observation files required as input for the algorithm. When radar information is lacking the algorithm will stop. When Satellite imagery is lacking the algorithm will use the less oldest image available. In an updated version the classification should be solely based on radar observation, despite the fact that the latter method may have a lower performance.

The input files are located in a predefined directory structure

The predictors with the highest correlation to the predictand are determined in a pre-study using the R statistical package(http://www.r-project.org/). From the radar and satellite files the predictors are determined for each area of interest around 26 stations. The area of interest is defined as a circle with a radius of 15 km around the airport reference point (ARP). The location, METAR code and identification number of each aerodrome are obtained from a separate input file.

The radar signals are contoured starting at 14 dBz with 17 steps of 2.5 dBz till 56.5 dBz. The highest occurring contour number within the area of interest or the highest contour number encompassing the area of interest has a high correlation with the predictand.

Also the contrast between the maximum and non zero minimum of the radar signal correlated to the predictand. The latter correlation appeared in the 2013 release of the software for a number of aerodromes

From the satellite observations within the area of interest the contrast (maximum – minimum) in the reflection channel HRV correlated significantly to the predictand during daytime. Also the average cloud top temperature appeared in the R study as a predictor, under the condition that it is not classified as a cirrus cloud. The difference between spectral channels 12.0 um and 10.8 um can distinguish semitransparent cirrus clouds from other clouds. The average cloud top temperature is determined by applying a rudimentary cloud mask where pixels with a brightness temperature in the 10.8 um channel below 268 K are classified as cloudy. SAFNWC *www.nwcsaf.org* provides a more accurate cloud mask. It is not implemented here as the availability of the cloud mask demands too much time. Here the production time is not the bottle neck. The transport of the data between the various platforms introduces an unacceptable latency for operational implementation .

During night time the areal fraction of pixels within the cloud for which a brightness temperature difference between channel 3.9 um and 10.8 um is negative (BT3.9 -BT10.8 < 0) also appeared as a predictor. The night time is defined there where HRV channel value is smaller than 39 counts. The same rudimentary cloud mask as above is applied BT10.8 < 268 K.

Predictor coefficients and thresholds

The supervised Cb classification for 2010 done by forecaster is used to determine per aerodorme the three predictors with the highest correlation to the predictand. This may differ per considered season. Using the R glm function the predictor coefficients are

determined.

Predictor coefficient determination is done in a scripting environment which converts the coefficients and their associated predictors in an equation which can be directly incorporated into the software.

Another script is used to determine per aerodrome and per season the probability threshold for which the highest CSI score is obtained. These thresholds can also be directly incorporated into the software.

The scripting generation of predictor equations and threshold values fed directly into the software minimizes errors by transferring these values.

Appendix 5. Implementation

The ACTUAL implementation in 2011 involves several platforms.

The main software package runs on the APL. It consists of Fortran and “C” coded programs and c-shell scripts.

The radar data is already available on the APL.

The required satellite data is produced on the operational Cinesat system. Via Vivid the satellite results are copied into a prescribed directory on the APL. As there is some time variety in the availability of the files on Cinesat Vivid checks frequently whether the files are available.

Next to software also scripts on the APL had to be modified for an optimal timing of the start of the run. Given the time of availability of the satellite files (HH+17,47) and the required time (HH+20,50) to incorporate this observation into the METAR (HH+25,55) optimization of timeliness is essential.

CIBIL collects and distributes the XML file from the APL to the ADCMs.

A smooth transition from test-CIBIL to CIBIL was done in the morning on March 9, 2011.

The only hick-up in AUTO-METAR Cb production was a complete outage of satellite data. In April 2011 there was no data from the satellite nor from the operational back-up satellite for a few hours on one day.

Datastreams

The algorithm runs in an **APL** environment which is only accessible from APL ${HOME} .
All software, fortran and “C” code and “C”-shell scripts are located in:
${HOME}/MODELLEN/BEELDEN/Cb

The algorithm uses as input radar observations and satellite observations.
All the subsequent paths starting with “/net/” can be accessed from any KNMI workstation

The radar files (e.g. RAD_NL21_PCP_NA_201108080850.h5) are distributed by the **OMNIVOOR** or **OMBE** imagery system. They have a resolution of 2.5 x 2.5 km^2 and are available on the **APL** platform in the directory:
/net/apl/apl/data/RADAR/INPUT/

Four satellite files
MET9_120-108_Cb-NL_1011231230.h5
MET9_39-108_Cb-NL_1011231230.h5
MET9_HRV_Cb-NL_1011231230.h5
MET9_IR108_Cb-NL_1011231230.h5
are produced on the operational Cinesat system ”**bvlcinesat**”. They are produced as soon as the observation files are available.
The “**VIVID**” system collects the files by ftp from
/net/bhlbcs02/data/cinesat_oper/out/export
and stores them in the directory
/net/apl/apl/data/Cinesat/
The “**VIVID**” system attempts every minute to collect the files, as there is not a fixed availability time due to small deviations of broadcasting, and data traffic.

The algorithm collects the data and produces output files (radarCb_201108081145.xml).

Please note the subtle (CB versus Cb) but essential differences with the Meteo France based algorithm output files (radarCb_201108081140.xml) which are stored into */net/apl/apl/data/RADAR/Cb*

An APL script merges radarCb_201108081140.xml and radarCb_201108081145.xml into one radarCb_201108081145.xml in the output directory:
/net/apl/apl/data/Cb

Allthough the file name of the output file "radarCb_YYYYMMDDHHmm.xml" contains "radar", the content is based on both radar and satellite. The time stamp of radarCb_201108081140.xml is the start of the radar observation. The time stamp of radarCb_201108081145.xml is the moment that the message is issued, which is five minutes after the radar observation starts. Due to software dependencies the format of the resulting xml file is very limited in its format freedom. Only in the last line there is room for additional information on used satellite, time stamp and other information.

The **CIBIL** system collects the radar output file from the APL by ftp every five minutes and distributes it to the **ADCM** at the various airports. Within the ADCM the radar.xml files is used next to lightning data to come to a Cb classification, which is used for METAR, SPECIAL and ACTUAL reports. The **ADCM** combines the Cb classification with Ta-Td information to come to a cloud base height. Should the base height data lead to an inconclusive result a cloud base height of 1500 ft is reported.
It is underlined here that the algorithm using radar and satellite information only provides a Cb classification and coverage and does NOT provide any information on the cloud base height.

For the North Sea platforms **CIBIL** combines the XML files with ceilometer and lightning to produce a METAR. This enables a software change to determine the cloud base height using ceilometer and Ta-Td together.

The data flow and file names are depicted in Figure below.
The dependency on Cinesat can become an issue in the future. There have been no updates of Cinesat since 2007.

Dependencies

The algorithm only produces output when radar and satellite data is available. The assumption is that the radar data is always present. Should satellite data lack than the algorithm will look for satellite data of one time step earlier. It is also checked whether the operational satellite is replaced by the backup satellite.

The repeat cycle of the radar is five minutes, that of the satellite data is 15 minutes. This means that one satellite image will be used three times in combination with different radar inputs. The best collocation in time and space is the combination of satellites image at HH+00, 15, 30 and 45 minutes (start time of image observation) with radar image of HH+ 15, 30, 45, 00 (end time of observation) minutes. The other combination's will have an offset in observation time of five or ten minutes. It has not been studied what the impact of

this offset is on the classifications because it is not feasible as there is no independent and validated data set available which provide Cb classifications with a five minutes repeat cycle.

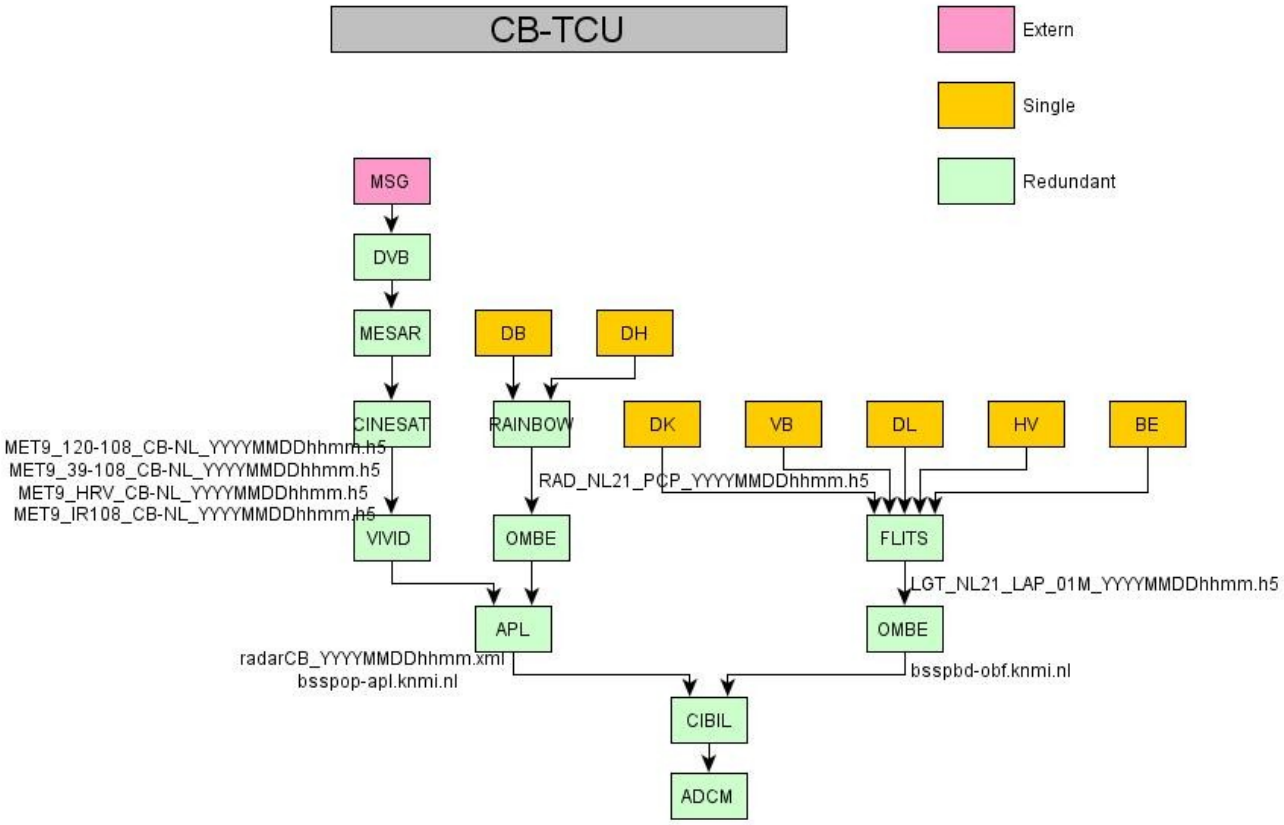

Figure A5. The data streams and file names as applied in the Cb-Tcu algorithm. The ADCM produces the METAR, ACTUAL and SPECIAL message. Courtesy W. Wauben. The separate systems should be identifiable within the "blue print of KNMI". MSG meteosat second generation satellite DVB digital video broadcasting DB de Bilt DH den Helder DK De Kooy VB Valkenburg DL Deelen HV Hoogeveen BE Beek

Lacking of satellite data should be reported in the XML file.

The presence of the radar files will not assure that both radars are functioning. Should one of the radar be out of function then this will lead to deteriorated results. There is no fall back option for this.
Lacking of radar information should be reported in the XML file.
The last line of the XML file includes all relevant times used at the creation of the XML file
Example
<!-- METAR time=201407021025 utc RADAR time= 201407021015 utc SATELLITE time=201407020945 utc -->

Appendix 6: The coefficients and the predictors

Summerday

The next lines, containing predictors and coefficients, are the required input for the algorithm.
Here
kans(i) represents the exponential denominator of the logistic probabilistic equation for station 1 (EHAM)
The numbering of stations in accordance to the list in table 4.1, alphabetic order of the stations.
pre(18,i) represents the highest occurring radar contour number.
pre(30,i)-pre(29,i) represents the contrast in the radar observation between the maximum and minimum (non-zero) precipitation intensity
pre(93,i) represents the average of the cloud top temperature
pre(94,i) represents the areal fraction where the brightness temperature difference between the 3.9 um and the 10.8 um channel is below zero is valid (T03.9-T10.8 <0)
pre(97,i) represents the difference between the maximum and minimum occurring value in the HRV channel
The index i in kans(i) refers to the alphabetic order of station as given in table (4.1)

kans(1)=-5.005148+0.563032*pre(18,1)+0.000977*(pre(30,1)-pre(29,1))+0.021035*pre(97,1)
kans(2)=-4.192553+0.356401*pre(18,2)+0.001890*(pre(30,2)-pre(29,2))+0.020869*pre(97,2)
kans(3)=-4.512681+0.414435*pre(18,3)+0.001445*(pre(30,3)-pre(29,3))+0.024944*pre(97,3)
kans(4)=-4.674758+0.001038*(pre(30,4)-pre(29,4))+0.638536*pre(93,4)+0.017866*pre(97,4)
kans(5)=-4.752277+0.414525*pre(18,5)+0.001318*(pre(30,5)-pre(29,5))+0.024438*pre(97,5)
kans(6)=-4.849494+0.001856*(pre(30,6)-pre(29,6))+0.445414*pre(93,6)+0.022618*pre(97,6)
kans(7)=-4.226944+0.334157*pre(18,7)+0.001936*(pre(30,7)-pre(29,7))+0.022258*pre(97,7)
kans(8)=-4.002909+0.387155*pre(18,8)+0.001737*(pre(30,8)-pre(29,8))+0.022231*pre(97,8)
kans(9)=-4.544155+0.428406*pre(18,9)+0.001570*(pre(30,9)-pre(29,9))+0.024202*pre(97,9)
kans(10)=-4.039726+0.308764*pre(18,10)+0.002109*(pre(30,10)-pre(29,10))+0.016926*pre(97,10)
kans(11)=-3.536002+0.260909*pre(18,11)+0.002010*(pre(30,11)-pre(29,11))+0.015208*pre(97,11)
kans(12)=-3.345408+0.376033*pre(18,12)+0.001891*(pre(30,12)-pre(29,12))+0.013778*pre(97,12)
kans(13)=-3.898231+0.346122*pre(18,13)+0.001729*(pre(30,13)-pre(29,13))+0.016604*pre(97,13)
kans(14)=-4.931388+0.510528*pre(18,14)+0.001343*(pre(30,14)-pre(29,14))+0.021763*pre(97,14)
kans(15)=-4.713504+0.498964*pre(18,15)+0.001551*(pre(30,15)-pre(29,15))+0.021339*pre(97,15)
kans(16)=-4.167577+0.410839*pre(18,16)+0.002801*(pre(30,16)-pre(29,16))+0.019947*pre(97,16)
kans(17)=-4.341123+0.409585*pre(18,17)+0.001828*(pre(30,17)-pre(29,17))+0.021887*pre(97,17)
kans(18)=-5.940921+0.292810*pre(18,18)+0.753382*pre(93,18)+0.019456*pre(97,18)
kans(19)=-4.308098+0.432553*pre(18,19)+0.001662*(pre(30,19)-pre(29,19))+0.018023*pre(97,19)
kans(20)=-5.680149+0.501368*pre(18,20)+0.480081*pre(93,20)+0.020773*pre(97,20)
kans(21)=-4.257932+0.001903*(pre(30,21)-pre(29,21))+0.462372*pre(93,21)+0.017968*pre(97,21)
kans(22)=-4.975038+0.359778*pre(18,22)+0.002036*(pre(30,22)-pre(29,22))+0.024464*pre(97,22)
kans(23)=-3.424113+0.311675*pre(18,23)+0.001864*(pre(30,23)-pre(29,23))+0.019869*pre(97,23)
kans(24)=-4.254710+0.418030*pre(18,24)+0.001325*(pre(30,24)-pre(29,24))+0.021313*pre(97,24)
kans(25)=-3.889209+0.386215*pre(18,25)+0.001837*(pre(30,25)-pre(29,25))+0.017960*pre(97,25)
kans(26)=-4.418287+0.469358*pre(18,26)+0.001499*(pre(30,26)-pre(29,26))+0.020858*pre(97,26)

Summer night

kans(1)=-4.045229+0.482925*pre(18,1)+0.001465*(pre(30,1)-pre(29,1))+0.782631*pre(93,1)*pre(94,1)

kans(2)=-3.793898+0.453560*pre(18,2)+0.001491*(pre(30,2)-pre(29,2))+0.709827*pre(93,2)*pre(94,2)

kans(3)=-3.545076+0.467205*pre(18,3)+0.001470*(pre(30,3)-pre(29,3))+0.739188*pre(93,3)*pre(94,3)

kans(4)=-2.963092+0.215276*pre(18,4)+0.001152*(pre(30,4)-pre(29,4))+0.827244*pre(93,4)*pre(94,4)

kans(5)=-3.521369+0.439741*pre(18,5)+0.001798*(pre(30,5)-pre(29,5))+0.548301*pre(93,5)*pre(94,5)

kans(6)=-3.217309+0.503695*pre(18,6)+0.001419*(pre(30,6)-pre(29,6))+0.771269*pre(93,6)*pre(94,6)

kans(7)=-2.913615+0.452748*pre(18,7)+0.001373*(pre(30,7)-pre(29,7))+0.674099*pre(93,7)*pre(94,7)

kans(8)=-2.775414+0.447234*pre(18,8)+0.001805*(pre(30,8)-pre(29,8))+0.294568*pre(93,8)*pre(94,8)

kans(9)=-3.313099+0.406833*pre(18,9)+0.002223*(pre(30,9)-pre(29,9))+0.591239*pre(93,9)*pre(94,9)

kans(10)=-3.217997+0.311830*pre(18,10)+0.001087*(pre(30,10)-pre(29,10))
+0.819669*pre(93,10)*pre(94,10)

kans(11)=-2.870764+0.310888*pre(18,11)+0.002112*(pre(30,11)-pre(29,11))
+0.530747*pre(93,11)*pre(94,11)

kans(12)=-1.953290+0.321046*pre(18,12)+0.002216*(pre(30,12)-pre(29,12))
+0.286220*pre(93,12)*pre(94,12)

kans(13)=-2.941589+0.363141*pre(18,13)+0.002027*(pre(30,13)-pre(29,13))
+0.553764*pre(93,13)*pre(94,13)

kans(14)=-3.595595+0.380259*pre(18,14)+0.065709*(pre(30,14)-pre(29,14))
+0.639209*pre(93,14)*pre(94,14)

kans(15)=-3.104404+0.516562*pre(18,15)+0.002148*(pre(30,15)-pre(29,15))
+0.322778*pre(93,15)*pre(94,15)

kans(16)=-2.423604+0.364648*pre(18,16)+0.001894*(pre(30,16)-pre(29,16))
+0.391221*pre(93,16)*pre(94,16)

kans(17)=-2.441915+0.309969*pre(18,17)+0.002230*(pre(30,17)-pre(29,17))
+0.522658*pre(93,17)*pre(94,17)

kans(18)=-3.127027+0.282932*pre(18,18)+0.002196*(pre(30,18)-pre(29,18))
+0.650571*pre(93,18)*pre(94,18)

kans(19)=-2.880456+0.392727*pre(18,19)+0.001486*(pre(30,19)-pre(29,19))
+0.537378*pre(93,19)*pre(94,19)

kans(20)=-3.451520+0.434030*pre(18,20)+0.045205*(pre(30,20)-pre(29,20))
+0.535971*pre(93,20)*pre(94,20)

kans(21)=-3.035430+0.205029*pre(18,21)+0.001575*(pre(30,21)-pre(29,21))
+0.756056*pre(93,21)*pre(94,21)

kans(22)=-3.118787+0.337508*pre(18,22)+0.003159*(pre(30,22)-pre(29,22))
+0.544256*pre(93,22)*pre(94,22)

kans(23)=-3.284205+0.470768*pre(18,23)+0.001611*(pre(30,23)-pre(29,23))
+0.705458*pre(93,23)*pre(94,23)

kans(24)=-3.732134+0.464259*pre(18,24)+0.001957*(pre(30,24)-pre(29,24))
+0.670624*pre(93,24)*pre(94,24)

kans(25)=-2.497732+0.391845*pre(18,25)+0.001720*(pre(30,25)-pre(29,25))
+0.371168*pre(93,25)*pre(94,25)

kans(26)=-3.188830+0.402032*pre(18,26)+0.001971*(pre(30,26)-pre(29,26))
+0.577265*pre(93,26)*pre(94,26)

Winter day

kans(1)=-8.768599+0.459746*pre(18,1)+1.559562*pre(93,1)+0.020084*pre(97,1)
kans(2)=-10.601483+2.846091*pre(93,2)+0.790690*(pre(30,2)-pre(29,2))+0.012741*pre(97,2)
kans(3)=-7.287225+0.274382*pre(18,3)+1.326403*pre(93,3)+0.015586*pre(97,3)
kans(4)=-4.792377+0.520206*pre(93,4)+0.001881*(pre(30,4)-pre(29,4))+0.019711*pre(97,4)
kans(5)=-8.479504+1.886269*pre(93,5)+0.011642*pre(97,5)+0.159743*(pre(93,5)*pre(18,5))
kans(6)=-5.112664+0.904797*pre(93,6)+0.001997*(pre(30,6)-pre(29,6))+0.018422*pre(97,6)
kans(7)=-2.781194+0.278792*pre(18,7)+0.003144*(pre(30,7)-pre(29,7))+0.015931*pre(97,7)
kans(8)=-4.676150+0.536810*pre(93,8)+0.909339*(pre(30,8)-pre(29,8))+0.015544*pre(97,8)
kans(9)=-4.266510+0.415463*pre(18,9)+0.002117*(pre(30,9)-pre(29,9))+0.012894*pre(97,9)
kans(10)=-4.316424+0.470980*pre(93,10)+0.002029*(pre(30,10)-pre(29,10))+0.021133*pre(97,10)
kans(11)=-3.364756+0.292419*pre(18,11)+0.002592*(pre(30,11)-pre(29,11))+0.018905*pre(97,11)
kans(12)=-5.450531+0.770105*pre(93,12)+0.624467*(pre(30,12)-pre(29,12))+0.019687*pre(97,12)
kans(13)=-2.814321+0.255334*pre(18,13)+0.002714*(pre(30,13)-pre(29,13))+0.016412*pre(97,13)
kans(14)=-7.465661+0.315049*pre(18,14)+1.170047*pre(93,14)+0.020644*pre(97,14)
kans(15)=-4.609739+0.505378*pre(18,15)+0.002286*(pre(30,15)-pre(29,15))+0.021326*pre(97,15)
kans(16)=-7.060140+0.357967*pre(18,16)+1.474034*pre(93,16)+0.017480*pre(97,16)
kans(17)=-6.465545+0.312999*pre(18,17)+1.231456*pre(93,17)+0.021053*pre(97,17)
kans(18)=-7.407702+0.329326*pre(18,18)+1.738058*pre(93,18)+0.015465*pre(97,18)
kans(19)=-6.942599+0.323352*pre(18,19)+1.338032*pre(93,19)+0.019606*pre(97,19)
kans(20)=-8.987710+1.968117*pre(93,20)+0.016790*pre(97,20)+0.137454*(pre(93,20)*pre(18,20))
kans(21)=-7.456365+1.541178*pre(93,21)+0.019721*pre(97,21)+0.109744*(pre(93,21)*pre(18,21))
kans(22)=-3.444531+0.238488*pre(18,22)+0.002749*(pre(30,22)-pre(29,22))+0.015711*pre(97,22)
kans(23)=-6.804436+1.218520*pre(93,23)+0.653290*(pre(30,23)-pre(29,23))+0.015939*pre(97,23)
kans(24)=-7.362115+1.470175*pre(93,24)+0.013403*pre(97,24)+0.130746*(pre(93,24)*pre(18,24))
kans(25)=-5.707278+0.561712*pre(93,25)+0.850236*(pre(30,25)-pre(29,25))+0.023650*pre(97,25)
kans(26)=-8.812819+1.738990*pre(93,26)+0.016786*pre(97,26)+0.139644*(pre(93,26)*pre(18,26))

Winter night

kans(1)=-4.212144+0.563237*pre(18,1)+0.058473*(pre(30,1)-pre(29,1))+0.616219*(pre(93,1)*pre(94,1))

kans(2)=-2.896279+0.171752*pre(18,2)+0.002135*(pre(30,2)-pre(29,2))+0.453886*(pre(93,2)*pre(94,2))

kans(3)=-3.064745+0.291470*pre(18,3)+0.002608*(pre(30,3)-pre(29,3))+0.372357*(pre(93,3)*pre(94,3))

kans(4)=-4.984703+-0.030399*pre(18,4)+1.422150*pre(93,4)+1.040895*pre(94,4)

kans(5)=-3.523589+0.088751*pre(18,5)+0.417120*(pre(30,5)-pre(29,5))+0.723013*(pre(93,5)*pre(94,5))

kans(6)=-6.654496+0.296140*pre(18,6)+1.938398*pre(93,6)+1.157439*pre(94,6)

kans(7)=-4.825637+0.186539*pre(18,7)+1.324623*pre(93,7)+1.438616*pre(94,7)

kans(8)=-2.801990+0.349355*pre(18,8)+0.002378*(pre(30,8)-pre(29,8))+0.502063*(pre(93,8)*pre(94,8))

kans(9)=-3.472123+0.270135*pre(18,9)+0.002386*(pre(30,9)-pre(29,9))+0.678602*(pre(93,9)*pre(94,9))

kans(10)=-4.991683+0.196885*pre(18,10)+1.400937*pre(93,10)+1.265117*pre(94,10)

kans(11)=-4.580928+0.303738*pre(18,11)+1.044949*pre(93,11)+1.686967*pre(94,11)

kans(12)=-2.494288+0.333564*pre(18,12)+0.002505*(pre(30,12)-pre(29,12))
+0.598659*(pre(93,12)*pre(94,12))

kans(13)=-4.312087+0.303239*pre(18,13)+1.023539*pre(93,13)+1.324932*pre(94,13)

kans(14)=-3.441762+0.403842*pre(18,14)+0.002253*(pre(30,14)-pre(29,14))
+0.519303*(pre(93,14)*pre(94,14))

kans(15)=-2.931117+0.396201*pre(18,15)+0.084684*(pre(30,15)-pre(29,15))
+0.498709*(pre(93,15)*pre(94,15))

kans(16)=-5.306368+0.298030*pre(18,16)+1.465592*pre(93,16)+0.659303*pre(94,16)

kans(17)=-4.604095+0.354896*pre(18,17)+1.157853*pre(93,17)+1.138649*pre(94,17)

kans(18)=-4.718265+0.380595*pre(18,18)+0.933844*pre(93,18)+1.744414*pre(94,18)

kans(19)=-4.345935+0.349664*pre(18,19)+0.870867*pre(93,19)+1.346895*pre(94,19)

kans(20)=-3.809774+0.497100*pre(18,20)+0.001548*(pre(30,20)-pre(29,20))
+0.753395*(pre(93,20)*pre(94,20))

kans(21)=-5.460806+0.339693*pre(18,21)+1.315791*pre(93,21)+1.524863*pre(94,21)

kans(22)=-5.574109+0.352615*pre(18,22)+1.330417*pre(93,22)+1.321132*pre(94,22)

kans(23)=-2.870671+0.168681*pre(18,23)+0.265967*(pre(30,23)-pre(29,23))
+0.359997*(pre(93,23)*pre(94,23))

kans(24)=-3.942523+0.329958*pre(18,24)+0.002105*(pre(30,24)-pre(29,24))
+0.721757*(pre(93,24)*pre(94,24))

kans(25)=-5.569308+0.337655*pre(18,25)+1.431346*pre(93,25)+0.921379*pre(94,25)

kans(26)=-3.042133+0.281514*pre(18,26)+0.002059*(pre(30,26)-pre(29,26))
+0.655902*(pre(93,26)*pre(94,26))

Appendix 7: **Forecaster manual by Pieter Arts to evaluate Cb occurrence.**

Handleiding CB/TCU, Pieter Arts. January 2015.

Omwille van verbetering en validatie van het CB/TCU-algoritme van het KNMI, is het noodzakelijk te beschikken over waarnemingen van het optreden van CB/TCU in de nabijheid van vastgestelde locaties. Hiertoe zal een meteoroloog de verleden situatie op de locaties moeten beoordelen en aangeven of er wel/niet sprake was van CB/TCU binnen een straal van 15 km.
Het KNMI algoritme maakt gebruik van radar- en satelliet-informatie. De meteoroloog zal bij het aanmaken van de CB/TCU database zich vooral laten leiden door radarbeelden, die Rudolph van Westrhenen klaar zal zetten. Ook bestaat er een mogelijkheid om satellietbeelden op een cinesat machine klaar te laten zetten (door Paul de Valk).

Naast bovenstaande primaire informatie heeft de beoordelend meteoroloog zelf de mogelijkheid om o.a. de volgende bronnen te raadplegen:
http://oper.knmi.nl/archiefviewer/ (o.a. weerkaarten, progtemps, etc ……)
http://www.knmi.nl/klimatologie/daggegevens/onweer/ (handige onweerkaartjes)
http://www.wunderground.com/history/ (metar gegevens)
http://www.sat.dundee.ac.uk/abin/browse/modis als alternatief voor de cinesat beelden (wel zal je jezelf eenmalig moeten registreren voor een username en wachtwoord).

De uitkomsten van de meteoroloog moeten worden ingevuld in een Excel-bestand. Afhankelijk van de behoefte van Paul zijn er 2 verschillende invulformulieren. Het eerste formulier behelst 26 locaties en het tweede formulier 8 locaties. De locaties zijn ruwweg van noord naar zuid gerangschikt, zodat dit het invullen vergemakkelijkt.

- Verander als eerste de tekst in cel A1 door daar de juiste datum in te voeren
- Standaard staat er een “-” ingevuld voor alle andere gevallen dan de volgende:
- “C” = CB
- “T” = TCU
- “?” = CB/TCU op de rand van de 15 km cirkel, of als je twijfelt of het CB/TCU is.
- “F” = relatief veel valse echo’s binnen de 15 km cirkel.
- Als er een radarbeeld mist zet je in de kolom AB “niet beschikbaar”.

Tot slot, sla je het Excel bestand op een logische manier en plek op (bv op de N-schijf).

Appendix 8: Clutter

In a late stage of the study the impact of distorted radar signals by atmospheric phenomena, also named clutter has an impact on the performance of sea platforms. A rudimentary clutter filter was applied: where the rain intensity was more than 40 mm/hr the classification was set to non-Cb.

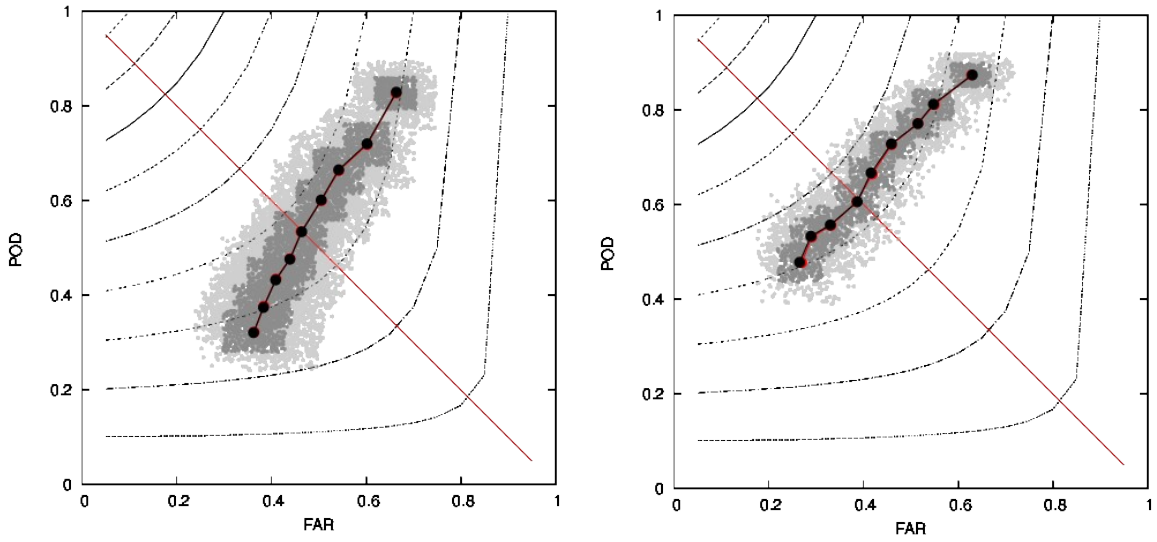

Figure that shows the impact of clutter removal on the pod far diagram for a sea station EHMG during day time in the summer of 2010. There is a significant increase in CSI from 0.37 to 0.45 due to clutter removal, shown in the right image.